UNIVERSIDAD COMPLUTENSE DE MADRID
FACULTAD DE CIENCIAS QUÍMICAS

TESIS DOCTORAL

Lysosome-dependent cell death: molecular players and implications for disease

Muerte celular dependiente de lisosoma : reguladores moleculares y consecuencias en la neurodegeneración

MEMORIA PARA OPTAR AL GRADO DE DOCTOR

PRESENTADA POR

Ana Serrano Puebla

Directora

Patricia Boya

Madrid 2019

UNIVERSIDAD COMPLUTENSE DE MADRID
Facultad de Ciencias Químicas

CONSEJO SUPERIOR DE INVESTIGACIONES CIENTÍFICAS
Centro de Investigaciones Biológicas

Lysosome-dependent cell death: molecular players and implications for disease

Muerte celular dependiente de lisosoma: reguladores moleculares y consecuencias en la neurodegeneración

Memoria presentada por Ana Serrano Puebla para optar al grado de Doctora en Bioquímica, Biología Molecular y Biomedicina por la Universidad Complutense de Madrid

VºBº de la Directora de Tesis
Patricia Boya

VºBº del Tutor
Ismael Galve-Roperh

Ana Serrano Puebla

2018

AGRADECIMIENTOS

Quería agradecer haber llegado hasta aquí a la doctora Patricia Boya. Patri, gracias por darme la oportunidad de haber estado en tu laboratorio donde no solo me has enseñado a ser buena científica, sino a hacerme mayor, a relativizar las cosas y a intentar disfrutar de cada momento de la tesis, aunque bien sabes que no ha sido un camino facil.

Gracias a mis compañeros de laboratorio, el día a día sería un aburrimiento sin vosotros. Gracias Bea, por ser una amiga, por estar siempre dispuesta a ayudar y por escucharme constantemente. Gracias amiga y una compañera de vida, aunque no sabemos qué caminos nos deparan, ya sabes que aquí estoy. Gracias Elena, por tu ayuda en el día a día, por tus ironías, tus gracias y por ser mi cerebro y profesora de historia. Gracias Raquel por traer siempre tan buen flow, por tus risas y por mantener la calma en esta loca de la vida. Gracias por estar siempre dispuesta a echar un cable. Gracias Nacho, chiqui, por recordarme lo mucho que te gustaron las prácticas conmigo y por mantener tan buen rollo en el laboratorio. Gracias por tus ánimos Nata, una pena haber coincidido tan poco contigo, pero creo que eres un ejemplo a seguir. Gracias también a los que ya no están: Esther, ya sabes que no es poco lo que te agradezco, fuera y dentro del laboratorio. Lorena, compañera de tardes, gracias por todas las cosas buenas. Gracias Lucía, por ser mi primera profe en el laboratorio y ser paciente con mis manos sacando retinas. Gracias Marta, un placer coincidir contigo cuando sólo eramos pollitos recién salidas del cascarón.

Gracias a todos aquellos del 3D Lab, los que siguen y los que ya se marcharon: Alberto, Patri V, Noemí, Marisa, Mariano, María Platón. Gracias por escuchar, por ayudar, por los indios o las pepitas. Gracias a los que, de una manera u otra, han estado de mi mano en el CIB: Alessandra, qué de historias tenemos juntas, vidas paralelas que parecen encaminarse. Albert y Paco, a ver cuando salís de argumosa. A Joan. A todos los chiquis: Ignacio, gracias gorrión, nos vemos en vallehermoso o en mondo. Patri L y Natalia, gracias equipo femenino de la casa rural. Gracias Néstor, por tu paciencia.

Gracias a los servicios del CIB: a la gente del animalario, especialmente a Carlos y a Dani; a microscopía confocal, Maite y Gema, gracias por vuestra ayuda constante; a Fernando, el rey de la microscopía electrónica; gracias también a Carmen y a Zahira. Gracias a la gente del CIB, que aunque nunca hemos trabajado juntos, siempre ha sido un placer coincidir con vosotros: Luque, Rafa, Juan, Barbara, Concha.

Gracias amigas, sois mi segunda familia, mi equipo vallecano: Sofi, Vero, Patri y Sara. Os quiero amigas, gracias por todos estos años, horas de terapia, feminismo y diferentes parques del barrio conquistados. Gracias por estar siempre, por escuchar mis 19 audios de 10 segundos y por ser mi segunda familia. Me habéis apoyado muchísimo estos años. No sabemos a donde nos llevará el destino, pero sé que nuestra amistad irá creciendo con los años. Gracias a mis compañeros de universidad: Eu, Noelia, Raquel, Anabel, Silvia, Isa. No sabemos donde acabarán nuestras carreras, solo espero seguir estando al día de vuestras peripecias.

Muchas gracias queridos amigos de casa y salidas: Martina, te quiero mucho amica! Ojalá sigamos creciendo y que nunca acaben nuestras horas de terapias juntas. Gracias por escucharme los días que me subía por las paredes. Gracias por las cervezas, fiestas y momentos yoguis juntas. Víctor, gracias por sacarme a bailar y charlar tanto conmigo. Creo que ni la boca de Soraya conseguiría separar esta amistad. Oli, gracias pelirrojo! Por escuchar, debatir y sacarme a mover las caderas. Ojalá acabemos en Tailandia, confío en ti. Jose, gracias por seguir con vida después de la línea jaja gracias por escucharme y animarme siempre que llegaba a casa. Pablo, gracias por mostrarme hombres feministas con más fuerza que yo, por crear las mundialmente conocidas miserias y por cuidarme a los juanes. Gracias por escucharme tanto! Gracias Elena, por no dejar que la tienda de campaña saliera volando gracias al peso de tus pestañas –sin eso, hoy no estaría aquí ;) y Lucía, gracias vecina del centro, por tu sonrisa y tus ganas de ayudar.

Gracias Copenhague! Por tantos momentos hygge: Sara, Carlota, Alex, Tamara, Guille, Elio, Ollie, Alberto I love you guys, ya sabeis que me podeis

encontrar entre los matorrales del distortion gritando *felichitá*! Quizás volvamos a vivir estas cosas de nuevo muy pronto.

Thanks to Dr. Marja Jaattela, for the opportunity to stay in her laboratory for 6 months. Thanks to Elisabeth, Elena, Kristina, Jano, Jonathan, Knut, Allie, Siri for giving me really nice moments and for making me fell like at home. Thanks Marie and Boris for being my danish-russian family.

Gracias papá, por comprender, ayudarme y escucharme siempre que lo he necesitado. Gracias por darme tan buenos principios. Gracias María, por hacerme sentir parte de tu familia, por animarme en el día a día. Gracias abuela por todo. Os quiero mucho.

Gracias mamá, por estar, de alguna manera, tan cerca de mí. Esta tesis está dedicada a ti. Sin tus enseñanzas, tu fuerza y tus sonrisas, incluso en los peores momentos, no habría llegado a este día. Ahora sólo me queda crecer, y lo haré, de alguna manera, gracias a ti.

INDEX

RESUMEN

La muerte celular dependiente de lisosoma es un tipo de muerte en el que la estabilidad de la membrana se pierde, llevando a la liberación del contenido lisosomal al citosol. Parte de las proteínas del lumen lisosomal son activas en el citosol, lo que desencadena el corte de múltiples proteínas citoplasmaticas, llevando a muerte celular. Además, la autofagia, mecanismo necesario para la homeostasis celular, requiere de lisosomas en correcto estado para poder ser efectiva. En esta tesis, el papel de la autofagia y la estabilidad lisosomal fue estudiado en un modelo murino de degeneración retiniana llamado *retinitis pigmentaria,* demonstrando que en un modelo de ratón de esta enfermedad, la muerte celular dependiente de lisosoma está ocurriendo. Estos resultados nos llevaron a estudiar el mecanismo de esta muerte en modelos deficientes de autofagia, descubriendo que la proteína Atg7, necesaria para la inducción de la autofagia, podría tener un papel fundamental en la composición lipídica del lisosoma, afectando directamente a la estabilidad lisosomal.

ABSTRACT

Lysosomal-dependent cell death is a kind of cell death which is characterized by the lost of the lysosomal stability, leading to the release of the lysosomal content to the cytosol. Some of the lyososomal protein are active in the cytosol, leading to the cleavage of several cytoplasmic proteins, promoting cell death. In addition, autophagy, which is a necessary mechanism for the cellular homeostasis, needs functional lysosomes to be effective. In this thesis, autophagy role and lysosomal stability was studied in a mouse model of a retinal degeneration disease called *retinitis pigmentosa,* demonstrating that in this model of the disease, lysosomal dependent-cell death is happening. These results leaded us to study this cell death mechanism in autophagy-deficient models, demonstrating that the protein Atg7, necessary for autophagy induction, could present a fundamental role in the lysosomal lipidic composition, afecting to the lysosomal stability.

ABBREVIATIONS

ADCD: autophagy-dependent cell death

AMD: Age-Related Macular Degeneration

BafA1: Bafilomycin A1

BMP: bis(monoacylglycero)phosphate

BSA: bovine serum albumin

CAD: cationic amphiphilic drug

CMA: chaperone-mediated autophagy

DAPI: 1,4-diamino-2-fenilindol

DTT: dithiothreitol

FBS: fetal bovine serum

GCL: ganglionar cell layer

INL: inner nuclear layer

IPL: inner plexiform layer

LDCD: lysosome-dependent cell death

LMP: lysosomal membrane permeabilization

LLOMe : Leu-Leu-OMe

LSD : lysosomal storage disorder

LTR: LysoTracker Red

MMP : mitochondrial membrane permeabilization

MPP+: neurotoxin 1-methyl-4-phenylpyridinium

MTDR: MitoTracker Deep Red

NGS: normal goat serum

ONL: outer nuclear layer

OPL: outer plexiform layer

PAS: pre-autophagosome structure

PBS: phosphate buffer saline

PE: phosphatidylethanolamine

PFA: paraformaldehyde

ROS: Reactive Oxidative Species

SDS: Sodium Dodecyl Sulfate

TSA: trichostatin A

INTRODUCTION

1. INTRODUCTION

1.1 AUTOPHAGY

Autophagy is a term formed by two Greek words: “auto” means “self”; “phagy” means “eating”. In that way, “autophagy” or “self-eating” is the mechanism that cells use to degrade and recycle intracellular components including proteins and even whole organelles by delivering and degrading them inside lysosomes. (Boya et al., 2013). Three types of autophagy have been described, depending on the way the intracellular material is delivered to lysosomes: macroautophagy, chaperone-mediated autophagy or microautophagy (Figure 1.1).

Macroautophagy is the best well known type of autophagy. During the macroautophagy, the formation of the double-membrane vesicles is mandatory. This structure is called autophagosome and it is in charge of sequestering components to be degraded. Finally, autophagosome fusses with lysosome. Several proteins are implicated in this mechanism. This thesis will go in deep later into this type of autophagy.

Chaperone-mediated autophagy (CMA) is a selective type of autophagy where the proteins with KFERQ-like pentatide motif are recognized by the chaperone Hsc70 and delivered to the lysosomes (Cuervo and Dice 1996). The translocation of the proteins to the lysosomal lumen needs channels generated by the lysosomal-associated membrane protein type 2A (Lamp2A) and the presence of the chaperone heat shock chaperone 70 (Hsc70) (Salvador et al., 2000). Interestingly, this type of autophagy only occurs in mammalian cells.

In mammals, **microautophagy** is the less characterized type of autophagy. This system, only present in yeast, implies the invagination of the lysosomal membrane to imbibe the compounds to degrade (Sahu et al., 2011). There are two types of microautophagy: non-selective, which degrade portions of cytosol randomly; or selective, degrading specific organelles: micromitophagy (mitochondrias), micronucleophagy (nucleus), or micropexophagy (peroxisomes) (Mijaljica et al., 2011).

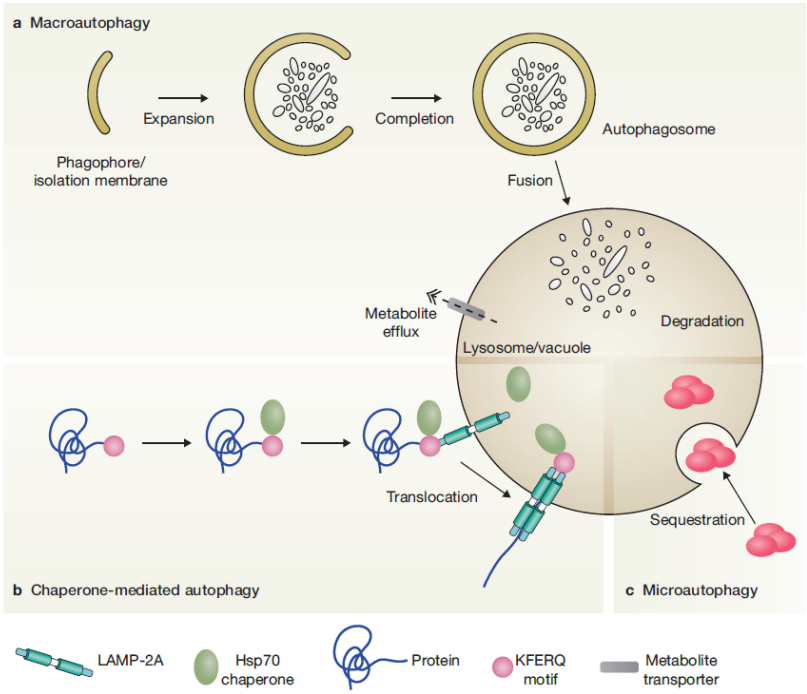

Figure 1.1. Types of autophagy. (A) Macroautophagy, characterized by the formation of autophagosomes. **(B)** Chaperone-mediated autophagy (CMA), the proteins with the KFERQ motif are recognized and carried to the lysosome. **(C)** Microautophagy, direct invagination of the lysosomes of the compounds to degrade. Figure taken from Boya et al., 2013.

Autophagy can be non-selective, when autophagy degrades bulk cytoplasm to recycle compounds and get energy to survive to unfavorable situations, such as starvation; or highly selective, when autophagy targets specifically intracellular components such as organelles and intracellular bacteria. This type of autophagy has promoted a new understanding of this process due to the new roles that it can present. For example, controlled mitophagy (mitochondrial-specific autophagy) promotes a metabolic switch during retinal development (Esteban-Martinez et al., 2017). Selective autophagy is described further (apart 1.1.1.2).

1.1.1 Macroautophagy

Hereinafter, this book will refer to macroautophagy simply as autophagy. Christian de Duve discovered autophagy due to his observations in rat liver where he studied cellular enzymes, identifying a novel intracellular granule that he called “lysosome” (De Duve et al., 1955). Subsequent experiments performed later by Prof. Yoshinori Ohsumi of defective mutants in the yeast *Saccharomyces cerevisiae* promoted the discovery of the

proteins implicated in this degradation process (Tsukada and Ohsumi, 1993). For these discoveries, Yoshinori Ohsumi was awarded with the Nobel Prize in the year 2016. Ohsumi thought that, if autophagy was happening in yeast, inhibition of vacuolar enzymes would result in the accumulation of cytoplasmic vacuoles. He created random mutants of the vacuolar proteases to identify the phenotype of vacuolar accumulation, discovering the proteins implicated in autophagy in yeast (Takeshige et al., 1992; Tsukada and Ohsumi, 1993). The proteins that he found have been conserved through the eukaryotic evolution (Feng et al., 2013), pointing out the importance of this process. However, several genes appear in mammals and not in yeast, indicating the increase in the complexity of the system and the addition of new functions. In addition, proteomic analysis demonstrated the complexity of the interaction between the proteins implicated in autophagy (Behrends et al., 2010). Nowadays, 40 autophagy-related genes are known in yeast (Liu et al., 2017), considering genes implicated in the regulation and machinery of autophagy, as well as genes implicated in the selective autophagy, such as receptors. Nevertheless, the autophagy-related proteins are implicated in other mechanisms in the cellular homeostasis (as this book will explain in the apart 1.1.1.3).

Autophagy is characterized by the formation of autophagosomes. These autophagosomes are transient organelles, with a half-life of 10 minutes before fussing with the lysosome. Due to the dynamism of this process, the exploration of autophagy has been an arduous challenge to researchers. The inhibition of the lysosomal activity and discovery of a specific marker of the autophagosome (Kabeya et al., 2000), together with the ability to perform ATG-specific mutants has busted research in this field (Ohsumi, 2014).

1.1.1.1 Macroautophagy phases

Autophagy process is divided in several phases: autophagy induction, nucleation and elongation of the autophagosomal membrane; fusion with lysosome and recycling of the compounds obtained after the degradation (**figure 1.2**).

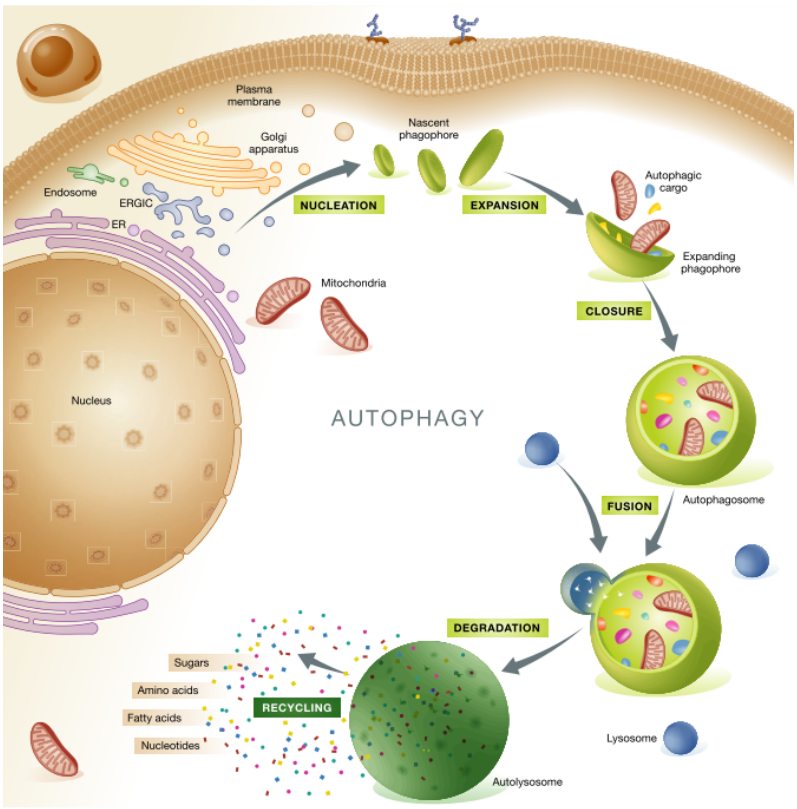

Figure 1.2. Macroautophagy phases. Induction and nucleation of the autophagosome are the first steps of macroautophagy. Then, autophagosome expansion and closure need to happen to degrade the obsolete material. The last step is the fusion of autophagosome with lysosome to degrade the compounds to recycle, such as sugars, amino acids, fatty acids or nucleotides. Figure taken from Galluzi et al., 2015.

Before the **induction of autophagy**, several kinases such as TOR (mTOR in mammals) or AMP-activated protein kinase (AMPK) are in charge of regulating this process. TOR is able to inhibit to the initiation complex, formed by Atg1-Atg13-Atg17 in yeast. Atg13 is hyperphosphorylated under nutrients-presence conditions by TOR complex. But, Atg13 is dephosphorylated when autophagy is induced (Scott et al., 2000). In mammals, the complex ULK1/2, homolog of Atg1, interacts with Atg13. ULK1 can be activated by (AMPK)-dependent process (glucose starvation) or AMPK-independent process (amino acid starvation). When this happens, mTOR1 complex phosphorylates ULK1/2 and Atg13, avoiding the interaction between ULK1 and AMPK. But, in starvation, mTOR is released from this complex, leading to the activation of ULK1/2. Ambra1 and Beclin1 are also phosphorylated by ULK1. These interactions promote the localization of these proteins to the autophagosome formation (Kim et al., 2011).

During autophagosome **nucleation** in yeast, Atg9 is a transmembrane protein that is present in sites in membranes where the double membrane begins its formation. This double membrane is called phagophore is going to appear. The mammalian homolog

Atg9A localizes in the trans-Golgi network in nutrient-rich conditions. Atg9 has more homologs, for example Atg9B, which is present in placenta (Yamada et al., 2005). Atg9 and Atg16L appear in separate populations and subsequently they fuse during the autophagosome formation.

Mammalian cells have two kind of phosphoinositide 3-kinase that are involved in autophagy regulation: class I and class III. These proteins are homologous of Vps34. These components are part of three complexes: firstly, Ambra1 and Beclin1 regulate Atg14 complexes; secondly, the UVRAG complex has a protein called UVRAG, which participes in endocytosis and autophagy; thirdly, the KIAA0226/Rubicon complex, which regulates negatively autophagy (Feng et al., 2014).

The **formation and elongation** of the autophagosome is regulated by Atg9. Additionally, two highly complexes are involved in this step. These multiprotein complexes are called conjugation systems. Both complexes are ubiquitin-like conjugation systems, and are formed by Atg5-Atg12 and Atg8/LC3/GABARAP-phosphatidylethanolamine (PE) (Mizushima et al., 2003). Atg7 directly activates and transfers Atg12 to Atg5. Atg5 present two UBL domains, but when the Atg5-Atg12 conjugated is formed, three UBL domains are activated. These three UBL domains recruit the factors needed for the elongation of the autophagosome. Additionally, Atg16L1 is implicated in this complex, ensuring the association between the complex and the pre-autophagosome structure (PAS). The aim of this complex is to give E3-like activity to Atg8 (LC3 in mammals), to induce the connection with PE (Kabeya et al., 2000).

Atg8 is synthetized as a cytosolic protein, and it is processed by Atg4. After that, Atg8 is activated by Atg7 and transferred to Atg3 to be linked to the PE. In humans, there are six homologs of Atg8: LC3A, LC3B, LC3C, GABARAP, GABARAPL1 and GABARAPL2. The LC3s are encoded by four genes: MAP1LC3A, MP1LC3B, MAP1LC3B2 and MAP1LC3C (Wild et al., 2014). The LC3B is the most studied Atg8 protein to date. This protein is attached to the autophagosomal membrane during their formation and maturation. While LC3B is in the cytosol, it is called LC3-I, nevertheless, as soon as LC3B is lipidated and attached to the membrane, it is called LC3-II.

The final step in autophagy is the autophagosome **fusion** with lysosomes. Previous results demonstrated that the SNARE protein family has a major role in the fusion of the membranes (Wang et al., 2016). Interestingly, Atg8 could be implicate in the fission of the autophagosomal and lysosomal membrane by tethering (Nguyen et al., 2016). The lumen of the autophagosome is degraded by lysosomal enzymes. The resultant molecules are transported from the lysosome to the cytosol through permeases for the last step of **recycling**. This step is crucial to transform autophagy, not only in a cleaning mechanism, but providing novel pathways to get energy.

Importantly, LC3B is attached to the autophagosomal membrane, and the lysosomal proteases degrade LC3-II. The part attached to the external membrane come back to the cytosol, after Atg4 break the connection with PE (Tanida et al., 2004). LC3B is the unique marker for autophagosomes to date. In fact, the relative quantity of LC3-II sights the autophagosomal amount. (Mizushima, 2004). But, due to the dynamism of the autophagosomes, autophagic flux is necessary to be determined (Mizushima and Yoshimori, 2007).

1.1.1.2 Selective autophagy

The selective autophagy of organelles is crucial to maintain cellular homeostasis (Anding et Baehrecke, 2017). The selective autophagy implies the specific recognition of the cargo to be degraded by specific receptors. All of them present an initial signaling that induces events, molecules that tag the cargo to be degraded and the elimination of the cargo through autophagy. The organelles described to have specific degradation are mitochondrias, peroxisomes, lysosomes, endoplasmic reticulum, nucleus, protein aggregates, proteasomes, lipid droplets and polyribosomes (Reggiori et al., 2012). In addition intracellular bacteria are also degraded via selective autophagy.

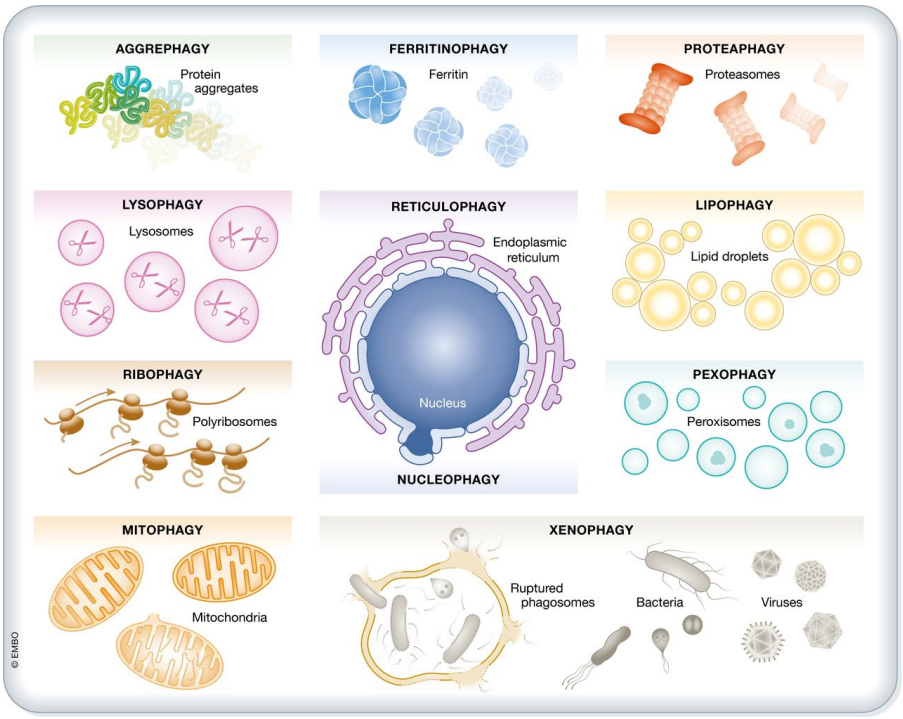

Figure 1.3. Selective autophagy. *Autophagy can degrade specifically cellular compounds to determine cellular development or to clean specific material from the cytosol. From Galluzi et al., 2017.*

Mitophagy, or the specific degradation of mitochondria was firstly observed by de Duve (De Duve and Wattiaux, 1966), and then described in 2005 (Lemasters, 2005). Mitochondria can be depolarized by several stimuli, such as hypoxia, chemical uncouplers of oxidative phosphorilation or ROS. It has been demonstrated that this process is quite important for several circumstances, such as during development to change the metabolic profile (Esteban-Martinez et al., 2017). There are several proteins implicated in mitophagy, but the best-known mitophagy-related proteins are Pink1 and Parkin. These proteins act as receptors during mitophagy and are linked to Parkinson disease (Lazarou et al., 2015; Eiyama et al., 2015). When mitochondrial membrane potential is compromised, ubiquitinated Pink1 accumulates in the mitochondrial surface and Parkin amplifies the signal of Pink1. This high-ubiquitnated signal can be recognized by autophagy receptors and take the mitochondria to autophagosomes (Lazarou et al., 2015). Further experiments are demonstrating that these are not the only receptors for mitophagy. For example, Mitofusin-1 and Mitofusin-2 are proteins implicated in the fusion and fission of mitochondrial, but Mitofusin-2 serves as a receptor for Parkin translocation to damaged mitochondria (Gegg et al., 2010).

Lysophagy is the specific degradation of lysosomes, recently defined by Hung and colleagues (Hung et al, 2013). Lysosomes are the stomach of the cells, and some damage in the lysosomes can promote cellular distability, leading to cell death (Hasewaga et al., 2013). Lysophagy can be induced by several stimuli, such as silica crystals or photodamage (Hung et al., 2013). Lysophagy still presents several questions to be solved, but the methods to monitor this mechanism are being defined. For example, light damage allows studying the exact place of the damaged lysosomes, giving the opportunity to study lysophagy (Chu et al., 2017; Otomo et Yoshimori, 2017). Additionally, it has been demonstrated that, after lysosomal damage, LC3 and galectin-3 are recruited to the lysosome. Interestingly, galectin-3 colocalizes in damage membrane with p62 in mouse embryonic fibroblasts (Chauhan et al., 2016). Moreover, ubiquitination of damage lysosomes is involved in damage recognition and recruitment of autophagic machinery (Yoshida et al., 2017). Nevertheless, lysophagy still has many questions to be solved, for example, which are the mechanisms able to induce the ubiquitination of damaged lysosomes, or what is the signal received by galectin-3 to bind to damaged membranes.

Pexophagy, is the specific degradation of peroxisomes, small organelles implicated in the catabolism of fatty acids and the reduction of ROS. Due to the role of removing oxidative stress, peroxisomes are essential for the cellular homeostasis. In some situations, peroxisome-specific degradation is activated, for example after the treatment with hypolipidemic drugs (Till et al., 2012) or in amino acid starvation (Sargent et al., 2016).

Additionally, **ER-phagy** or **reticulophagy** is the specific degradation of endoplasmic reticulum (Bernales et al., 2006). ER-phagy is activated after the unfolded protein response (UPR) and ER-associated degradation (ERAD) (Wang and Kaufman, 2016).

Nucleophagy; because nucleus contains genetic material of the cells, degradation could be detrimental for the cells; but nucleophagy involves only a partial fragment of nuclear components. This includes portions of the nuclear envelope with pre-ribosomes, but excludes chromosomal DNA or nuclear pore complexes (Farré et al., 2009).

All of these mechanisms lead to show how delicate autophagy is. Slight control of autophagy lead to the cell not only to obtain energy through bulk-degradation, but specific organelles degradation to get different objectives: survival, metabolism profile change or

overpass stress damage. To discover the molecular mechanisms will be relevant for future researches.

1.1.1.3 Autophagy-independent functions of Atg proteins

Autophagy proteins present roles in other processes in the cell. The novel autophagy-independent roles are being studied. The research about this is complicated due to the different role of autophagy in the tissues. **Beclin1**, as defined previously, participates in the induction of autophagy. Beclin1 is present in the Vps34 complex I and II. In 2011, by using an autophagy inhibitor called spautin-1, Liu and colleagues demonstrated that Beclin1 expression regulates the levels of p53 by increasing the ubiquitination (Liu et al., 2011). P53 is called the "guardian of the genome" due to his role to prevent tumor and take care of the genome stability. P53 is mutated in 50% of human tumors (Vousden and Prives, 2009). If Beclin1 is able to control the levels of p53, this indicates that Beclin1 has an important role in oncogenic control. However, p53 is also able to control autophagy (Tasdemir et al., 2008).

Other example is **FIP200** (FAK family-interacting protein of 200 kDa); FIP200 is a protein equivalent of the yeast gene Atg17. FIP200 is participating in the complex ULK1/Atg13/Atg101 for autophagy induction (Hara et al., 2008). In 2016, FIP200 knock-in mutant allele was generated, leading to the study of FIP200 role in embryogenesis, cell survival and tumor growth (Chen et al., 2016). They used a mutant of FIP200 called FIP200-4A. FIP200-4A presented a mutation in the region where the protein interacts with Atg13. The protein FIP200-4A blocked autophagy in mouse embryonic fibroblasts, but, although FIP200 knock-out mice were lethal during embryogenesis, FIP200-4A leaded the complete embryogenesis in mouse, suggesting that FIP200 presented an autophagy-independent role and related to embryogenesis. Additionally, FIP200-/- phenotype during development is very similar to other Atg deficient knock-out mouse models.

Other examples are the ubiquitin-like **Atg8 family of proteins**. Atg8 is the yeast protein and it presents 6 orthologues in humans, as commented previously. Interestingly, these proteins interact with 67 other proteins, including GTPases (Wang et al., 2012). The GTPases are proteins with multiple roles in the cell, such as cycle progression, gene expression, migration or signaling. For example, non-lipidated LC3 is a regulator for viral

replication; Coronaviruses and mouse hepatitis virus are RNA viruses that induce accumulation of endoplasmic chaperones in double membrane vacuole coated by non-lipidated LC3: the down-regulation of LC3 –but not of autophagy- inhibited coronavirus infection.

Additionally, other non-ubiquitin-like Atg proteins present autophagy-independent roles. For example, **Atg16L** present a crucial role for hormone secretion of PC12 cells. Knock-down of Atg16L causes a reduction in the secretion, independently of autophagic activity (Ishibashi et al., 2012).

Other examples are the proteins **Atg5** and **Atg7**. During the attachment to the bone, osteoclasts become polarized. For this mission, lysosomal enzymes such as cathepsin K need to be secreted to the *resorptive space*. Atg5 and Atg7 are needed for the localization of secretory lysosomes during the polarization of the osteoclasts (DeSelm et al., 2011). Additionally, Atg7 has been implicated in more roles; for example, a recent study demonstrated that autophagy and cell cycle arrest are synchronized during starvation. In starved MEFs, Atg7 is essential for the interaction with p53 and for the transcriptional activation of the cell cycle inhibitor p21CDKN1A. These results indicate that Atg7 is also implicated in cell cycle arrest (Lee et al., 2012). Furthermore, Atg5 and Atg7 are implicated in adipogenesis in mice. Adipose tissue is smaller than compared to the wild-type in animals knock-out for these proteins. It is evident that Atg5 and Atg7 present a role autophagy-independent due to the inhibition of autophagy leads to an accumulation of the lipid droplets (Baerga et al., 2009; Zhang et al., 2009).

In addition, in germ-specific knock-out for Atg7 mice, it was observed that the animals were sterile. Acrosome is a lysosome-related organelle that plays an important role during fertilization in the sperm nucleus. The authors observed that germ-specific Atg7 knock-out presented a deficiency during the formation of the acrosome, leading to the infertility. Interestingly, Atg7 regulates another protein called Golgi-associated PEDZ and coiled-coil motif-containing protein (GOPC), proteins implicated in acrosome formation. This publication suggests that Atg7 is regulating, through other proteins, the acrosome formation (Wang et al., 2014).

It is important to understand that autophagy is implicated at several levels in the cellular processes, but further non-autophagy roles of the Atg machinery are being unraveled. Moreover, the knock-out mice of the Atg proteins demonstrate different phenotypes, from embryogenesis to tumors in adulthood. Definitely, autophagy, cell death and cell proliferation are processes quite related, with similar molecular mechanisms.

1.1.2 Autophagy and neurodegeneration

Intracellular aggregates are common in neurodegenerative diseases. Mutations in proteins contribute to diseases, such as α-synuclein in **Parkinson's disease**; expanded polyglutamine zones in Huntingtin in Huntington's Disease. The importance of autophagy has been previously described. For example, knock-out mice for Atg7 and Atg5 present neurodegenerative phenotype, suggesting the importance of autophagy-related proteins in pathologies (Hara et al., 2006). Autophagy is a regulator of the levels of protein aggregates, such as polyglutamine huntingtin in Huntington's Disease (Ravicumar et al., 2002); mutant α-synuclein in Parkinson's Disease (Webb et al., 2003); mutant TDP-43 in ALS 7 and tau proteins in some dementias (Berger et al., 2008). In addition, Parkinson's disease presents deficiency in Pink1 and Parkin genes, suggesting the meaning of mitophagy in this illness. Additionally, to their role in mitophagy, Parkin1 has been described to be involved in the degradation of α-synuclein (Lonskaya et al., 2013).

Alzheimer Disease is characterized by the accumulation of amyloid-β plaques. Interestingly, accumulation of autophagosomes was observed in affected neurons (Nixon et al., 2005). Some experiments have demonstrated problems in lysosomal function due to the mutations in the presinilin family. These mutations result in autophasosome accumulation. Further, deletion of cystatin B (an inhibitor of lysosomal proteases) in an Alzheimer Disease mouse model improved mouse cognitive performance (Yang et al., 2011). Moreover, Beclin1 presents reduced levels of mRNA in Alzheimer Disease brain, suggesting the importance of autophagy in this disease (Pickford et al., 2008).

In **Huntington Disease,** it has been described autophagosomes accumulation in biopsies of patients. Additionally, several autophagy markers such as p62 or LC3 appear increased. Interestingly, autophagosomes were not degraded. Interestingly, targeting autophagy induction could be a new therapy for the treatment of this disease. For example, the

rapamycin analog CCI-779 induced autophagy-dependent degradation of the accumulated huntingtin aggregates and improved motor phenotype in transgenic mice (Ravicumar et al., 2002). Moreover, trehalose, a disaccharide that induces autophagy, also improved motor function and extended lifespan in transgenic mice (Tanaka et al., 2004)

These publications demonstrate that autophagy could be a therapeutic target to induce during neurodegenerative diseases which present aggregates accumulation as origin of the disease. Additionally, it is important to look for therapies that avoid the phenotype of the disease from the origin and prevent the accumulation of the proteins. This thesis is focused in retinal neurodegeneration diseases, but these groups of diseases will be explained later in the introduction.

1.1.3. Autophagy in cancer

The role of autophagy in normal cells presents high complexity and it is tissue-dependent. For example, autophagy is essential in brain, muscle and liver due to the necessary removal of damaged organelle. Otherwise, autophagy presents a intricate role in cancer, as a tumor suppressor or tumor-helper. Autophagy can be a tumor suppressor, for example the gene Beclin1 is monoallelic in 40-75% of human breast, prostate and ovarian cancer (Aita et al., 1999; Liang et al., 1999). Additionally, deficiency in Atg5 or Atg7 can induce liver tumors in mice (Takamura et al., 2011). These results indicate that autophagy acts as a tumor suppressor.

On the other hand, autophagy can be a tumor promoter. Autophagy is increased in hypoxic tumor regions (essential for tumor cell survival) (Degenhardt et al., 2006), and it is also increased in RAS-transformed cells (Guo et al., 2011). The genetic context that promotes autophagy as a tumor promoter is poorly understood. Autophagy helps in the growth and progression of tumors due to the ability of reducing the environmental stimuli. Several advanced tumors exhibit an increase autophagic flux (Mikhaylova et al., 2012). These experiments support the idea that autophagy is helping during tumorigenesis and tumor development.

It will be necessary to understand which are the circumstances that promote that autophagy induces tumor cell death, or tumor development. Genetic context, type of tumor, or

deficiency of autophagy-related proteins could affect to the unbalance of the different roles of autophagy.

1.2 LYSOSOMES

Lysosomes are acidic organelles discovered by Christian de Duve in 1950´s (De Duve and Wattiaux, 1966). Lysosomes are membrane-bound organelles with acidic lumen. Lysosomes are ubiquitous and they present more than 60 hydrolytic enzymes and other transmembrane proteins implicated in the maintenance of the acidic gradient, as ATPases that pump protons to the lysosomal lumen and other proteins in charge of the molecular export through the lysosomal membrane.

Lysosomes are implicated in multiple mechanisms: degradation of external compounds through phagocytosis; degradation of internal compounds through endocytosis or autophagy – and this include the three types of autophagy: macroautophagy, chaperone-mediated autophagy and microautophagy. The molecules obtained are transported to the cytosol via transport channels or release to the extracellular space via exocytosis. Additionally, lysosomes have an important role as calcium storages (Churchill et al., 2002).

Lysosomal biogenesis is regulated by the transcription factor EB (TFEB) due to his ability to promote expression of most of the lysosomal proteins. This transcription factor binds to the coordinated lysosomal expression and regulation (CLEAR) promoter (Sardiello et al., 2009). Additionally, to the biosynthetic pathway, endocytic pathway is implicated in lysosomal biogenesis: early endosomes are completed with hydrolases until the complete maturation. It is important to understand how lysosomal biogenesis works due to the possible therapeutic functions it can present; for example, it has been demonstrated that an increase in the lysosomal amount can improve several protein aggregate-related diseases, such as Parkinson or Alzheimer (Napolitano and Ballabio, 2016). Until now, it has been described that TFEB is regulated by mTOR complex 1. In normal situations, mTOR phosphorylates TFEB and recruits it in the cytoplasm. As commented previously, mTOR is inactivated during starvation, leading to TFEB to be dephosphorylated and translating to the nucleus, where promotes the transcription of the CLEAR gene network (Settembre et

al., 2013). Recent studies have demonstrated that TFEB can be activated independently of mTOR. The serine/threonine kinase Akt (protein kinase B) controls TFEB activity after trehalose treatment, an mTOR-independent autophagy inducer. Akt phosphorylated TFEB at Ser647 and represses TFEB nuclear translocation. Trehalose administration reduces the phenotype in a mouse model of neurodegenerative disease that shows intralysosomal accumulation (Palmieri et al., 2017). Although lysosomes biogenesis is poorly understood, other protein implicated in this mechanism has been recently found. In *Drosophila* model of eye degeneration of tauopathy or amyotrophic lateral sclerosis diseases, Mask, an Ankyrin-repeat and KH-domain containing protein, is able to boost the ATPase activity in a TFEB-independent manner (Zhu et al., 2017). Futher studies are needed to understand the mechanisms of lysosomal biogenesis.

As expected, lysosomal **hydrolytic enzymes** are essential to preserve lysosomal function. Lysosomal hydrolases digest macromolecules in an acidic environment (lysosomal lumen pH is about 4,5-5), but some of them are also active at higher pH, such as cathepsin B, D, L. This is the reason why lysosomal leakage is a scene that can induce cell death, as when enzymes leak to the cytosol; they are able to degrade cytoplasmic proteins. This process of leakage is called lysosomal membrane permeabilization (LMP), a multi-pathway process that in most of the cases induce cell death.

1.2.1 Lysosomal membrane permeabilization

Lysosomal membrane permeabiliation (LMP) is a perturbation of the lysosomal membrane that induces the release of the lysosomal enzymes to the cytosol. Interestingly, lysosomes do not change their morphology during LMP (Brunk and Ericsson, 1972). This fact has resulted in reduced interest in this mechanism until new methods to assess LMP have been developed. In addition, LMP has been recently studied due to the fact that cathepsins are able to trigger cell death through conserved executors of cell death, such as caspases.

Lysosomes can be damaged under many different scenarios (**figure 1.4**). For example, lysosomes can be damaged by free radicals. Oxidative stress induces damage in the lipids of the lysosomal membrane or impairment in the lysosomal enzymes. Moreover, an increase in H_2O_2 levels reacts with the redox-active iron in Fenton-type reactions, inducing the production of the highly reactive hydroxyl radicals (Kurz et al., 2008a). This process can be blocked by using desferoxamine acting as an iron chelator (Krenn et al., 2015). Additionally, antioxidants have been demonstrated to protect against oxidative stress induced LMP (Kurz et al., 2008b).

Lysosomotropic agents form a group of weak bases compounds that accumulate inside lysosomes due to their detergent-like properties. These compounds are able to damage lyosomal membranes. Some examples of lysosomotropic agents are ciprofloxacin (Boya et al., 2003), sphingosine (Kågedal et al., 2001) or siramesine (Ostenfeld et al., 2008). Some of these lysosomotropic agents have been proposed as anticancer treatment, such as siramesine (Ostenfeld et al., 2005). The lysosomotropic agents are usually trapped in lysosomes, such as silica crystals or nanoparticles, used as LMP inductors. Additionally, some detergents, such as Leu-Leu-OMe (LLOMe), act as lysosomotropic agents. LLOMe has been proposed as an apoptotic inducer compound but his activity depends on the levels of cathepsin C to promote lysosomal damage (Thiele and Lipsky, 1985). Recently, new data support that sub-apoptotic concentration of LLOMe induces LMP in the lysosomes in Hela cell line due to the loss of proton gradient and release to the cytosol of lysosomal markers, but there was no evidence of release of cathepsin B and L into the cyotosol (Repnik et al., 2017). The authors proposed that LLOMe do not induce cathepsin release but induce lysosomal-dependent cell death through proteolysis signaling.

As mentioned above, released cathepsins can trigger the degradation of cytoplasmic proteins. Additionally, some cytoplasmic proteins are able to induce LMP. For example, the group of Torriglia demonstrated that calpain1 causes LMP by cleavage of Lamp2 in rat brains. Lamp2 degradation was rescued by using calpain inhibition or MEFs Lamp2 -/-. These data suggested that calcium-activated calpain1 was inducing Lamp2 cleavage (Villalpando-Rodriguez and Torriglia, 2013).

Another important fact for lysosomal stability is the membrane lipidic profile. Researchers have used a model system of Parkinson's disease called BE (2)-M17 neuroblastoma cells

treated with the neurotoxin 1-methyl-4-phenylpyridinium (MPP+). They observed that MPP^+ induced cholesterol accumulation in pre-apoptotic cells. When they treated the cells with U18666A, an intracellular cholesterol transport inhibitor, they observed a reduction in lysosomal damage and cell death. This suggests that increased lysosomal cholesterol is inducing a release of the lysosomal content to the cytosol (Eriksson et al., 2017). Additionally, our group observed that Parkinson's Disease displayed LMP in neuronal cells. Interestingly, enhacement of lysosomal biogenesis improved the phenotype in the cells (Dehay et al., 2010).

Additionally, several proteins are able to stabilize lysosomal membranes. For example, it has been demonstrated that Hsp70 interacts with BMP and induces a decrease in the acid sphingomyelinase (ASM) (Perdersen et al., 2010). Hsp70 deletion induces LMP and cathepsin release, leading to cell death (Nylandsted et al., 2014). This enzyme is in charge of transforming ceramide to sphingomyelin. This data is quite important because it has been demonstrated that an increase in sphingomyelin species implies lysosomal destability (Petersen et al., 2013).

LMP has not only been observed in vitro but also *in vivo*, during physiological conditions. For example, during the regression of the mammary gland after lactation, LMP-mediated cell death is activated. During the involution, lysosomes of the mammary gland undergo LMP through Stat3, which upregulates caspases 3, 6 and 7 (Kreuzaler et al., 2011). In addition, other authors studied the role of calpains during the mammary gland involution. They demonstrated that calpains are able to proteolyze subunit b_2 of the v-type H^+ ATPase and Lamp2, demonstrating that the calpain-induce cleavage in Lamp2 is a process that can happen in mammary gland tissue (Arnandis et al., 2012).

Neutrophile cell death presents LMP during infection and inflammation after *Escherichia coli* infection (Loison et al., 2014). In this case, neutrophils present the release of the serine protease PR3, leading to cleaved caspase 3 and cell death. The use of DFO rescues from the neutrophil cell death. Additionally, in macrophages infected by *Legionella pneumophila*, a bacterial protein called RpsL induces LMP in the macrophage to induce a productive infection (Zhu et al., 2015). Interestingly, when macrophages are infected by pneumococci, they induce suicide through cathepsin D release (Bewley et al., 2011). These

results demonstrate the importance of the LMP due to the ability of be a homeostatic response that occurs *in vivo*.

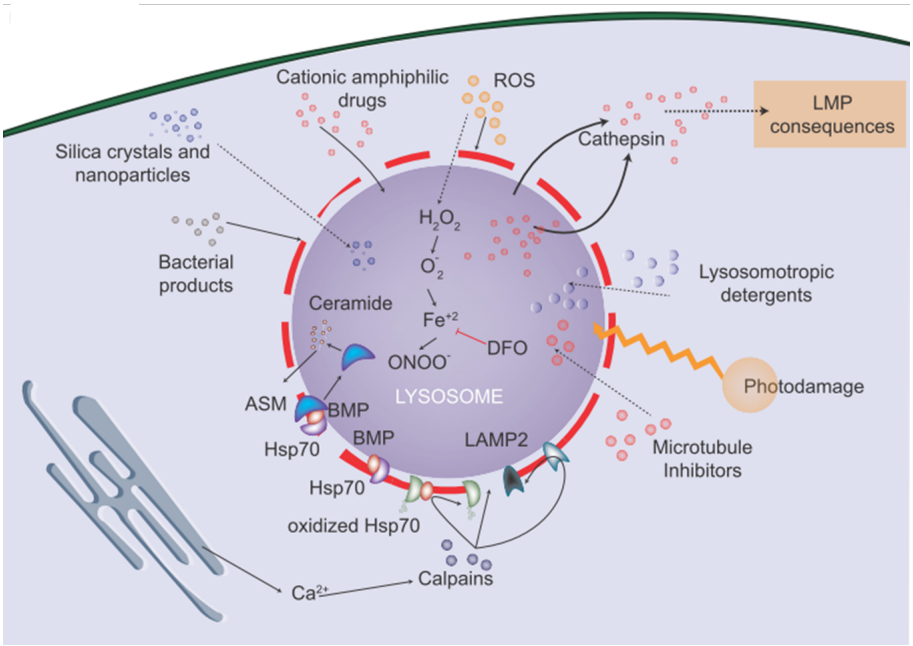

Figure 1.4. Inducers of lysosomal membrane permeabilization. *Reactive oxygen species can pass through the lysosomal membrane; free iron can induce the Fenton reaction; lysosomotropic detergents and some antibiotics can destabilize lysosomal membrane. All of these circumstances induce LMP. Additionally, photodamage or activated calpains target several lysosomal proteins, such as Lamp2 and Hsp70. From Serrano-Puebla and Boya, 2015.*

LMP induces a cell death defined by the Nomenclature Committee on Cell Death as **lysosome-depedent cell death (LDCD)** (Galluzi et al., 2018). This type of cell death will be commented in the appart 1.3.3. Understanding deeply the mechanisms that promote LMP is indispensable to avoid lysosome-dependent cell death or induce these mechanisms to trigger cancer cell death.

1.2.2 Lysosomes and neurodegeneration

LMP has been observed in several models of neurodegenerative diseases. First, this condition was observed in models of stroke. In 1996, Yamashima and colleagues described the first evidence of a pathway that implicates a calcium-calpain dependent lysosomal damage (Yamashima et al., 1996). They demonstrated that the mechanism of postischaemic hippocampus neuronal death, there is an increase in the intracellular calcium levels, leading to calpain activation that induced lysosomal destabilization. Later, in 2012, it was demonstrated that the molecular target of calpain in this model is the protein Hsp70,

leading to cell death associated to a necrosis-like phenotype (Zhu et al., 2012). Interestingly, the motor cortex is protected against ischemia neuronal cell death, suggesting that this kind of cell death is cellular dependent (Zhu et al., 2012).

Other example of LMP-related neurodegenerative models are some models of Parkinson's disease treated with the parkisnsonin toxin MPP+. Interestingly, rapamycin was able to attenuate the neuronal death phenotype in the mouse model (Dehay et al., 2010). Another publication demonstrated that mutations in presinilin-1 (PS1) found in Alzheimer Disease causes lysosomal disturbance through cleaving v-ATPases (Lee et al., 2010). Interestingly, this phenotype is ameliorated by increasing lysosomal biogenesis. Moreover, cultured neural stem cells presented lysosomal damage after using chloroquine (HCQ) or bafilomycine A1 (BafA1) treatment. Fascinatingly, in this Alzheimer Disease model, Atg7 downregulation ameliorate this phenotype (Walls et al., 2010).

In the retina, it has been demonstrated that lysosomal stability is crucial for retinal homeostasis. For example, in retinal detachment in rats, calpains are activated triggering photoreceptor cell death (Chinskey et al., 2014). They did not study lysosomal stability, but it will be interesting to unravel how calpain activation leads to LMP under these conditions. In addition, retinal degeneration has also been described in the mouse model knock-out for acid sphingomyelinase (ASM). ASM knock-out is a mouse model which presents a deficiency in the acid sphingomyelinase activity. This model is used as a Niemann Pick type A mouse model. This mouse model presents an attenuated response in ERG, thin retinal layer and lipofuscin accumulation (Wu et al., 2015). Interestingly LMP and cathepsin release is also observed in Niemann Pick type A, a lysosomal storage disorder (LSD) with mutations in the ASM gene (Gabandé-Rodriguez et al., 2014).

LSD's are a heterogeneous group of inherited diseases characterized with the lack of one lysosomal enzyme. This defect promotes the accumulation their substrate in the lysosomal lumen, such as glycoproteins, lipids, glycoaminoglycans. All the LSD's share similar clinical characteristics and some of them include retinal neurodegeneration. For example, the accumulation of sphingolipids in the cell promotes macular degeneration (Chen et al., 2014). For example, Niemann Pick type C present impaired retinal function by ERG (Claudipierre et al., 2011). Finally, the Hexb-/- and b-Gal -/- mouse model, monetizing

Sandhoff disease show accumulation of storage material in retinal ganglion cells (Denny et al., 2007).

In conclusion, these evidences demonstrate that lysosomal function is essential for neuronal cells. Understanding the mechanisms will be crucial to find potential targets for new therapeutic strategies for these diseases.

1.2.3 Lysosomes and cancer

As lysosomes present all these degradative enzymes inside they can be exploited to kill cells. This advantage can be used to fight against cancer and LMP can represent be a new therapeutic approach in apoptosis-resistant tumors. Some compounds, like cationic amphiphilic drugs (CADs) are being started to be used to kill cancer cells.

CADs include hundreds of pharmacologic agents used to treat a broad spectrum of common diseases, e.g. psychiatric disorders, allergies, heart diseases and infections (Kornhuber et al., 2010). They are characterized by a hydrophobic ring structure and a hydrophilic side chain with a cationic amine group. In acidic milieu, the basic amine groups are protonated allowing an up to 1000-fold drug accumulation inside acidic lysosomes (Trapp et al., 2008). The incorporation of CADs into membranes in the lysosomal lumen neutralizes the negative membrane charge thereby inhibiting the function of several lysosomal lipases, including ASM. The inhibition of ASM promotes the accumulation of sphingomyelin (Kolzer et al., 2004). Cancer cells are especially sensitive to the accumulation of sphingomyelin (Barcelo-Coblijn et al., 2011, Teres et al., 2012, Petersen et al., 2013), which may explain why CAD's, that are effective acid sphingomyelinase inhibitors, display selective cytotoxicity towards transformed cells (Petersen et al., 2013, Sukhai et al., 2013, Jahchan et al., 2013, Shchors et al., 2015).

Other compounds, such as silica crystals or nanoparticles, have been used as new therapies against cancer through cathepsin release and lysosome-dependent cell death (Gutierrez et al., 2016; Domenech et al., 2013). New windows of therapy have been launched after these experiments, leading to the cancer fight another option by using the powerful proteolytic bombs inside the cells: the lysosomes.

1.3 CELL DEATH

Cell death is a natural process that occurs under physiological conditions and is necessary to change cellular profiles in tissues, to balance the mitotic process in physical limited tissues, such as the intestine, and to renovate tissues to improve their function. Cell death is defined as the point of no-return, when the cell is no longer been functional (Galluzi et al., 2012). It could be presented in the nature as a suicide form, or as the mechanisms of killing other cells; for example, cell death can be found in the immune system, when the natural killer cells find tumor cells. Additionally, excessive cell death can be found in several diseases, such as in neurodegeneration. Conversely, reduced cell death can be associated to cancer.

Historically cell death has been classified by morphological criteria. Recently, the recommendations of the Nomenclature Committee on Cell Death have unified the nomenclature depending on the morphological and molecular characteristics. The Nomenclature Committee on Cell Death had described these types of cell death: **apoptosis** is the most well-known process, characterized by cascade activation and chromatin condensation. **Necrosis** is characterized by the break in the plasma membrane and loss of the intracellular content; **autophagy-dependent cell death (ADCD)** is characterized by the massive accumulation of autophagosomes without chromatin condensation. These three types of cell death have been the most described, but new types of cell death are appearing with the researches progress. For example, **mitotic catastrophe** is a type of cell death characterized by aberrant mitosis and cell death in mitosis or in the next step of the interphase. It is still under debate because it is not a cell death process *perse*, but it is a consequence of an oncosuppresive pathway. **Pyroptosis** is another mechanism introduced in 2000 (Brennan et Cookson, 2000). However, pyroptosis can present apoptotic or necrotic characteristics.

Lysosome-dependent cell death (LDCD) is another type of cell death described by the new nomenclature. Nowadays, lysosome-dependent cell death is described as the lysosomal disruption and lysosomal membrane permeabilization. This situation appears in several physiopathological situations, such as during mammary gland involution, aging or neurodegeneration. The LMP leads to lysosomal content release, but the pathways

downstream have not been elucidated. Sometimes, lysosomes appear permeabilized before the mitochondria, leading to activate other pathways, such as apoptosis or pyroptosis.
One feature of lysosomal-related cell death is that inhibiting LMP or blocking the cathepsin activity delay the cell death.

1.3.1 Apoptosis

Depending on where the death signals are coming apoptosis can be distinguished in two types. The extrinsic apoptosis describes the situation where apoptosis signals are extracellular signals which bind to transmembrane receptors. For example FAS/CD95 ligand, tumor necrosis factor alfa or TNF family (Galluzi et al., 2012). The intrinsic apoptosis pathway is triggered by intracellular signals, such as DNA damage, oxidative stress, and accumulation of unfolded proteins in the endoplasmic reticulum or increase of cytosolic calcium. Both of these pathways converge in changes in the mitochondrial membrane potential. Mitochondrial membrane is permeabilized, forming a pore with the proapoptotic members of the BCL-2 protein and cytochrome c is released and triggers the formation of the apoptosome, and the activation of caspase 9 and caspase 3 (Galluzi et al., 2012). AIF and ENDOG are proteins that appear in the nucleus, mediating the DNA fragmentation.

1.3.2 Autophagy-dependent cell death (ADCD)

The term **autophagy-dependent cell death** (ADCD) was described by Christian de Duve (De Duve et al., 1955). Although autophagy is a protective process that happens in several circumstances to prevent necrosis or apoptotic cell death, for example during starvation, ACD has been termed to describe the situations when the cells die by autophagy. This cell death is characterized by the accumulation of autophagosomes preceded by an increase in the autophagic flux. If inhibition of autophagy does not prevent cell death, this process is not autophagic cell death. This process has been observed during fly development. one example is during the regression of the salivary glands in *Drosophila melanogaster* (Baehrecke, 2003).

ADCD also has been shown to occur in apoptotic-resistant cells, for example in the absence of Bax and Bak (Shimizu et al., 2004; Yu et al., 2004). Interestingly, these cells

can die with autophagic inductors, and this kind of cell death can be avoided by using autophagy inhibitors, or silencing autophagy-related proteins, such as Atg5 (Shimizu et al., 2004). Importantly, autophagy is necessary, but not sufficient to induce ACD because it needs more death signals, like c-Jun N-terminal kinase (JNK). JNK appears increased when ACD is happening (Shimizu et al., 2010). Molecular participants in ACD should be discovered to understand the differences and specificity of this kind of cell death.

1.3.3 Lysosome-dependent cell death (LDCD)

LMP can induce cell death through several pathways. For example, it has been observed that LMP triggers apoptosis in a caspase dependent or independent manner. Additionally, LMP can activate inflammasome, inducing cytokines release and activating macrophages – process called pyropoptosis. The common condition for LMP-induced cell death is that it is able to prevent them by using cathepsin inhibitors. The common patterns between one pathway and another remain still unknown. To discover whether the origin of the induction of LMP is releasing one pathway or another would be interesting to understand how the lysosomal-induced cell death mechanism is happening. Interestingly, transformed cells have an increased sensitivity to LMP inducers (Pedersen et al., 2013), which have promoted a recent interest in the research of this field, looking for new therapeutic targets to kill cancer cells.

LMP promotes the release of cathepsins to the cytosol. Most of the cathepsins remain inactive at neutral pH, except cathepsin B, D and L. These three cathepsins can trigger a cascade of molecular events, activating cell death. For example, cathepsins are able to cleave the BH3-only protein Bid or Noxa, inducing mitochondrial membrane permeabilization (MMP). Bid induces conformational changes in Bax and Bak, which trigger classical apoptosis cascade: MMP, cytochrome c release and caspase activation (Eno et al., 2013). Occasionally, LMP can induce cell death through a caspase-independent pathway. For example, LMP can trigger cell death in a caspase-independent manner after oxidative stress (Mannick et al., 2001) or siramesine (Česen et al., 2013). The reason could be that caspase present oxidative places in their catalytic sites that can be affected by oxidative stress. Another example is in ATP depletion circumstance, cell death presents a shift between caspase-dependent apoptosis to necrosis pathway. For example, N-(4-hydroxyphenyl) retinamide, which is a vitamin, induce cell death in retinoblastoma tumor.

This compound induces lactate dehydrogenase release, disruption of mitochondrial transmembrane potential and ATP depletion. Under these circumstances, cathepsin D is released from lysosomes. Interestingly, Pepstatin A rescued cell viability and reduced DNA fragmentation, which indicates that cathepsin D was able to fragment DNA, inducing another pathway of LMP-induced cell death (Venè et al., 2007).

A variety of silica crystals and protein aggregates disrupt lysosomal integrity and activate the NRLP3 inflammasome, inducing cytokine release and activating macrophages/microglia and cell death. Atherosclerotic lesions present cholesterol crystals that can induce inflammatory response. When cholesterol crystals are injected in mice, acute inflammation and cathepsin B and cathepsin L release was observed. The cathepsin release leads to inflammasome activation (Duewell et al., 2010). Additionally, in Alzheimer's Disease, the peptide amyloid Aβ induces inflammasome activation through lysosomal destabilization (Halle et al., 2008).

Depending on the stimuli that induce LMP, the response can be totally different. It would be important to unravel which the molecular mechanisms are, and whether the molecular pathway depends on the LMP-inducer agent. This difference could set the release of cathepsins, or the differences in the proteins catalizes by the cathepsins.

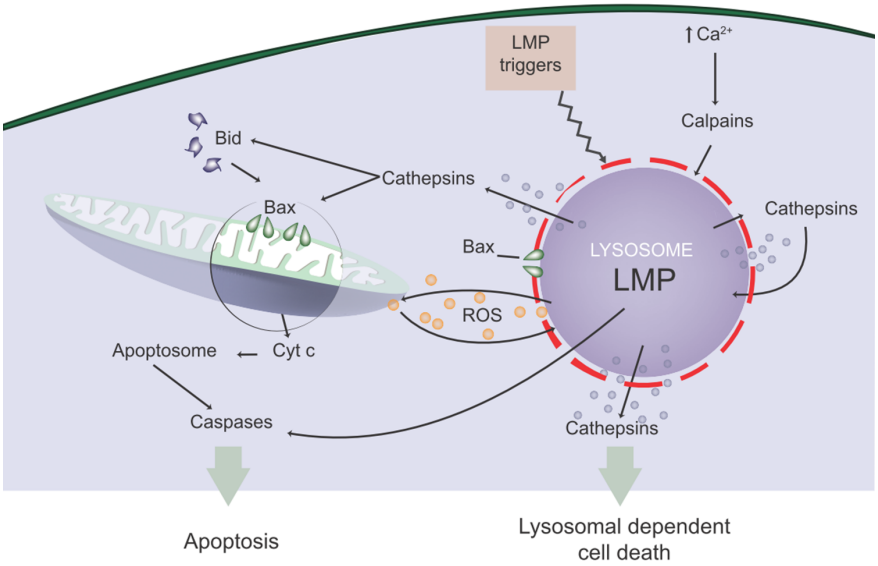

Figure 1.5. Consequences of lysosomal membrane permeabilization. *Cathepsin release after LMP induces different types of cell death: caspase-dependent cell death, caspase-independent, pyroptosis or autophagic cell death.*

1.3.4 Pyroptosis

Pyroptosis is a form of cell death characterized by the activation of caspase 1. Cells are able to activate caspase 1 after the formation of a multiprotein complex, the inflammasome. This response was observed in the inflammatory response, leading to cytokines and cathepsins release and cell death (Galluzzi et al., 2012). It has been described that some protein aggregates and some crystals are able to induce the NRLP3 inflammasome, and this activation can be block by using cathepsin inhibitors (48). For example, flagellin, one component of the flagella of Gram positive and negative bacterial, is able to induce LMP. This LMP causes capase-11 dependent and independent responses, and inflammasome activation (Lage et al., 2013). But, the molecular pathways that link inflammasome and cathepsin release are poorly understood. Further studies are needed to unravel how the connection between LMP and inflammation is.

1.4 VERTEBRATE RETINA

1.4.1 Retina: structure and function

Vertebrate retina is a layered and structured tissue with several cell types integrated in a complex organ. The function and morphology of this tissue is delicately organized to connect every circuit to produce a visual output. Five major neuronal cell classes constitute the retina: photoreceptors, horizontal cells, bipolar cells, amacrine cells and ganglion cells; and a non-neuronal cell type, the Müller glia. All these cells are intrinsically connected in a complex structure, divided in several layers depending on the higher content of nuclei or axons: outer nuclear layer (ONL), outer plexiform layer (OPL), inner nuclear layer (INL), inner plexiform layer (IPL) and ganglion cell layer (GCL). After the GCL, optic nerve will connect with the primary optic cortex (Jones et al., 2012)

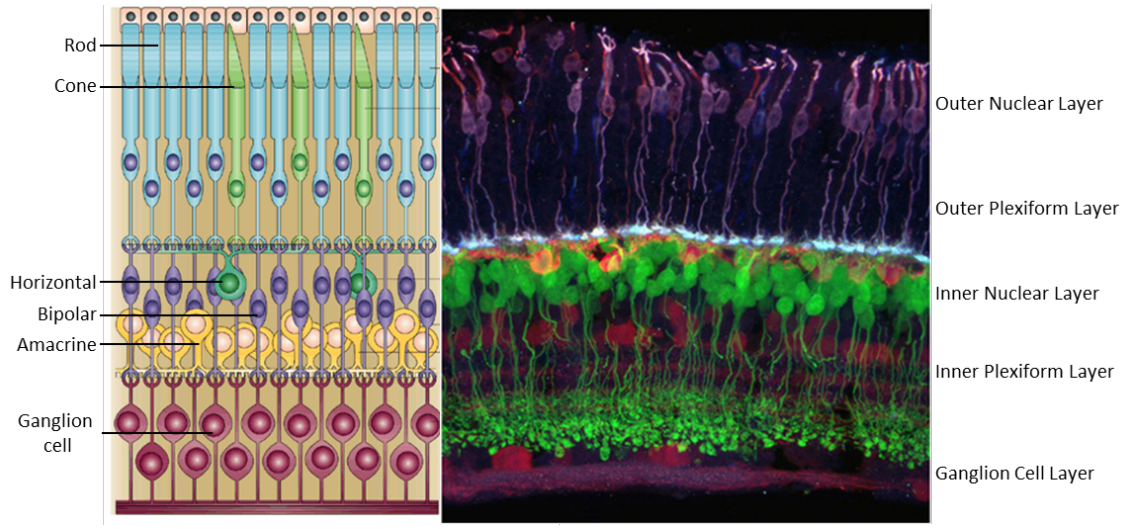

Figure 1.6. Retinal structure. *Retina is compouned by 5 cellular types: photoreceptors (cones and rods), horizontal, bipolar, amacrine and ganglion cells. These types are situated in layer: outer nuclear layer, outer plexiform layer, inner nuclear layer, inner plexiform layer and ganglion cell layer. Modified from Kumar, 2001 and Morgan and Wong, 2005.*

There are two types of photoreceptors: cones and rods. Rods are activated under low light conditions. Cones are in charge of color recognition, they are less sensitive, but they act faster during the phototransduction. Photoreceptors are able to transform the electron energy from the light to synaptic information. Synaptic transmission between photoreceptors and bipolar cells is modulated by horizontal cells. Additionally, bipolar cells can be divided in two types: those that depolarize (ON) and those that hyperpolarize (OFF) to increments the light signal. The ganglion cells project their axons to the visual center in the brain. The ganglion cells connect with bipolar and amacrine cells in the INL. Excitation of amacrine cells regulates the ganglion signaling thought the contact with the ganglion axons (Jones et al., 2012; Vuong and Hedges, 2017).

1.4.2 Photoreceptor Cell Death

Photoreceptors are cells under constant stress due to their high metabolic activity in the presence of light. The current theory is that apoptosis is the most common cell death during retinal development (Young et al., 1984), while other types of programmed cell death have been described in retinal pathological processes. In photoreceptor for example, pharmacological inhibition or genetic manipulation of caspase cascade, typical apoptosic executors, does not avoid cell death (Yoshizawa et al., 2002). It has been described that the type of cell death in retinal degeneration depends on the energy availability. For example, if there is an ATP depletion, necrosis can be activated (Lui et al., 2004). In addition, light-

induced photoreceptor damage activates apoptotic mechanism (Chang et al., 1993). But the events ocurring in inherited retinal degenerations present alternative features different from apoptosis.

Interestingly, it has been observed that in most instances, retinal neurodegeneration is caused by rod degeneration. However, cones will die after rod degeneration. This phenomenon is called **secondary cell death**, and it has been observed for example, when rods present a mutation that induce photoreceptor cell death. This phenomenon could be explained by the loss of structural support (Sahel et al., 2001), or by the loss of trophic support, as for example, the rod viability factor (Mohand-Said et al., 1998). Additionally, dying rods may release toxic compounds to the envionviment.

Several cascades have been characterized during photoreceptor cell death. First, c**yclic nucleotide signaling.** The cyclic nucleotides can be adenosine monophosphate (cAMP) and cyclic guanosine monophosphate (cGMP). These both molecules regulates intracellular signaling. For example, it has been demonstrated that cGMP can induce cell death (Ficuss, 2002). Several mutations in mouse models involve cGMP metabolism, leading to retinal degeneration. For instance, mutations affecting the cGMP-hydrolyzing PDE6 have been found in 10% of human retinitis cases. cAMP appears to be essential for cellular survival. cAMP mediates the activation of protein kinase A, which phosphorilates cAMP response element binding protein (CREB), a transcription factor for neuronal survival (Mantamadiotis et al., 2002). Inherited retinal pathologies present huge changes in **gene transcription**, involving this gene expression to cell survival or cell death.

Calcium influx. Excessive calcium influx has been described as a one of the principal factor in photoreceptor degeneration. Calcium activates several proteins such as calpains in rd1 photoreceptors (Paquet-Durand et al., 2006) and rd10 (Arroba et al., 2011). On the other hand, calcium causes ATP depletion by activating calcium extrusion mechanisms, like ATPases required to take sodium outside (Gerini et al., 2005). Additionally, calcium influx can promote ER stress. ER stress is higly connected to cell death. In summary, intracellular calcium increase can lead to several situations, such as energetic colpase or activation of calcium-related proteins.

Calpain activation. Calpains are proteins with 14 isoforms and they are implicated in cell death. These proteins can be blocked by the specfic inhibitor calpastatin. Inhibition of calpastatin with calcium leads to its autocleavage, leading the calpains activation. In retina, pharmacological inhibition of calpains can block cell death (Araújo et al., 2004). In fact, calpains function is still poorly understood due to the large number of potencial substrates. One of that substrate is arrestin, a component of the phototransduction cascade, which block the interaction between rhodopsin and transducin (Azarian et al., 1995). Additionally, increased cathepsin activity has been showed in the rd1 (Ahuja et al., 2008). More factors affect to the photoreceptor cell death, such as **oxidative stress**, **PARP activity** or **DNA fragmentation**.

The photoreceptror cell death is well described in the rd1 mouse model. In this case, rd1 mouse model does not present any apoptotic-signal marker, such as cytochrome c release, cleavage of Bcl-2 and activation of proteins such as p53 or caspases (Doonan et al., 2003). PDE6 inhibition induced rod and cone cell death. The use of calcium channels blockers prevent retinal degeneration (Frasson et al., 1999). Sancho-Pelluz and colleguaes proposed a model for the photoreceptor cell death of the rd1 mouse model (Sancho-Pelluz et al., 2008). Deregulation of cGMP levels induced by the mutation in PDE6 gene is the begining of the neurodegeneration. High levels of cGMP leads to the activation of cGMP channels. This triggers a calcium-dependent processes. High intracellular calcium levels activate AC, leading to the production of cAMP 116. Additionallyt, cAMP activates PKA, which can activate CREB. But, paradoxically, CREB appears downregulated in this model, so it is supossed to be a negative feedback mechanism. Downregulation of CREB reduces the transcription of CREB target genes, such as calpastatin. Decrease in calpastatin levels leads to the calcium-mediated activation of calpains. Calpains have a large number of possible targets, such as PARP or cathepsins, which appear increase in rd1 model. In conclusion, photoreceptor cell death presents different features to other cell death types.

1.4.3 Autophagy in Photoreceptors

Autophagy, as mentioned before, is a fundamental process that it has a relevant importance in the nervous system. Our lab has been studying the role of autophagy in the retina for several years our data and other laboratories data have demonstrated the essential role of autophagy to support retinal homeostasis (Boya et al., 2016). A pioneer experiment

demonstrated that squirrels presented less mitochondria and different cone morphology during hibertnation due to autophagy activation in photoreceptors (Reme and Young, 1977). After this research, several experiments demonstrated the importance of autophagy in the retina, such us the demonstration that autophagosomes were present in dying ganglion cell during retinal development (Hornung et al., 1989).

One way to study the importance of autophagy in the retina is to study retinal function and development in autophagy-deficient animal models. The first mouse with a photoreceptor-specific deficiency was generated by crossing ATG7flox/flox mice with rod-specific LMOP-Cre mice (Chen et al., 2013). The animals did not present alterations in the retinal under normal light conditions. However, these animals presented severe neurodegeneration after 2h of intense illumination (Chen et al., 2013). Other example studied is the Atg5 deficiency. Mice with $Atg5^{flox/flox}$ were crossed with rhodopsin-iCre-75. These animals $Atg5^{\Delta Rod}$ presented a massive loss of photoreceptors in 20 weeks, which suggest that Atg5 is essential for photoreceptors viability (Zhou et al., 2015a).

Several autophagy-deficient mouse models die after birth, such as the knock-out mice of Atg3, Atg5, Atg7 or Atg9 (Ichimura et Komatsu, 2011), which difficult the study of the visual function; in fact, other models die during the development, such as Beclin1 knock-out mouse model or Ambra1gt/gt. However, Atg4B knock-out mice, which present a normal lifespan, do not present any histological alteration in the eye under basal conditions (Mariño et al., 2010;) but they are more sensitive to optic nerve axotomy (Rodriguez-Muela et al., 2012). Other animal models have been used to study eye development and function. For example, Ambra1 knock-out in zebrafish present smaller eyes (Benato et al., 2013);

In addition, a recent report shows an important variation in the LC3 levels depending on the hour of the day in mice, being the highest peak of LC3 several hours after the light activation, and an important decrease at the first moment of darkness (Yao et al., 2014). More researchers showed the relation between retina and circadian cycle. For example, it has been demonstrated that age-related ocular diseases, a group of diseases that include glaucoma, diabetic retinopathy, age-related macular degeneration, cataract and diabetic retinopathy can be ameliorated with melatonin, the hormone generated during the sleep

time (Crooke et al., 2017). One possible explanation is that melatonin is affecting to sirtuins, proteins related with autophagy.

1.4.4 Autophagy in other retinal diseases and aging

As has been shown previously, autophagy is essential in retinal development and function. This implicates that autophagy must be active to avoid retinal diseases. In **glaucoma**, benefits of autophagy have been evidenced. Glaucoma is a group of molecular diseases characterized by the default of the optic nerve function. However, after axonal damage, a well described model of glaucoma and other diseases, autophagy is highly induced in the retina to avoid ganglionar cell death; nevertheless, animals Atg4B and Atg5 flox/flox presented an increase in cell death in ganglion cells (Rodriguez-Muela et Boya, 2012).

Another example of the importance of autophagy in the retina is the **light-induced damage**. To expose retina to light damage can damage the retina irreversibly. Autophagy induction was observed in illuminated retinas, more specifically, in photoreceptors and in retinal pigmentary epitelium (RPE) (Remé et al., 1999). Interestingly, the lack of some autophagy-related proteins induces an increase in the susceptibility in the retinal degeneration. As commented previously, when animals with rod-specific Atg7-deficiency (Atg7 flox/flox;LMOP-Cre) were exposed to light at 5000 Lux for 2 h, the mouse model Atg7 flox/flox;LMOP-Cre showed photoreceptor degeneration with thiner ONL and disrupted photoreceptor structure (Chen et al., 2013). In the same way, Beclin1-deficiency is increasing the susceptibility after light-induced damage (Chen et al., 2013). Interestingly, Atg5-deficiency was studied by using a model of rod-specific Atg5-deficiency, called Atg5flox/flox;iCre75. Exposing the mice, there was observed that Atg5-lack affected to the retina, but not only after light exposition. Additionally, the lack of Atg5 in the RPE induced a diminished photoreceptor response (Zhou et al., 2015b). These results after light damage and axotomy suggest a role of autophagy to survive to retinal damage.

Age related macular degeneration (AMD) is a complex group of disease characterized by the affection to the macula, the central region of the retina. In this case, the RPE is the one which degenerated during AMD. The RPE is found outside the photoreceptors and this group of cells is in charge of degrading the photoreceptor outside segments (POS) from the

photoreceptors. Autophagy is acting during the degradation of POS. Several experiments have demonstrated that blocking autophagy with 3-MA was increasing the levels of lipofuscin when RPE cells were fed with POS; additionally, autophagy stimulation with rapamycin treatment was inducing viability increase in RPE cells and a reduction of lipofuscin (Mitter et al., 2014). Molecular models have demonstrated that the balance between cholesterol and ceramide is affecting to the lysosomal stability and autophagy flux in the RPE under AMD illness (Toops et al., 2015). Not only in cellular models, but animal models have demonstrated that autophagy presents an important role in AMD. Rapamycin ameliorates the degenerative process in several animal models, such as a mouse with a deficiency in the mitochondrial respiration (Zhao et al., 2011a) and the OXYS rat (Kolosova et al., 2012).

Aging causes retinal dysfunction as a consequence of retinal degeneration and loss of retinal cells (Militant and Lombardini, 2014). In humans, it has been observed that retinal dysfunction is associated with rod and cones loss (Weleber, 1981). Interestingly, aging is associated with a reduction of autophagy process and a decrease in the cleaning pathways, such as the ubiquitin proteasome activity (Martinez-Lopez et al., 2015). Our group has demonstrated that autophagy flux is decreased with aging in mouse (Rodriguez-Muela et al., 2012) as well as reduced mRNA expression of some autophgy-related genes, such as Atg7 and Beclin1; additionally, accumulation of p62, ubiquitin and lipofuscin was observed in mice from 12 and 22 months. These effects were comparable to Atg5flox/flox nes-cre, animals with a lack in Atg5 during the development. Interestingly, chaperone mediated autophagy (CMA) was increased in both animal models, suggesting a cross-talk between both types of autophagy to maintain cellular homeostasis (Rodriguez-Muela et al., 2012). All of these mechanisms demonstrate the desvasting process of aging. To elucidate the mechanisms is important to prevent visual dysfunction associated to aging.

1.4.5 Retinal dystrophies: *Retinitis pigmentosa*

Retinitis pigmentosa (RP) is a group of heterogeneous and and inherited dystrophies mutations. Most cases of *retinitis pigmentosa* are monogenic but this disease is really heterogeneous genetically, in fact, investigators have identified at least 45 loci (http://www.sph.uth.tmc.edu/Retnet/disease.htm). Interestingly, these mutations cause a similar phenotype, characterized by photoreceptor degeneration and cell death. The

photoreceptor cell death leads to blindness. In humans, these diseases have an estimated incidence of 1 in 4.000 so it is classified as a rare disease (Rossmiller et al., 2012). The genes more known implicated in this disease are genes related to the phototransduction cascade, such us rhodopsin, rod cGMP-phosphodiesterase α-subunit or rod cGMP-phosphodiesterase β-subunit; additionally, genes related to the vitamin A metabolism, such as ATP-binding cassete protein A4 or retinaldehyde binding protein; genes related to structural or cytoskeletal; genes related to signaling, (Fagerberg et al., 2014; Wang et al., 2017).

Some patients develop visual loss during their childhood, but most of the patients present a pattern of difficulties in the dark adaptation during the adolescence; later, they present loss of peripheral vision, tunnel vision and complete loss of the central vision by the age of 60. Rods, the photoreceptors in charge of the achromatic dark vision, are the first to die. After them, cones, the photoreceptors responsible for the colour vision and the acuity in light situations, also die during the seconday cell death. The ONL of the retina from the patients is dramatically thinner than a healthy retina. Several methodologies had been approached to identify *retinitis pigmentosa* in the patients: dark adaptation tests, contrast sensitivity, Slit-lap biomicroscopy or electroretinograms (ERGs). This last technique is used either in human and mice. It is a technique that measures the electrical response of the retina based in giving flashes of light to the retina and harvest the information through an electrode. The expectations for the cure of *retinitis pigmentosa* are quite positive. Several treatments have been demonstrated to improve the phenotype of this disease. For example, patients administrated with vitamin A, vitamin E or both presented a better response in ERG test than those who were not taking vitamins (Clowes, 1993). Some of these recomedations can delay the neurodegeneration, but this disease has no cure yet.

The photoreceptors respond to light due to opsin, a visual pigment, and retinal, a chromophore. Retinal isomerizes to trans for photon absorption. In that way, rhodopsin catalyzes the activation of transducin. This protein is a G-protein, which stimulates cyclic uanosine monophosphate phosphodiesterase (cGMP PDE) to catalyze cyclic guanosine monophosphate (cGMP). The decrease of cGMP induces a closure in the cGMP channels (Palczewski, 2006). But, in darkness, cGMP channels are open and transporting sodium and calcium to the inner of the cells. The influx of cations induces a depolizarization of the membrane.

Several animal models have been used to study *retinitis pigmentosa*. Some of the models are use due to their mutation occurs in the nature: dogs, cats and chicken. Additionally, several models are product of transgenic modifications, providing models of diseases to develop curative strategies: rat, mouse and pig. In this thesis, only one mouse model was used, the rd10 mice. The first retinal degeneration mouse model was the rd1 (rd from retinal degeneration) (Pittler et al., 1993). This model presents a mutation in the rod photoreceptor-specific phosphosidsterase gene Pde6b (Gargene et al., 2007). This mouse model presents a degeneration of the retina which begins at postnatal day P10. Retina is completely lost close to postnatal day P21 (Bowes et al., 1990). The rd10 mouse model presents a mutation in the same gene but the neurodegeneration is delayed. This mutation leads to an increase cGMP and cell death close to postnatal day P25 (Barhoum et al., 2010). After 2 months of age, the mice are completely blind. This model provides a better pharmaceutical therapy due to the longer photoreceptor survival in comparison with rd1. There are more rd mouse model, such as rd4, with a chromosomic inversion; rd8, after a mutation in the gene CRB; or the rd16, with a depletion in a centrosomal proteins CEP290 (Rivas and Vecino, 2009)

Several therapeutic approaches have been tried in rd10 mouse model. For example, expression of human proinsulin in the mouse model rd10 is able to reduce cell death in the retina from the murine model. The human proinsulin decreased cell death and preserved visual response as determiend by ERG (Corrochano et al., 2008). Additionally, due to features observed in this mouse model, such us inflammation, microglial activation and reactive gliosis, the study of antagonists against the proneurotophin–$p75^{NTR}$ axis has been described (Platón-Corchado et al., 2017).

1.4.6 Histone deacetylases in *retinitis pigmentosa*

Histone acetylases (HATs) and histone deacetylases (HDACs) are enzymes that promote addition or removal of acetyls in lysine residues. These proteins were first known by relaxing chromatin structure and allowing access to transcription factors. In addition, recent studies have shown that these enzymes can also act in non-histone proteins and are implicated in cellular vital functions. In fact, HDACs have been considered as crucial target in several diseases, such as cancer, autoimmune or inflammatory diseases (Tang,

2013). The HDACs can be classified into four families: class I, compound by HDAC1, 2, 3 and 8; class IIa, compound by HDAC 4, 5, 7 and 9; class IIb, compound by HDAC6 and 10; and IV, compound only by HDAC11. In addition, there is another group of deacetylases called sirtuins or class III. HDACs are essential in the cellular homeostasis, although, interestingly, the pharmacologic HDAC inhibitors do not result in catastrophic effects. In fact, the HDAC inhibitors are well tolerated *in vivo* and block numerous disease-associated gene expression (Haberland et al., 2009). In relation with our work, previous evidences in the rd1 mice have demonstrated that HDACs activity is increased in photoreceptors and this imbalance has an important role in rd1 photoreceptor degeneration. In this model, HDAC inhibition protects from photoreceptor death (Sancho-Pelluz et al., 2011).

Recent studies have shown that acetylation/deacetylation processes are implicated in autophagy, modifying the autophagy activity, in most cases, triggering autophagy. For example, SIRT1, one member of the sirtuin family, induces autophagy by deacetylating factors such as Atg5, Atg7 or LC3 in starvation conditions (Lee et al., 2008). In mouse embryonic fibroblasts, the deacetylation of p53 by HDAC1 induces autophagy (Contretas et al., 2013), and in Huntington disease, HDAC6 was established as a mediator of aggregates degradation by autophagy because of its interaction with microtubules (Iwata et al., 2005). These studies have demonstrated that deacetylation and autophagy are related processes, and this relationship could explain some disease-related effects. In addition, several evidences have demonstrated that acetylation can modulate the outcome and flux of autophagy (Bánreti, et al., 2013; Füllgrabe et al., 2013). HDAC research will help to ths scientific community to find out novel therapeutic pathways for retinal diseases.

OBJECTIVES

2. OBJECTIVES

The main objective of this thesis was to analyze the consequences of lysosome-dependent cell death in models of a neurodegenerative disease called *Retinitis pigmentosa*. In addition, we characterized the role of autophagy during lysosome-dependent cell death by using autophagy-deficient cell lines.

For these aims, the following objectives were proposed:

1. Determine the role of autophagy during photoreceptor neurodegeneration in a *Retinitis pigmentosa* mouse model, the Rd10 mice.
2. Assess lysosome stability during neurodegeneration in the Rd10 retinas.
3. Modulate autophagy and lysosomal activity during neurodegeneration to characterize the capacity of autophagy and lysosome to prevent or increase photoreceptor cell death.
4. Develop an *in vitro* model by using the calcium ionophore A23187 to mimetize the Rd10 phenotype.
5. Study the relation between lysosomal membrane permeabilization and autophagy at molecular level by using autophagy-deficient cell lines.
6. Assess viability and lysosomal activity in autophagy-deficient cell lines, specifically in Atg5- and Atg7- deficient cell lines under conditions of lysosomal stress.
7. Characterize the consequences of to lysosomal membrane permeabilization in autophagy-deficient cell lines.

MATHERIALS AND METHODS

3. MATHERIALS AND METHODS

3.1 ANIMAL PROCEDURES

3.1.1 MOUSE MODELS AND METHODS

3.1.1.1 Mouse models and housing

The CSIC and CIB ethics committee for animal experimentation approved the animal procedures used in this thesis. All the experiments were carried out in accordance with the European Union guidelines and the ARVO Statement for the Use of Animals in Ophthalmic and Vision Research. Wild-type and Rd10 mice are in C57BL/6J background and both strains were obtained from the Jackson Laboratory. The animals were exposed to 12:12 light: dark cycles, temperature of 20 degrees, food and water *ad libitum* at the CIB animal facility. Both males and females were used for the experiments. To avoid the circadian variations of autophagy in the retina, samples were always obtained at the same hour: 10 am.

3.1.1.2 Intravitreous and intraperitoneal injections

Intravitreous injections were done with a Hamilton syringe (Model 75 RN SYR). For intravitreal trehalose treatment, P19 mice were anaesthetized with isoflurane. Right eyes were injected with 1 µl of 30 mM trehalose in PBS and left eyes were injected as controls with 1 µl of 30 mM sucrose in PBS. Mice were euthanized at P22 and eyes or retinas were extracted and fixed in 4% (w/v) paraformaldehyde (PFA) in 0.1 M phosphate buffer pH 7.4 at 4 ºC overnight. Then, retinas were extracted and cell death detection was performed. *In vivo* rapamycin injections were performed from postnatal day P13 to postnatal day P23. The injections were done every two days. At P23, animals were sacrified and retinas were fixed with 4% PFA in 0.1 phosphate buffer at 4ºC. Then, TUNEL reaction was carried out as in apart 3.1.2.1.

3.1.1.3 Neuroretina dissection

Animals were euthanized by cervical dislocation and decapited. Eyes were enucleated and deposited in PBS. Using two dissection tweezers, neuroretina was separated from the pigmentary epithelium, sclera, crystalline and *ora serrata*.

For immunofluorescence, retinas were mounted in 0.44 µm nitrocellulose membranes (Sartorius, Göttingen, Germany) with the photoreceptors up. The mounted retinas were fixed in 4% PFA in 0.1 M phosphate buffer (PB), pH 7.14 overnight at 4 ºC or one hour at room temperature. After fixation, neuroretinas were washed with PBS 3 times for 5 minutes each. Finally, they were kept in the fridge until the moment of the immunofluorescence. For western blot or qPCR, neuroretinas were frozen at -80 ºC until the protein or RNA extraction.

3.1.1.4 Neuroretina organotypic culture

Neuroretinas were cultivated in defined medium serum-free R16 medium, described by Dr. P. A. Ekstrom (Caffe et al., 2001) at 37 ºC and 5% CO2 for 24 hours. After that time, neuroretinas were mounted in nitrocellulose or they were frozen at -80 ºC. The treatments used in this thesis are in the **table 1**.

Reactives	Provider	Reference	Concentration	Funtion
A23187	Sigma	C7522	5 µM	Calcium ionophore
ALLN	Sigma	208719	20 µM	Calpain inhibitor
Leupeptin	Calbiochem	108975	10 µM	Cathepsin inhibitor
Pepstatin A	Sigma	P5318	10 µg/ml	Cathepsin inhibitor
Rapamycin	Calbiochem	553210	200 nM	Autophagy inductor

Table 1. Treatments used in the neuroretina organotypic culture.

For autophagy flux assessment, neuroretinas were cultivated for 4 hours. One half was cultivated in vehicle in control medium, and the other half was cultivated with the lysosomal inhibitors: ammonium chloride (20 mM, Sigma, Missouri, USA) and leupeptin (100 µM, Calbiochem). After that, neuroretinas were froozen at -80 ºC until the protein extraction.

3.1.1.5 Eye cryosections

For cryosections studies, eyes were enucleated from the mice and fixed in 4% PFA overnight at 4 ºC. After that, eyes were washed 3 times with PBS and then the eyes were dehydrated by washes in sucrose diluted in 0.1 M phosphate buffer pH 7.14:

- Sucrose 15% (w/v) during 1 hour in the shaker
- Sucrose 30% (w/v) during 1 hour in the shaker

- Sucrose 50% (w/v) overnight in the shaker.

If the samples were not used at the moment, eyes were frozen in sucrose 50%. Eyes were imbibed in OCT (Tissue Tek, Sakura Finetek, Tokyo, Japan) in an Eppendorf tube for 30 minutes. After that time, eyes were placed in the Eppendorf lid with OCT to set up the eye. Eyes were oriented to get slices with optic nerve in the cryostat. Eyes were cut at 10 µm in a Leica CM 1800cryostat. The tissue sections were placed on glass slides (Superfrost® Plus, Thermo Scientific, Massachusets, USA). The tissue sections were kept at room temperature for 1 hour and then they were frozen at -20 ºC until immunofluorescence reaction.

3.1.2 CELULAR TECHNIQUES

3.1.2.1 Cell Death assay by TUNEL reaction

Cell death assay was assessed in whole mounted retinas by using the terminal deoxynucleotidyl transferase-mediated dUTP nick-end labeling (TUNEL) staining. Mounted neuroretinas were washed with PBS after fixation. The chromatin was opened with citrate buffer, heating it up in the microwaves for 5 minutes. After three washes with PBS, neuroretinas were permeabilized with Triton®X-100 2% (v/v) in PBS four times during 20 minutes each. Neuroretinas were washed 3 times with PBS. Then, neuroretinas were permeabilized with BGT (3 mg/mL BSA, 10 mM glicine y 0.25% Tritón X-100 in PBS) 3 times 30 minutes each. Neuroretinas were washed with PBS. Neuroretinas were pre-equilibrated during 30 minutes in equilibration buffer at room temperature. Then, TUNEL reaction was done during 1 hour at 37 ºC as in the protocol from Promega (Madison, Wisconsin, USA). Then, the reaction was stopped by washes with PBS and nuclei were stained with 1µg/µl of 1, 4-diamino-2-fenilindol (DAPI). Neuroretinas were mounted with 1, 4 – diazabacycle (2, 2, 2) octane (DABCO, Sigma, Missouri, USA) and analyzed by confocal microscope TCS SP5 (Leica, Watzler, Germany).

3.1.2.2 Quantification of cell death by TUNEL on mounted-retinas

At least four pictures were taken with confocal microscopy from every neuroretina. The pictures were done in the ONL to include the photoreceptors and to avoid other cell types. Every picture was done at the same distance from the optic nerve. Only TUNEL positive cells were quantified. For the quantification, the maximal projections from sections of 1

µm were used. The software used in the quantification was ImageJ 1.6.0 (National Institute of Health, USA).

3.1.2.3 Immunofluorescence in flat mounted retina

Mounted neuroretinas were washed with PBS after fixation and then permeabilized with 2% Triton®X-100 (v/v) in PBS four times during 20 minutes each, washed with PBS and blocked with BGT 3 times for 30 minutes and washed with PBS. Primary antibodies were incubated in 10% normal goat serum (NGS), 1% Triton®X-100 (v/v) in PBS overnight at 4 ºC in a humid chamber (**table 2**). After 3 washes with PBS, neuroretinas were incubated with secondary antibodies with the specific fluorophore (**table 3**) in the same equilibration buffer for 2 hours at room temperature. After several washes, neuroretinas were incubated with DAPI for 1 hour at room temperature and mounted with DABCO for the posterior visualization at confocal microscope.

3.1.2.4 Immunofluorescence in retina cryosections

Criosection samples were left at room temperature 5 minutes. The samples were delimited with the Immunopen. Samples were refixed in 4% PFA during 15 minutes and washed. If the protein of study is attached to cellular membrane, samples were immersed in cold methanol for 5 minutes; if the antibody stain transcription factor, we used citrate buffer for 5 minutes in the microwave. After several washes, samples were submerged in BGT 3 times for 5 minutes each in a humidity chamber. After washing, samples were blocked by 10% NGS, 1% Triton X-100 in PBS for 1 hour at room temperature. Primary antibodies were incubated in the same buffer overnight at 4C in the humidity chamber (**table 2**). After washing, secondary antibodies were incubated for 1 hour at room temperature (**table 3**). The nuclei were stained with DAPI as described before, and samples were mounted with DABCO. Samples were observed at the confocal SP5 Leica microscope.

Antibody	Provider	Reference	Species	Dilution
Anti-Ambra 1	Covalab	CVL-PAB0224	Rabbit	1:100
Anti-Cathepsin B	Santa Cruz	SC6490	Rabbit	1:50
Anti-Galectin-3	BD	556904	Mouse	1:100
Anti-Lamp1	DSHB	1D4B	Rat	1:50

Table 2. Secondary antibodies used in immunofluorescence of mounted or criosections of retinas.

Ab 2º	Provider	Reference	Species	Dilution
Alexa 488	Invitrogen	A11001	Polyclonal; Goat	1:200
Alexa 568	Invitrogen	A11004	Polyclonal; Goat	1:200
Alexa 647	Invitrogen	A21235	Polyclonal; Goat	1:200

Table 3. Secondary antibodies used in immunofluorescence of mounted or criosections of retinas.

3.1.2.5 Determination of cathepsin B activity by Magic Red reaction

The activity of cathepsin B in the retinas was measured with Magic Red Cathepsin B Assay Kit (Immunochemistry Technologies, Minneapolis, USA). The Magic Red Cathepsin B Assay is a red fluorogenic cathepsin B substrate. Magic Red was added to the medium the last 30 minutes of incubation protected from the light, following the manufacturer´s protocol. After that, neuroretinas were mounted in nitrocellulose filters, fixed in 4% PFA in dark conditions during 1 hour at room temperature. Neuroretinas were incubated with DAPI as described before, and samples were observed at the confocal SP5 Leica microscope.

3.1.2.6 Detection of mitochondria levels by flow cytometry

Mitochondria levels in the retina were studied by flow cytometry. Retinas from mice at postnatal day 20 and 30 were used for this assay. Neuroretinas were extracted from the eyes and placed in culture medium. Retinal cells were incubated with 0.5 mg/ml of trypsin (Worthington, Ohio, USA) for 5 minutes at 37ºC and dissociated by gentle pipetting. Trypsin effect was stopped by adding 1% (v/v) of FBS. Tubes were centrifuged at 450 g for 5 minutes. After decant the supernatant, retinas were incubated with 10 nM MitoTracker Deep Red (Thermo Fisher Scientific) in HBSS for 15 minutes at 37 ºC. At least 10.000 retinal cells were acquired in a FC500 flow cytometer (Beckman Coulter). Mean fluorescence in the FL4 channel of the live cell population was represented.

3.1.3 BIOCHEMICAL TECHNIQUES

3.1.3.1 Extraction and quantification of neuroretina proteins

Appropriate volume of lysis buffer was prepared: 150 µl per complete retina and 75 µl per half of retina in flux autophagy studies. Lysis buffer is prepared in distilled water with 50 mM of Tris-HCl pH 6.8, 10% of glycerol (v/v) and 2% Sodium Dodecyl Sulfate (SDS) (w/v), protease inhibitors (1 tablet for each 10 mL of buffer, Roche, Indianapolis, USA)

and phosphatase inhibitors (1 mM sodium orthovanadate, 5 mM sodium pyrophosphate, 1 mM sodium fluoride). Retinas were scraped in 1.5 ml Eppendorfs with a syringe plunger. After vortex the homogenate, samples were warmed up at 95 ºC for 14 minutes. For protein quantification, 5 µl of every sample were diluted 1:5 in distilled water. The kit BCA Protein Assay (Pierce, Thermo Fisher Scientific Inc, Illinois, USA) was used for the quantification and was measured in a wavelength of 540nm.

3.1.3.2 Immunodetection of proteins in membrane: Western blot

A fraction of 15 µg of cell lysate was supplemented with 10 mM of dithiothreitol (DTT) and 0.005% (w/v) of bromophenol. The samples were loaded in Criterion™ TGX Precast Midi Protein gels (Biorad, California, USA) and transferred onto PVDF membranes (Biorad, California, USA) by using the Trans-Blot® Turbo™ Transfer System (Biorad, California, USA). The membranes were activated in methanol and blocked in 5% (w/v) of milk in PBS-Tween for one hour. After blocking, primary antibodies were incubated in 3% (w/v) BSA in PBS-Tween for 16 hours at 4 °C in the shaker. The primary antibodies used in this thesis are in the **table 4**.

Ab 1º	Provider	Reference	Species	Dilution
Anti-AKT	Cell Signaling	9271	Rabbit	1:1000
Anti-Calpain	Calbiochem	MAB3083	Mouse	1:1000
Anti-COX4I1	Invitrogen	459600	Mouse	1:1000
Anti-ERK	Sigma	M5670	Rabbit	1:500
Anti-GAPDH	Abcam	ab8245	Mouse	1:2000
Anti-Lamp2A	Invitrogen	51-2200	Rabbit	1:1000
Anti-LC3	Nanotools	0260-100	Rabbit	1:1000
Anti-MAB	Milipore	MAB1273	Mouse	1:1000
Anti-p62	ENZO	PW9860	Rabbit	1:500
Anti-PS6	Cell Signaling	4856	Rabbit	1:1000
Anti-S6	Cell Signaling	2317	Mouse	1:1000
Anti-TIMM23	BD	611222	Mouse	1:1000
Anti-TOMM20	Santa Cruz	sc-17764	Mouse	1:1000
Anti-TOMM40	Santa Cruz	sc-11414	Rabbit	1:1000
Anti-tubulina	Covance	MMS-435P	Rabbit	1:500

Table 4. Primary antibodies used in retinal western blot.

After several washes with PBS-Tween, membranes were incubated with secondary antibodies conjugated for one hour at room temperature with peroxidase (DAKO P0448, Rabbit, Thermo Scientific 31430). Membranes were developed with the system Pierce ECL Blotting Substrate (Thermo Scientific, 32106) and using films Curix RP2 Plus film (AGFA). The films were digitalized and quantified with the software ImagJ 1.6.0.

3.1.3.3 ATP assay: determination of ATP levels in retinas.

ATP was quantified using the ATP Bioluminiscent Assay Kit HS II (Roche, Switzerland) in frozen retinas. 50 µl of dilution buffer and 50 µl of lysis buffer are added in each eppendorf, and incubated for 5 minutes at room temperature. After that, centifrugation was carried out for 1 minute at 10,000 X g at 4 ºC. 10 µl of the supernatant was diluted 1:2 with lysis buffer and quantified with the kit BCA Protein Assay (Pierce, Thermo Fisher Scientific Inc, Illinois, USA). The rest of the supernatant is used for measure ATP: 100 ng of every sample with 50 µl of dilution buffer in a plate with a black background. The measurement was done Measure the ATP in a Varioskan reader.

3.2 CELL CULTURE

3.2.1 MOUSE EMBRYONIC FIBROBLAST AND CANCER CELL LINES

Large T-transformed mouse embryonic fibroblasts Atg5+/+, Atg5-/-, Atg7+/+ and Atg7-/- were kindly provided by Prof. Noboru Mizushima at the University of Tokyo (Japan) and Prof. Komatsu (Tokyo Metropolitan Institute of Medical Science, Tokyo, Japan), respectively HeLa were obtained from the American Type Culture Collection (ATCC®, Rockville, Maryland, USA). The human breast adenocarcinoma cancer cell line MCF7 were obtained from Dr. Marja Jäättelä´s laboratory (Danish Cancer Society Research Center, Copenhagen, Denmark).

Mouse embryonic fibroblasts and HeLa were cultured in DMEN (Dublecco´s Modified Eagle Medium, GIBCO) supplemented with 10% FBS, 1% penicillin/streptomycin and 1% glutamine. MCF7 cell line was cultured with RPMI (GIBCO) supplement with 6% FBS and 1% penicillin/streptomycin. Cell lines were seeded at a density of 5.000-10.000 cells/cm^2 the evening before carry out the experiments.

3.2.2 IMMUNOFLUORESCENCE DETECTION

3.2.2.1 Immunofluorescence of cells seeded in cover-slips

Cells were seeded over sterilized glass cover-slips the day before the treatment. After the treatments, cover-slips were fixed with 4% PFA for 15 minutes and washed with PBS. The cover-slips were kept at 4 ºC. The permeabilization phase depends on the antibodies used. In general, 10% (v/v) SDS in PBS during 30 minutes was used for most of the antibodies. For proteins attached to membranes, cold methanol was used during 5 minutes for cleaning the cytoplasmic staining. After methanol permeabilization, 0.01% Triton 100X (v/v) in PBS was used. Primary antibodies were always incubated in 10% NGS and 1% Triton 100X in PBS and incubated for 1 hour at room temperature or overnight at 4ºC (**table 5**).. After 3 washes with PBS for 5 minutes, secondary antibody was incubated for 1 hour at room temperature in 10% NGS (**table 6**).

Ab 1º	Provider	Reference	Species	Dilution
Anti-Cathepsin B	Santa Cruz	SC6490	Policlonal; Rabbit	1:50
Anti-Galectin-3	BD	556904	Monoclonal; Mouse	1:100
Anti-Lamp1	DSHB	1D4B	Policlonal; Rat	1:50
Anti-LC3	Sigma	L7543	Policlonal; Rabbit	1:100
Anti-p62	Progen	GP62-C	Policlonal; Guinea Pig	1:100

Table 5. Primary antibodies used in immunofluorescence technique in cell lines.

Ab 2º	Provider	Reference	Species	Dilution
Alexa 488	Invitrogen	A11001	Polyclonal; Goat	1:200
Alexa 568	Invitrogen	A11004	Polyclonal; Goat	1:200
Alexa 647	Invitrogen	A21235	Polyclonal; Goat	1:200

Table 6. Secondary antibodies used in immunofluorescence technique in cell lines.

After several washes with PBS, 1 mg/ml of DAPI was incubated for 15 minutes at room temperature. One last wash of PBS and cover slips were mounted with Fluoromont-G (Cultek, Spain) and stored at 4 ºC until confocal analysis.

3.2.2.2 Lysosomal membrane permeabilization detection by galectin-3

Cover-slips were fixed with 4% PFA for 15 minutes, washed three times with PBS and permeabilized with cold methanol for 3 minutes. After several washes with PBS, anti-

galectin3 (BD, reference 556904; Mouse) as incubated for 2h at RT in 1% (w/v) BSA, 0.3% (v/v) Triton 100X in PBS in a dilution of 1:100 After several washes with PBS-Tween, secondary antibody was incubated in 1% (w/v) BSA, 0.3% (v/v) Triton 100X in PBS. After several washes of PBS-tween, nuclei were stained with 1mg/ml of DAPI and cover-slips mounted with Fluoromont G. Galectin-3 quantification was done in the microscope. Every cell had to present at least two galecin-3 puncta to be considered as a galectin-3 puncta positive cell.

3.2.2.3 Lysosomal leackage by cathepsin B release

To determine subcellular distribution of cathepsin B is a way to detect lysosomal membrane permeabilization. Cover-slips were fixed with 4% PFA for 30 minutes and cleaning three times with PBS. Cover-slips were permeabilized with cold methanol for 5 minutes. After several washes with PBS, anti-cathepsin B (Santa Cruz, SC6490, polyclonal rabbit) was incubated in 10% (v/v) SDS in PBS in a dilution of 1:50 for 2 hours at RT. After several washes with PBS-Tween, secondary antibody was incubated in 10% (v/v) NGS, 0,1% (v/v) Triton 100X in PBS. After several washes of PBS-tween, nuclei were stained with 1mg/ml of DAPI and cover-slips mounted with Fluoromont G. Cathepsin B quantification was done in the microscope. To consider one cell as positive, cathepsin B should appear as diffuse staining and not in dots. Colocalization with other antibody against lysosomal protein is a good option to detect if cathepsin B is outside lysosomes.

3.2.2.4 Acidic compartments staining: LysoTracker

LysoTracker is a fluorophore, which stains acidic compartments in cells. To study acidic compartments by immunofluorescence, 1 μM LysoTracker Red (Invitrogen, L7528) was added to the well in the last 30 minutes of the treatment. After this incubation, cover-slips were fixed with 4 % PFA during 30 minutes. Nuclei was stained with 1 mg/ml DAPI and cover-slips mounted with Fluoromont G.

3.2.2.5 Quantification of microscopy confocal images

Images from confocal were quantified with ImageJ 1.6.0 (National Institute of Health, USA). Java program was used to perform a protocol. The protocol was setting depending on the antibody. To perform the protocol, we performed a Java protocol. After that, the protocol was run automatically in ImagJ.

3.2.3 PROTEIN DETECTION OF MOUSE EMBRYONIC FIBROBLAST

3.2.3.1 Protein extraction

Cells were seeded in 6-well plate the day before carrying out the experiment. After the transfection or treatment, proteins were extracted from the plate by using 150 µl of lysis buffer. Lysis buffer was prepared as described in 3.1.3.1. The proteins were scraped with a syringe plunger and transferred to 1.5 ml Eppendorfs. Samples were warmed up at 95ºC for 14 minutes. The quantification of the cellular proteins was done as described in 3.1.3.1.

3.2.3.2 Immunodetection of proteins in membrane: western blot

The immunodetection of cellular proteins in membrane was done as described in 3.1.3.2.

3.2.4 TRANSMISSION ELECTRON MICROSCOPY

300,000 cells were seeded in 6 well plates. After the treatment, medium was removed and cells were washed with PBS and fixed with 3% glutaraldehyde (v/v) in PBS for one hour. After fixation, cells were washed with PBS. Cells were refixed with osmium 1% and ferricianure 0.8% in PBS for one hour. After PBS washes, cells were dehydrated with ethanol washes, from 30% to 100% gradually. Cells were infiltrated with epoxy LX 112 resin. Cells were polymerized for 24 hours at 60C. Ultramicrotomy and contrast with 5% of uranile acetate in PBS and lead citrate (Reynolds). The samples were visualized in transmission electron microscopy 1230 80kv with camera TVIPS 4KxK.

3.2.5 FLOW CYTOMETRY

25,000 cells were seeded in a 24-well plate the day before the experiment. After the treatment, wells were washed with 200 µl of PBS, and cells were detached with 200 µl of Trypsin (Thermo Fisher Scientific) at 37 ºC for 5 minutes. Trypsin action was stopped with 400 µl of serum-containing medium and the samples were transferred to cytometer tubes. After, tubes were centrifuged for 5 minutes at 140 g, medium was removed and medium with 1µM of propidium iodide (Sigma, P4864) was added. Death population was plotted. At least, 10,000 cells were adquired in a FC500 flow cytometer (Beckman Coulter).

3.2.6 DETECTION OF GENE EXPRESSION

3.2.6.1 Extraction of messenger RNA

300,000 cells were seeded in 6-well plate in a high confluency. After the treatments, cultures were stopped with TRIzol® Reagent (Thermo Fisher Scientific). Cell extract was moved to Eppendorfs and this extracted was passed 10 times through syringes of 0.8mm x 25 mm. Chloroform was added in the Eppendorf and cell extract was centrifuged at 1,400 g during 15 minutes at 4 ºC. Supernatants were kept and glycogen (Fisher, reference 10814010) and isopropanol was added. After gentle shaking, cells were centrifuge at 1,400 g for 10 minutes at 4C. Supernatant was removed and the samples were cleaned with ethanol 70% and centrifugated at 60 g, 5 minutes at 4C. Ethanol was removed and when the pellet was dry, samples were resuspended in RNase free water. To increase the solubility, samples were heating at 55 ºC. RNA amount was quantified in Nanodrop and stored at -80 ºC until use.

3.2.6.2 Reverse transcriptase reaction

The qRT-PCR was done in groups of 6 samples. 1 µg of RNA was retrotranscribed to cDNA by using the High-Capacity cDNA Reverse Transcription Kit with RNase Inhibitor (Applied Biosystems, Waltham, MA, USA) in a final volume of 13,2 µl. The next reactives were added to every sample: 2 µL buffer 10X, 2 µL Random Primers 10X, 0.8 µL de 25x dNTP Mix (100mM), 1 µL MultiScribe® Reverse Transcriptase (50 U/µL) and 1 µL of RNAse inhibitor (20 U/µL). The samples were mixed and the reaction was done in the thermocycler Light Cycler® 480 Instrument (Roche Diagnostics, Mannheim, Germany) with the next program: 25 ºC for 10 minutes, 37 ºC for 120 minutes, 85 ºC for 5 minutes and 4 ºC as final step.

3.2.6.3 Quantitative PCR

Taqman oligonucleotides for selected genes were designed according to the Roche software for quantitative real-time PCR (Roche Diagnostics, Mannheim, Germany). Assays were made in experimental duplicate and results normalized according to the expression levels 18S. The results were expressed using the method ΔΔCT (cycle threshold). The tagman oliglonucleotides used are shown in the **table 7**.

Gen	Taqman Reference
Lamp1	Mm00495262_m1
Maplc3b	Mm00458725_gl
Sqstm	Mm00448091_m1
TFEB	Mm00448968_m1

Table 7. Probes and references used for the qRT-PCR.

3.2.7 CELL LINE TRANSFECTION

300.000 cells were seeded in a 6-well plate the day before. Medium was removed and OPTIMEN was added to the wells. Transfection was done with 2 µg of DNA incubated with lipofectamin. After 25 minutes of incubation of DNA and lipofectamin, 400 µl of the mix was added to every well. After 4 hours, OPTIMEN medium was removed and, depending on the experiment, complete medium was added to the cells or cells were raised and seeded in a new plate.

3.2.8 LIPIDOMIC STUDY

For the lipid extraction, 1,2 millon cells were centrifuged at 140 g during 5 minutes. Cells were washed with Ammonium Acetate (Sigma) in H_2O and then centrifuged for 5 minute each, at 400X g and 4 ºC. The lipidomic service of the Danish Cancer Society Research Centre studied the lipidomic profile through HPLC.

3.3 STATISTICAL ANALYSIS

The data presented in this thesis was analyzed with the SPSS 21.0 software. If the samples were normal and homoscedastic, the comparision of means statistical significance was evaluated using the Student *t* test or analyzed with of variance analysis (ANOVA). In all cases, $p<0.05$ was considered stadistically significative. The data are represented as the means of the population ± the standar error from 3 independent experiments with triplicates.

RESULTS

4. RESULTS

4.1 RD10 MOUSE MODEL: AUTOPHAGY AND LYSOSOME-DEPENDENT CELL DEATH IN *RETINITIS PIGMENTOSA* MODEL

4.1.1 Rd10 retinas display photoreceptor cell death

Previous results in the Rd1 mouse model had demonstrated that the cell death is associated to calcium accumulation (Sancho-Pelluz et al., 2008) as phosphodiesterase mutation in this strain keeps calcium channels in the open conformation. To address this process in the Rd10 mouse model, a time-course of the intracellular calcium levels was performed. Previous data from our lab demonstrated that the peak of cell death in the Rd10 is at postnatal day P25. Wild-type and Rd10 retinas were used from animals at different ages: postnatal day P14, P18, P21 and P25. The retinas were dissociated and stained with Fluo-3 and analyzed by flow cytometry.

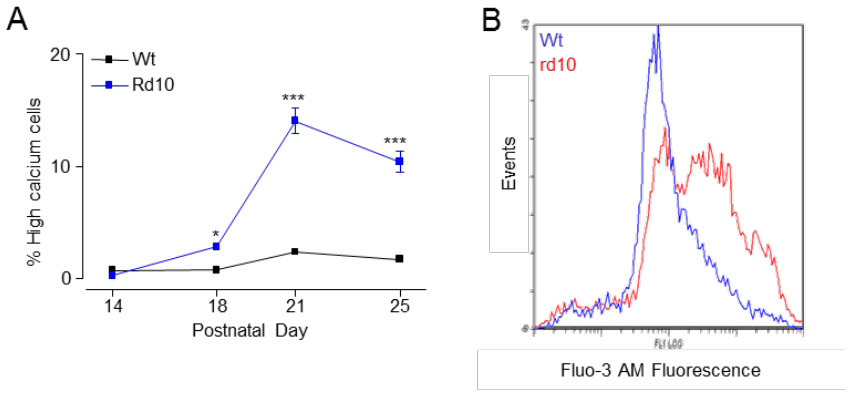

Figure 4.1 Rd10 retinas present an intracellular calcium influx. (A) Determination of the percent of cells with increased intracellular calcium in the retina at different postnatal days. Relative values ± SEM (*p<0.01, ***p<0.001). **(B)** Representative histogram of the levels of Fluo-3 in whole retinas from wild-type and Rd10 animals.

Analysis of Fluo-3 staining revealed a significant increase in the intracellular calcium influx in the Rd10 retinas from postnatal day P18. The number of cells with increased intracellular calcium levels is significatively higher in Rd10 than in wild-type from postnatal day P18 (**figure 4.1A**). As expected the fluorescence of Fluo-3 is higher in Rd10 retinas than in the wild-type retinas (**figure 4.1B**). These data indicated that calcium increase happens before the cell death peak.

Observing the increase of intracellular calcium in the Rd10 retinas, and due to the relation between intracellular calcium and the activation of the calpain family protein, immunoblotting of wild-type and Rd10 retinas at different postnatal days was performed to study the activation of calpain family proteins. The ages selected were: P15, when neurodegeneration was starting, P20, several days before the cell death peak; and P25, when the cell death peak was taking place.

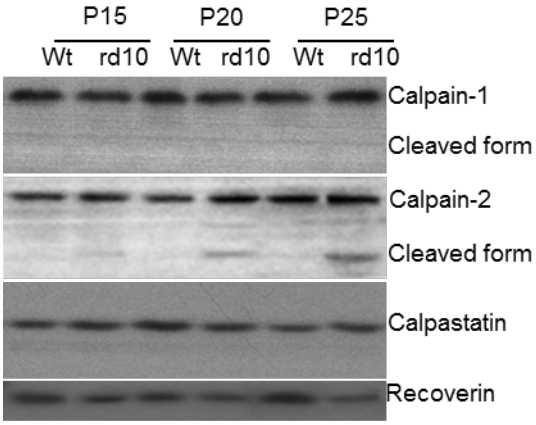

Figure 4.2 Activation of calpain-2 in the Rd10 retinas. Immunoblotting from retinal lysates from wild-type (Wt) and Rd10 retinas at postnatal day P15, P20 and P25. Every lane represent one different animal.

We observed that Rd10 retinas present cleaved calpain-2 at postnatal day P20 and P25 (**figure 4.2**), suggesting the calcium-induced calpain activation.

4.1.2 Autophagy in rd10 retinas

4.1.2.1 Detection of basal autophagy in Rd10 retinas

We were interested in understanding the dynamic of autophagy during the neurodegeneration in Rd10 retinas. To study the role of autophagy in a mouse model of retinal degeneration several autophagy related protein expression was assessed in wt and rd10 mice at different time postnatal days: P20, P30 and P60.

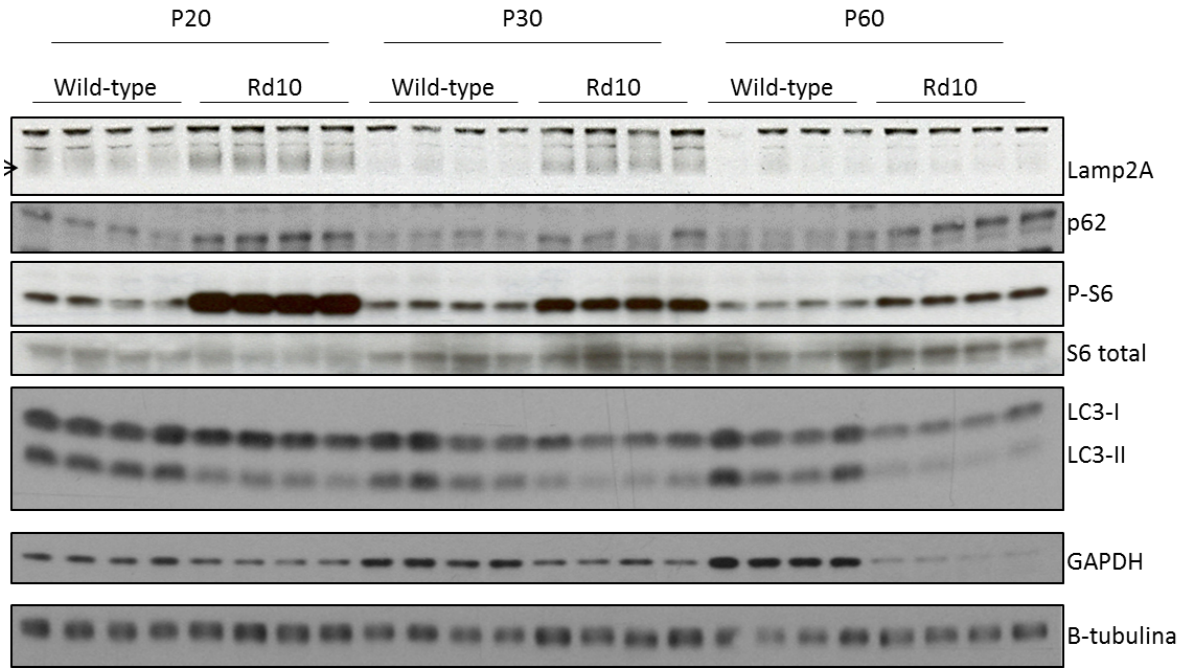

Figure 4.4 Autophagy study in wild-type and Rd10 retinas. Immunoblot of autophagy-related proteins in extracts from wild-type and Rd10 retinas. Animals were sacrificed at different ages: P20, P30 and P60. Every lane represented one retina representative from animal.

At postnatal day P20, before the cell death peak, LC3-II levels were decreased in Rd10 in comparison with wild-type retinas (**figure 4.4)**. Alternatively, p62, which is an autophagy substrate, is increased in the Rd10 retinas, suggesting autophagy blockade. In addition, this reduction of LC3-II is more pronounced in postnatal day P30 Interestingly, the levels of LC3II dissapered at postnatal day P60, suggesting that most of the autophagy process is taking place in the rods, as no rods are left at P60. Furthermore, the autophagy blockade was confirmed by the activation of mTOR as is evidenced by the increase in the phosphorylation of S6 in the Rd10 retinas. Interestingly, an increase in Lamp2A was observed in the Rd10 retinas at postnatal day P20 and P30. In conclusion these data suggest a block in autophagy in the rd10 retinas.

These data were confirmed by assessing the retinas of rd10 mice crossed with the GFP-LC3 mouse. **Figure 4.5** shows decrease GFP-LC3 staining in the ONL of rd10 retinas. In addition, Ambra1 staining was also reduced in retinal sections from GFP-LC3 and Rd10-GFP-LC3 animals at postnatal day P25.

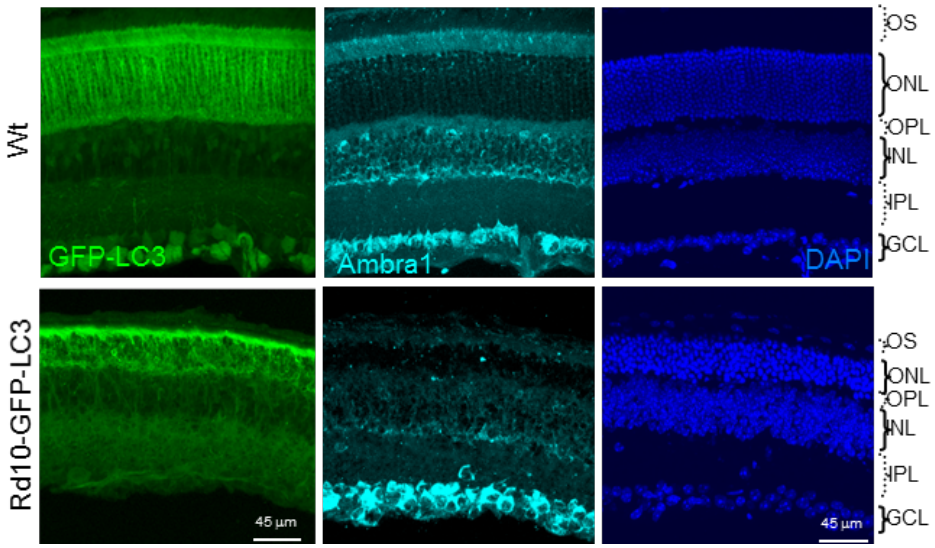

Figure 4.5 Staining of autophagic proteins was observed in Rd10-GPF-LC3. The retinal cryosections were stained with Ambra 1 (cyan) and DAPI (blue). LC3 is observed in green. Scale bar, 45 µm. GCL, ganglion cell layer; IPL, inner plexiform layer; INL, inner nuclear layer; OPL, outer plexiform layer; ONL, outer nuclear layer; OS, outer segment.

GFP-LC3 retinas presented a uniform pattern of LC3 staining in the ONL and the GCL. Moreover, Ambra1 was observed in the OS, INL and GCL. However, Rd10-GFP-LC3 cryosections presented a non-ubicuous GFP signaling and more accumulated in the ONL (**figure 4.5)**. Moreover, Ambra1 appeared more concentrated in the GCL.

4.1.2.2 Detection of Autophagy flux in Rd10 retinas

To assess in autophagy flux in Rd10 retinas, LC3-II was studied after lysosomal inhibition using protease inhibitors. For that goal, levels of autophagic proteins were studied after 24 hours of culture with proteases inhibitors: Pepstatin A, E-64d and Leupeptin A. For this experiment, whole retinas from wild-type and Rd10 animals at postnatal day P20 were incubated *ex vivo* in the presence and absence of protease inhibitors. Western blot was performed with the samples.

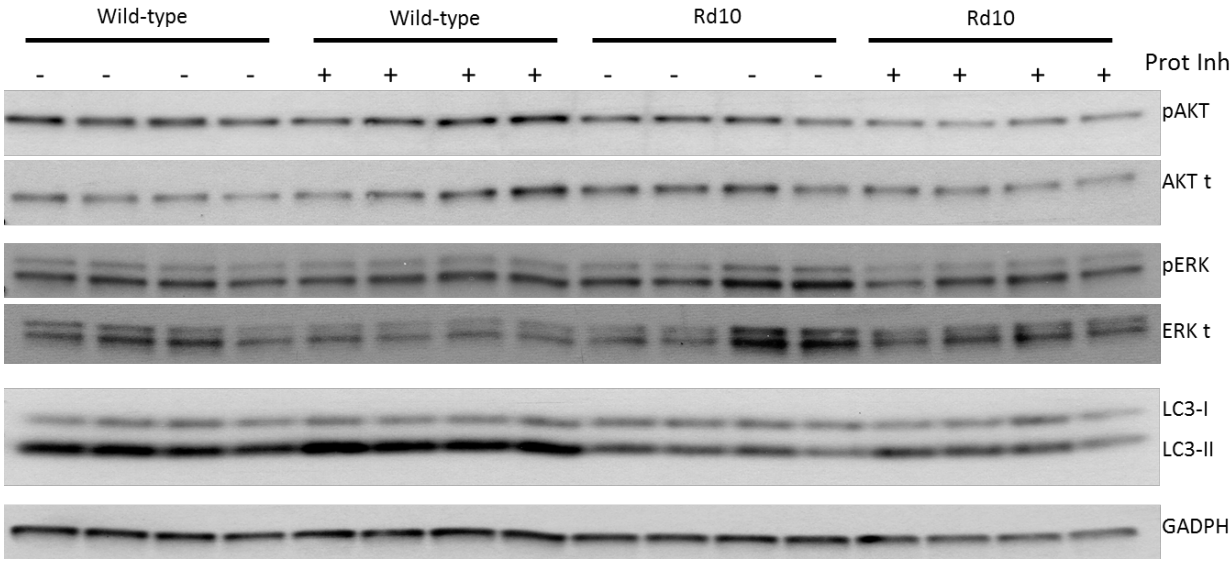

Figure 4.6 Western blot of autophagic proteins after 24 hours of incubation with protease inhibitors. Autophagy-related protein levels in the whole retina from wild-type and Rd10 of postnatal day P20. Every lane represented one retina.

The **figure 4.6** clearly shows that the levels of LC3-II in the Rd10 animals at postnatal day P20 do not increase in the presence of protease inhibitors while it did in wild-type retinas. This indicates that there is no autophagy flux in the Rd10 retinas. Moreover, Akt and phospho-Akt present similar levels of protein in wild-type and Rd10. Interestingly, phospho-ERK present an increase in Rd10 retinas, suggesting the activation of MAPK pathway, a well-known pro-survival signalling before degeneration.

We next assessed whether the block in autophagy flux was observed at different time points during neurodegeneration. For this experiment, half of the retinas were incubated in absence of protease inhibitors; the other halfs were incubated for 3 hours in "N/L" medium: fresh medium with Ammonium Chloride and 100 µm Leupeptin A. To confirm the autophagy flux blockade at different ages, wild-type and Rd10 retinas were isolated from animals from three different postnatal days: P16, P20, and P24.

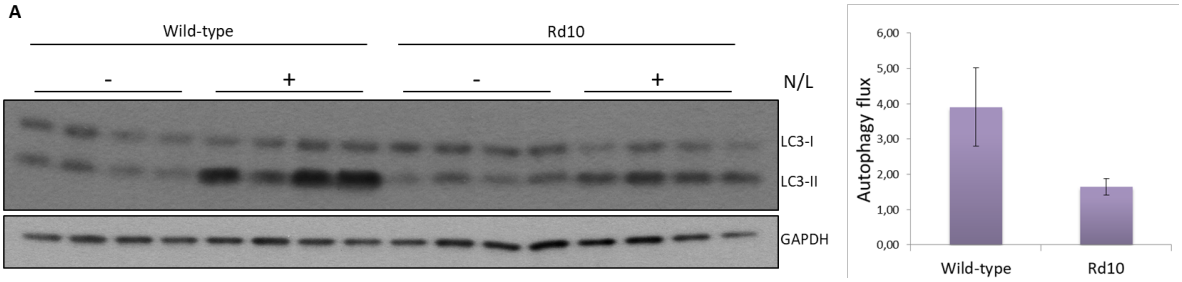

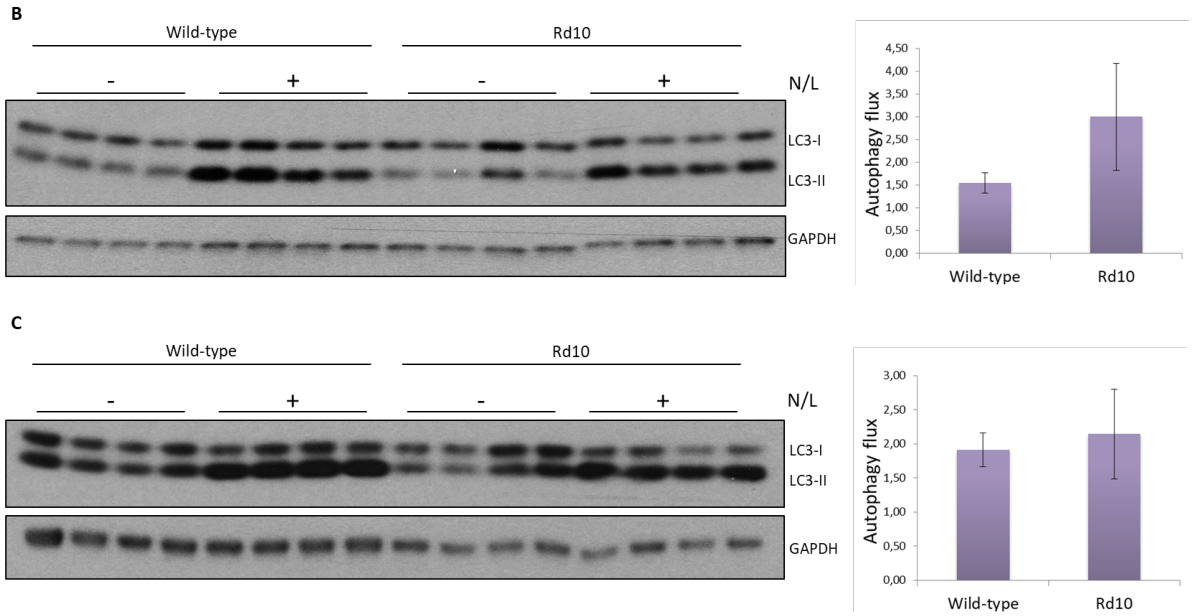

Figure 4.6 Autophagy and autophagy flux in wild-type and Rd10 retinas. Immunoblotting of LC3-I and LC3-II after 3 hours of ammonium chloride and Leupeptin (N/L) from isolated retinas from animals at postnatal day P16 **(A)**, P20 **(B)** and P24 **(C).** Every lane represented the half of the retinal cultured in absence of presence of N/L.Autophagy flux: LC3-II divided by GAPDH, and the coefficient between samples with N/L and control.

Differences in LC3-II protein levels were observed between protease inhibitor and N/L technique, being N/L more efficient blocking the autophagy flux. Moreover, wild-type retinas at postnatal day P16 presented an active autophagy flux, unlikely in the Rd10 retinas (**figure 4.6A**). Interestingly, the LC3-II protein levels become more similar to the wild-type retinas when the cell death peak was close at P20, but the variation in Rd10 retinas is elevated (**figure 4.6B)** and even more similar at P24 (**figure 4.6C**). In conclusion, autophagy flux was blockade before neurodegeneration.

4.1.3 Rd10 retinas present higher levels of mitochondria

The autophagy block observed in the rd10 retinas could be affecting the selective degradation of organelles such as mitochondria during mitophagy. For this reason, oxidative stress was studied by staining the retinas with dihydroethidium (DHE). DHE exhibits blue-fluorescence in the cytosol until oxidized, where it intercalates with cell's DNA, staining its nucleus a bright fluorescent red. After staining, retinas were studied by flow cytometry.

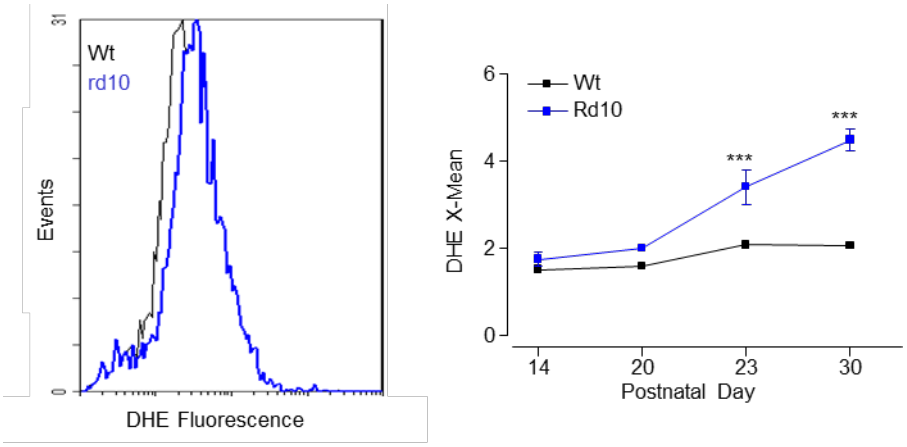

Figure 4.8 Rd10 retinas exhibit an increased in oxidative stress. Oxidative stress determination by using DHE staining.Histogram shows profile of Wt and rd10 retinas at P23 and the graphs display the quantification at different ages (*** p<0.005, n=4).

As it is shown in **figure 4.8**, Rd10 retinas have a significative increase in the levels of oxidative stress at postnatal day P23. After this result, mitochondria levels were studied by using MitoTracker Deep Red (MTDR) and probing for the staining by flow cytometry using a method recently described by our lab (Mauro-Lizcano et al., 2015) using wt and rd10 retinas at day P20 and P30.

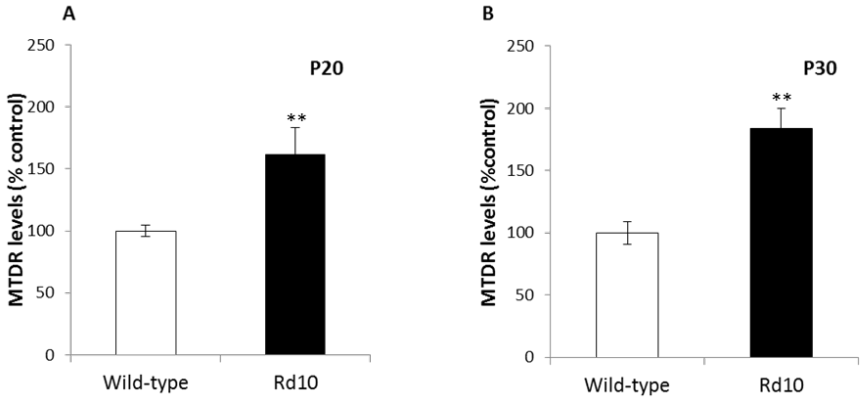

Figure 4.9 Levels of MTDR in complete retinas. The graphics represent the levels of MTDR relatively to wild-type retinas from the same age. **(A)** MTDR levels from postnatal day 20 retinas from wild-type and Rd10 animals. Mean ± SEM represented from 8 retinas per condition in 2 independent experiment. **(B)** MTDR levels from wild-type and Rd10 animals from postnatal day P30. Mean ± SEM represented from 8 retinas per condition in 2 independent experiments. ** p-value <0.01

Rd10 retinas displayed more MTDR fluorescence levels by flow cytometry that wild-type retinas at postnatal day P20 (**figure 4.9A**) and P30 (**figure 4.9B**). To verify these data by other method, we isolated retinas from wild-type and Rd10 mice from postnatal day 20 and 30 and evaluated the levels of mitochondrial proteins such as: COX4I1, TIMM23, TOMM20, and TOMM40 by immunoblotting.

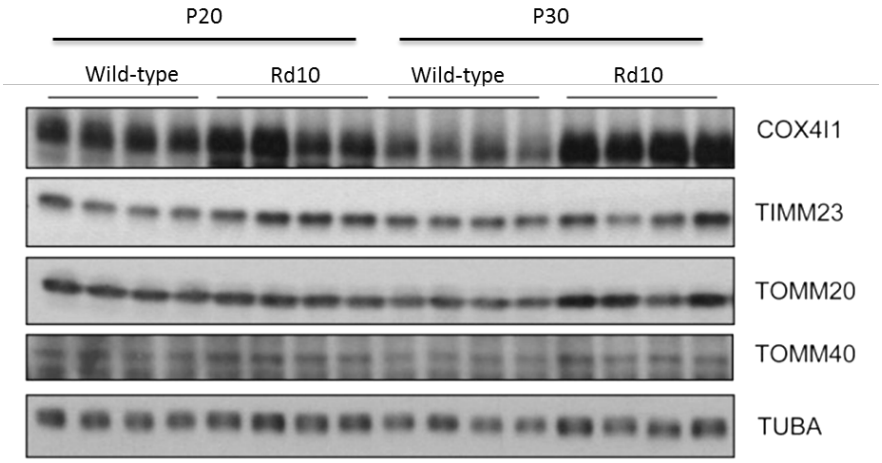

Figure 4.10 Mitochondrial proteins from wild-type and Rd10 retinas. Retinas from wild-type and Rd10 at postnatal day 20 and 30 were used to study mitochondrial protein levels. Every lane represented a different animal.

The immunoblotting demonstrated that COX4I1 and TOMM20 protein levels were higher in the Rd10 retinas than in the wild-type (**figure 4.10)**. Moreover, protein level of TIMM23 was increased in the Rd10 retinas. These data demonstrated that Rd10 retinas presented increased mitochondrial protein levels. To gain insight into these results, mitophagy and mitophagy flux were studied through two approaches: mitochondrial protein levels were studied by western, and inducing/blocking mitophagy with mitophagy inductors, such as CCCP; and mitophagy inhibitors, such as Ciclosporin A or FK506.

First of all, mitophagy flux was studied by immunoblotting after culture of Leupeptin A, E64d and Pepstatin A for 24 hours. For this aim, whole retinas from wild-type and Rd10 animals from postnatal day P20 were incubated in medium in the absence or the presence of the proteases inhibitors.

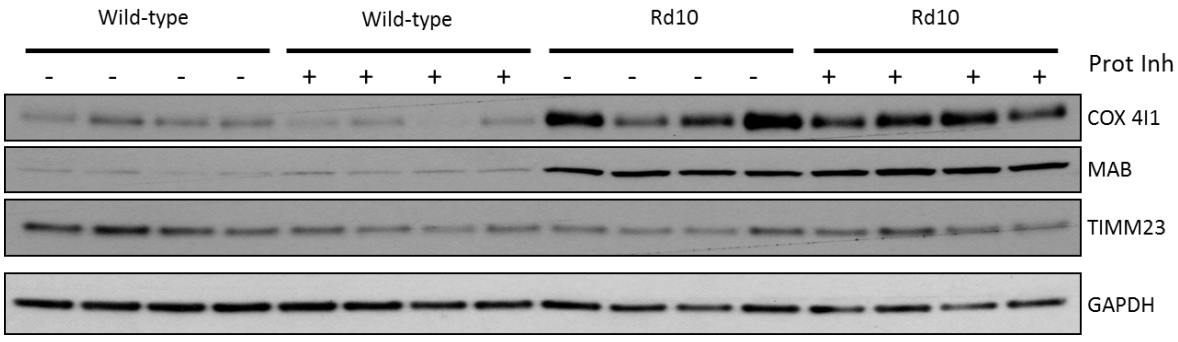

Figure 4.11 Mitochondrial protein from extracts of retinas incubated with protease inhibitors. Mitochondrial proteins from whole retinas of wild-type and Rd10 animals of postnatal P20 after 24 hours of culture in absence or present of Leupeptin A, E64d and Pepstatin A. Every lane is an individual retina. Prot Inh: protease inhibitor.

The levels of the mitochondrial proteins MAB, COX4I1 and TIMM23 were not increased in the retinas after 24 hours of incubation with protease inhibitors (**figure 4.11**).

Next retinas from wild-type animals were cultured with CCCP (25 µM), a mitophagy inductor; and CsA (10 µM) and FK, mitophagy inhibitors to confirm that there was no mitophagy in the retina. Wild-type retinas from animals at postnatal day P20 were isolated and cultured with the respective drugs. After the culture, retinal cells were dissociated, stained with MTDR and studied by flow cytometry.

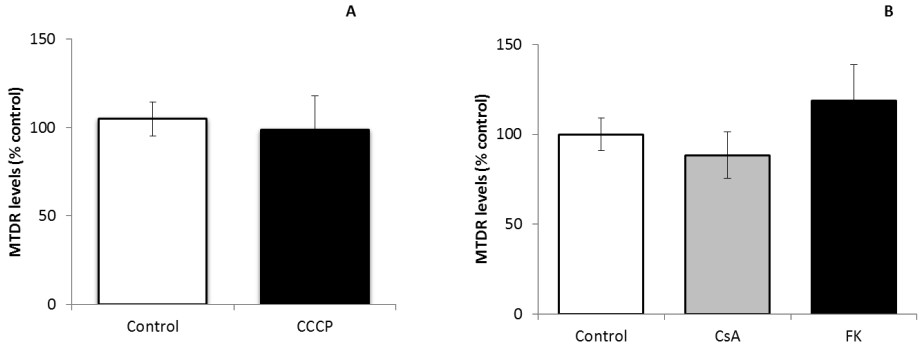

Figure 4.12 Basal and induced mitophagy in wild-type retinal. (A) Wild-type retinas at postnatal day 20 were treated with CCCP 25 µM for 24 hours to induce mitophagy. **(B)** Wild-type retinas at postnatal day 20 were treated with CsA and FK for 24 hours to block basal mitophagy. In total, 12 retinas were used in 4 different experiments for each basal and induced studies. No significative differences were observed. Mean ± SEM represented. 12 retinas per 4 independent experiments.

No mitophagy induction was observed in wildtype retinas after 24 hours of CCCP (**figure 4.12A**). Moreover, no increase of MTDR was observed after treatment with CsA and FK (**figure 4.12B**). The analysis of mitochondrial levels after mitophagy induction and mitophagy inhibition demonstrated that mitophagy was not happening in the wild-type retinas. But, as commented previously, Rd10 presented more mitochondrial protein levels, which could indicate an induction of mitochondrial biogenesis. Further experiments need to be done to understand mitochondrial dynamic in the Rd10 retinas.

4.1.3.1 ATP levels in rd10 retinas

Due to the difference in the mitochondria levels in the Rd10 retinas, ATP levels were studied in the whole retina comparing Rd10 mouse model to wild-type. For this experiment, wild-type and Rd10 animals of postnatal day 20 were used.

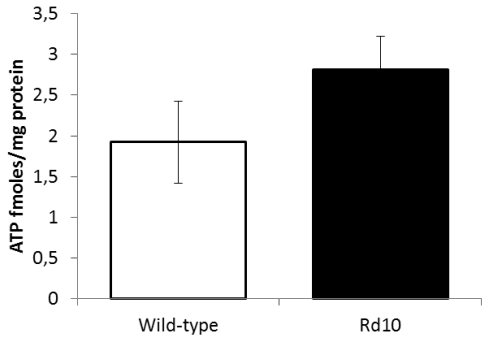

Figure 4.13 Study ATP levels in wild-type and Rd10 retinas. This table is representing fentomoles of ATP in the complete retina from wild-type and Rd10 retinas. Mean ± SEM represented. 6 animals per genotype were used in this study.

The mean of the levels of ATP were higher in the Rd10 retinas than in the wild-type retinas (**figure 4.13)**. As commented previously, Rd10 presented more mitochondrial protein levels and the retinas present a tendency displaying more ATP, which could indicate an induction of mitochondrial biogenesis or that rod have less mitochondria than cones, and since the rd10 retinas are enriched in cones due to rod death. These possibilities wait for further investigation.

4.1.4 Lysosomal membrane permeabilization in rd10 retinas

4.1.4.1 Colocalization of immunofluorescence of lysosomal markers

In order to understand why the Rd10 retinas displayed alterations in autophagy flux and due that calpain activation has been described to induce lysosomal damage, we decided to investigate whether lysosomes were altered in the Rd10 retinas. To detect whether the Rd10 mouse model presented lysosomal damage, retinas from wild-type and Rd10 animals from postnatal day P20 were stained with Lamp1, a lysosomal membrane protein, and Cathepsin B, a lysosomal protease able to be active in the cytosol. Colocalization of both proteins was studied in the Rd10 system and in the wild-type model by confocal microscopy.

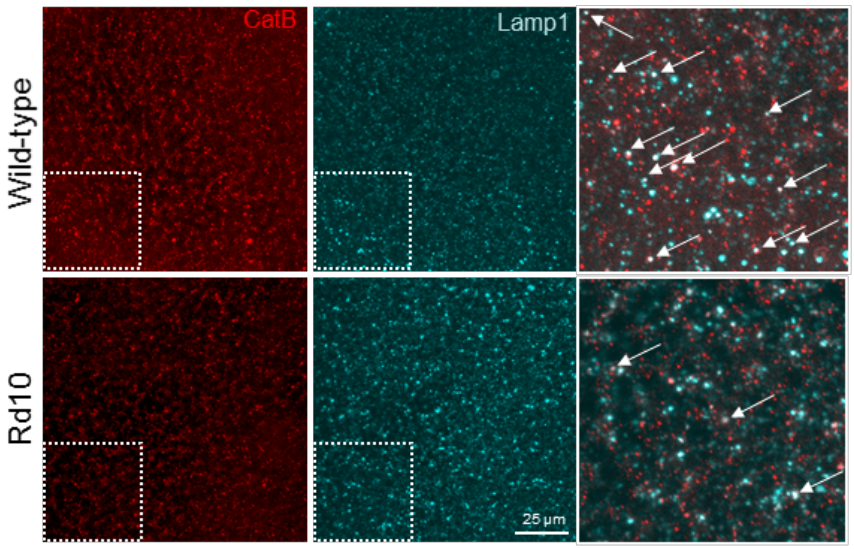

Figure 4.14 Immunofluorescence of lysosomal proteins in wild-type and Rd10 retinas. Staining of Cathepsin B (red) and Lamp1 (cyan) in mounted retinas of wild-type and Rd10 retinas at postnatal day P20. White narrows point the colocalization between both proteins. Scale bar 25 µM.

Rd10 retinas presented less colocalization between the lysosomal membrane protein, Lamp1, and the lysosomal protease, cathepsin B. These results suggested that the Rd10 retinas presented less colocalization between lamp1 and cathepsin B in the lysosomes (**figure 4.14**).

4.1.4.2 Magic-Red staining to study cathepsin B activity

To determine whether Rd10 retinas presented less cathepsin B in the lysosomes, cathepsin B activity assay was carried out. For this goal, retinas from wild-type and Rd10 at postnatal day P20 were cultured with magic red, a fluorogenic cathepsin B substrate that display red fluorescence. After the culture, retinas were flat mounted and observed by confocal microscopy.

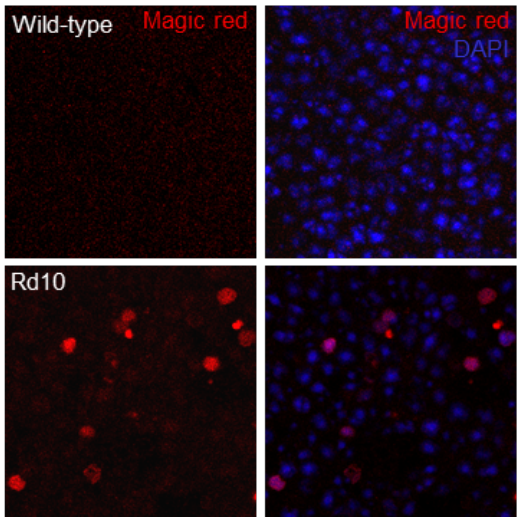

Figure 4.15 Magic red assay in wild-type and Rd10 retinas. Wild-type and Rd10 retinas were cultured with magic red, the fluorogenic cathepsin B substrate. Only outer nuclear layer was assessed by performing the maximal projection of the z-stack of the ONL. Three experiments, 4 animals each condition. Scale bar 25 µm.

Magic red staining presented puncta staning in the wild-type retinas, suggesting the lysosomal distribution of cathepsin B; alternatively, the Rd10 retinas presented a cytoplasmic and more intense magic red staining in comparison with the wild-type retinas (**figure 4.15**). This experiment commended that the localization of cathepsin B was cytosolic in the case of the Rd10 retinas due to the cytosolic staining. Additionally, this staining suggested that the enzyme was still being active even in the cytosol. These experiments suggested that the Rd10 retinas present LMP in the photoreceptors.

4.1.4.3 Galectin-3 to detect LMP

To further gain insight into the lyosomal damage in the Rd10 retinas, we used a recently and powerful methods by assessing LMP with galectin-3 staining in cell cultures (Aits S, et al.). Galectins are proteins with high affinity for the β-galactoside sugars (Barondes, et al.). Galectins are usually presented in the cytosol, but when lysosomes are permeabilized, galectins can go inside lysosomes and bind to the β-galactoside sugars from the lysosomal membrane. LMP can be studied by doing an immunofluorescence for galectin-3.

To assess if this technique was valid in retinas, wild-type retinas were treated with terfenadine, a cationic amphiphilic drug (CAD) well-known to induce LMP in cell lines. After 24 hours of culture, cathepsin B immunofluorescence was studied to analyze whether terfenadine was inducing LMP in the retinal system.

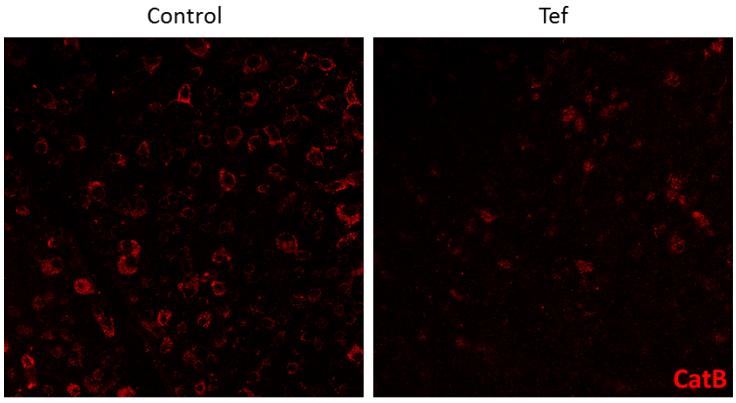

Figure 4.16 Immunofluorescence of Cathepsin B in wild-type mounted retinas. Wild-type retinas were incubated for 24 hours in the absence and presence of terfenadine. Scale bar 25 µm.

The immunofluorescence of cathepsin B after the treatment with terfenadine showed that the treatment with the CAD was affecting to the localization of the lysosomal protease cathepsin B in the retinas. The pictures demonstrated that terfenadine was inducing lysosomal damage in the retina due to the diffuse cathepsin B staining after terfenadine treatment in comparision with control (**figure 4.16**). For this reason, wild-type retinas treated with terfenadine were stained with galectin-3 and Lamp1.

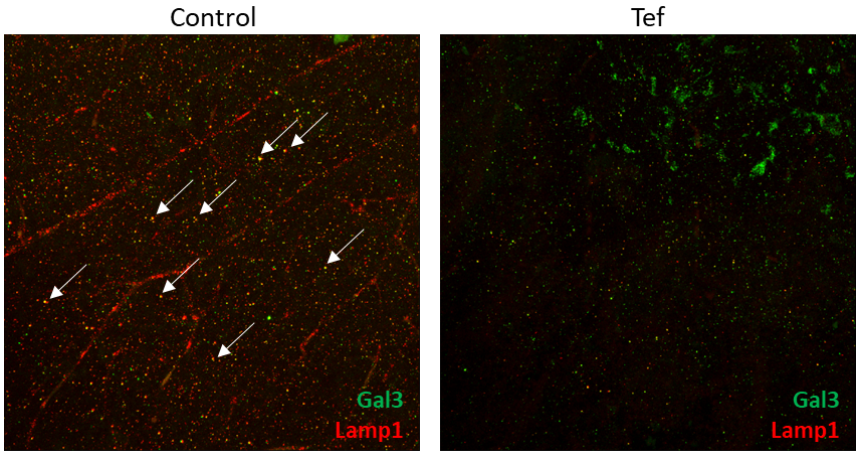

Figure 4.17 Immunofluorescence of galectin3 and lamp1 of mounted retinas. Mounted retinas from wild-type mice at postnatal day P20 were stained for galectin-3 and Lamp1 after 24 hours of absence or presence of terfenadine. White narrows indicate colocalization between galectin-3 and lamp1. Scale bar 25 µm.

Interestingly, control mounted retinas presented higher levels of colocalization between galectin-3 and lamp1 (**figure 4.17**). However, treated retinas with terfenadine present a decrease in lamp1 protein levels. Slices of retinas were studied to determine in which layer the colocalization of lamp1 and galectin-3 was happening. For that goal, wild-type retinas were cultured in control medium and terfenadine for 24 hours. After that, retinas were

fixed and immunofluorescence was carried out. In the microscope, slices of XZY were done to characterize the layers of the retinas.

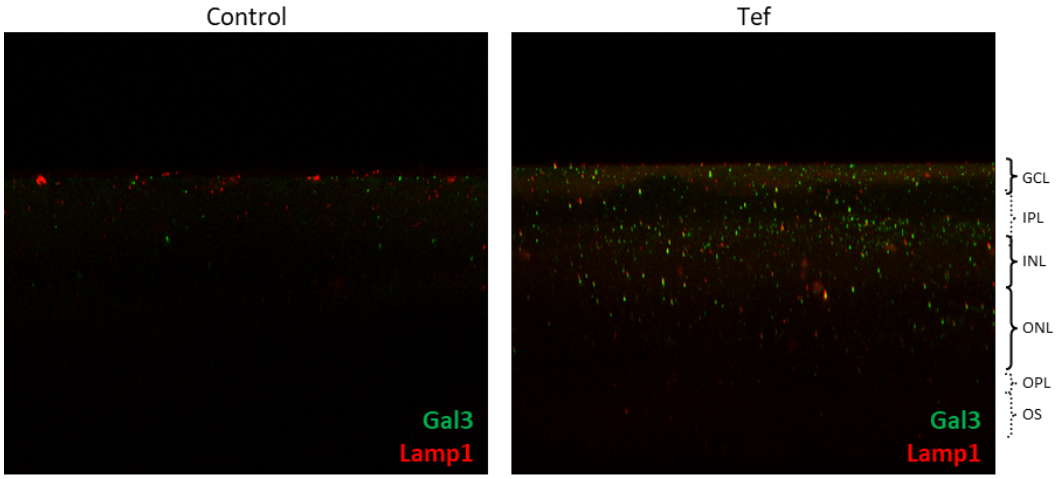

Figure 4.18 Colocalization of Lamp1 and galectin-3 in slices of cultured retinas. Immunofluorescence for galectin-3 and Lamp1 was completed in retinas after 24 hours of terfenadine treatment. GCL, ganglion cell layer; IPL, inner plexiform layer; INL, inner nuclear layer; OPL, outer plexiform layer; ONL, outer nuclear layer; OS, outer segment.

The XZY layout leaded us to observe the immunofluorescence in every layer **(figure 4.18)**. The colocalization of galectin-3 and Lamp1 was observed in the ganglion cell layer in the control retina. Additionally, the staining of galectin-3 and lamp1 after terfenadine treatment was higher when the retinas were observed in XZY layout. Interestingly, terfenadine treatment is inducing galectin-3 colocalization with lysosomes, but it is only observed in slices. Subsequently, Rd10 animals were studied to conclude if galectin-3 was a precise method to study LMP in the retina system.

Immunofluorescence of galectin-3 was studied in retinas from Rd10 animals at postnatal day P20. Retinas were isolated, immunofluorescence was done and mounted retinas and retinal slices were observed in the confocal microscopy.

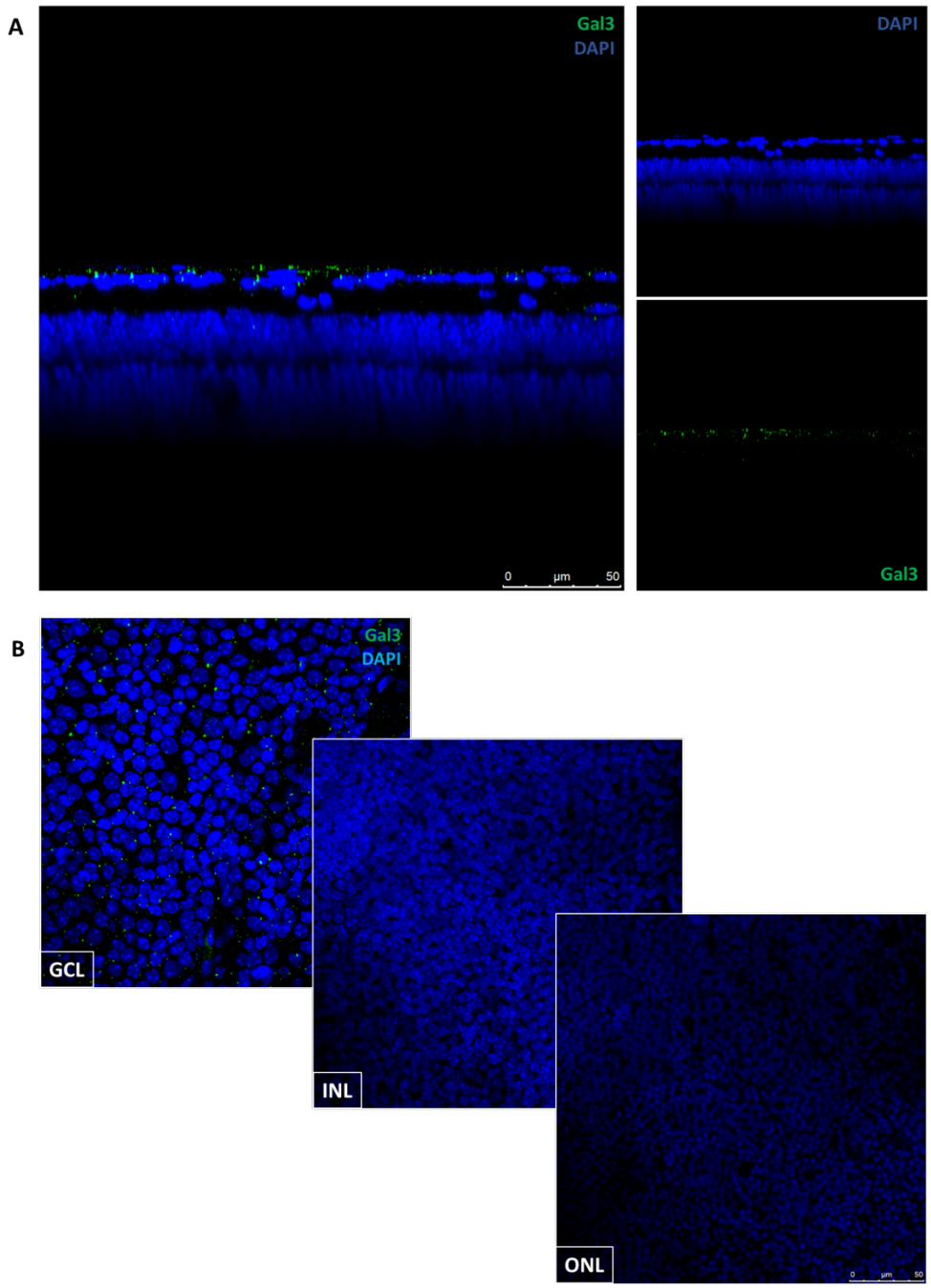

Figure 4.19 Immunofluorescence of galectin-3 in Rd10 retinas. Rd10 animal of post-natal day P20 were stained for galectin-3 (green) and DAPI (blue). **(A)** Slices of retinas from Rd10. **(B)** Pictures from GCL, INL and ONL. Scale bar 50 µm. Two experiments with 3 animals each.

Interestingly, the signaling of galectin-3 was observed in the GCL of the Rd10 retinas (**figure 4.19**). It has not been described that GCL presented LMP. In addition, ONL did not presented galectin-3 staining. Together these data show that galectin-3 cannot be used as a precise method to assess LMP in retinal tissue, as it is working in cells (see appart 4.2.1.1).

4.1.5 A23187-treated retinas: mimicking the rd10 model in wild-type retinas

4.1.5.1 Detection of cell death levels in A23187-treated wild-type retinas

The A23187 is a calcium ionophore procedent from the bacterial *Streptomyces chartreusensis*. A23187 interacts with Mn^{2+}, Ca^{2+} and Mg^{2+}, allowing them to cross the membrane to the cytoplasm increasing intracellular Ca^{2+} levels. In this thesis, A23187 has been used as a model for the Rd10, as it mimic the calcium increase found in these mice and in patients with *retinitis pigmentosa*. Calcium levels were studied in wild-type and A23187 treated retinas in comparison with Rd10 retinas.

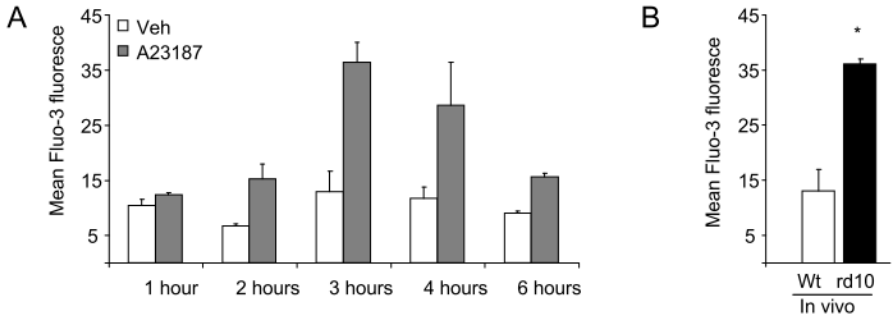

Figure 4.20 A23187 treatment induced similar levels of calcium as Rd10 retinas. (A) Flow cytometry analysis of calcium levels using Fluo-3AM in P20 wild-type retinas cultured for the indicated times with either vehicle (DMSO) or the calcium ionophore A23187. **(B)** P20 Wt and rd10 retinas were incubated in parallel with Fluo-3AM for comparison. *p<0.05, n=4.

A23187 treatment was inducing similar calcium levels as in Rd10 retinas **(figure 4.20)**. After this result, cell death levels were studied by TUNEL reaction and compare it with the levels in the Rd10 retinas at the peak of cell death. For this aim, wild-type retinas were treated with A23187 for 24 hours. After that, TUNEL reaction was carried out.

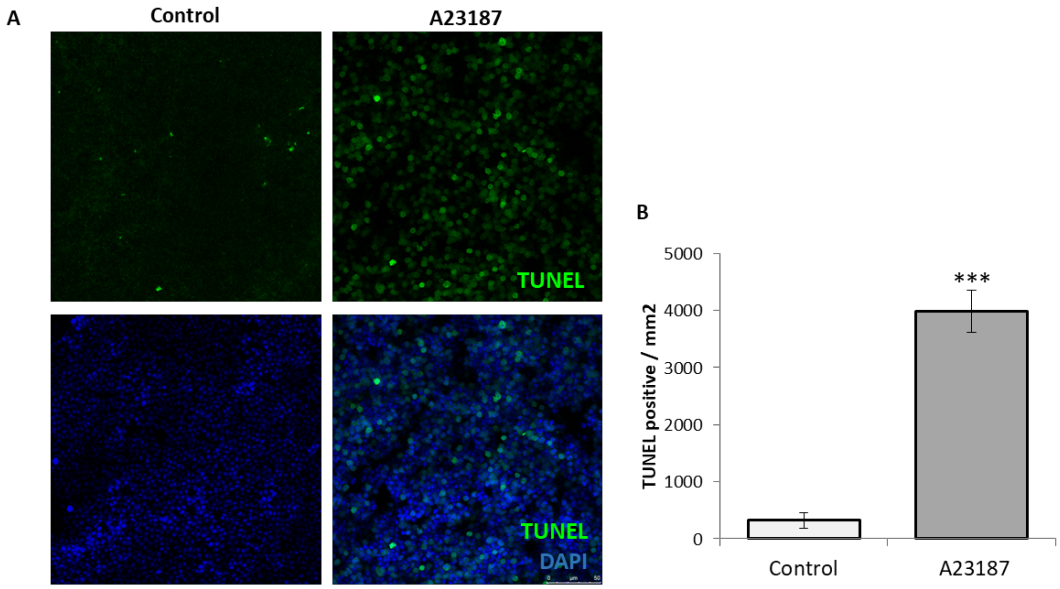

Figure 4.21 A23187 treatment is inducing cell death in wild-type retinas after 24 hours. (A) TUNEL reaction in mounted retinas. Scale bar 50 µm. **(B)** Quantification of TUNEL positive cells. Mean ± SEM of 4 retinas per condition of 4 independient experiments. (*** $p<0.001$). Student´s test.

A23187 treatment in retinas was inducing cell death in the wild-type retinas in a significative manner (**figure 4.21A and 4.21B**).

4.1.5.2 Autophagy blockade in A23187-treated wild-type retinas

Because of the autophagy blockade in the Rd10 retinas, autophagy protein levels were studied in A23187-treated retinas. For that aim, retinas from wild-type animals of postnatal day 20 were isolated and cultured for 24 hours with 5µM A23187. The contralateral retinas were cultured with protease inhibitors (Pepstatin A, E64d and Leupeptin) in order to measure autophagy flux. After the culture, the immunoblotting of autophagy-related proteins was developed.

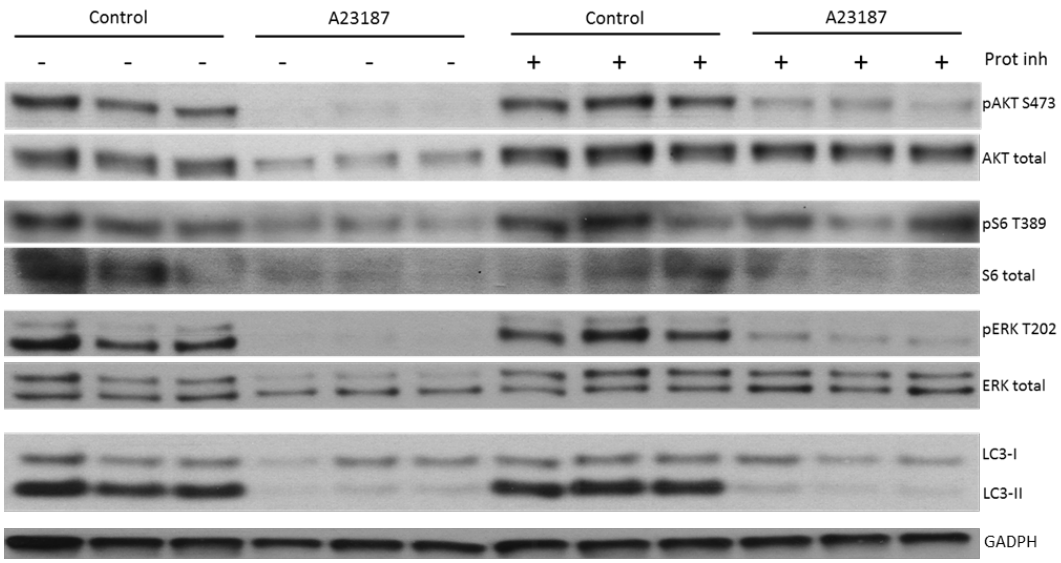

Figure 4.22. A23187 was inducing a decrease in autophagy-related proteins levels in wild-type retinas. Western blot from retinas of postnatal day 20 after 24 hours of A231287 treatment. Every lane represents one retina from different animals. The protease inhibitor treatment was done with retinas from the same animal. This is a representative image of three different experiments where 9 animals were used in total. "Prot inh": protease inhibitors.

A23187 treatment induced a decrease in LC3-II (**figure 4.22**), indicating that A23187 induces an autophagy blocked. Indeed, LC3-II reduction is still present in the combined treatment of A23187 and proteases inhibitors, demonstrating that autophagy flux is blocked with A23187. In conclusion, A23187-treatment induces basal autophagy and autophagy flux blocked, similarly to the phenotype observed in the Rd10. Additionally, A23187 treatment affected to the AKT and ERK protein levels. The decrease of protein levels of AKT and ERK could be related with the decrease of cellular viability, as it has been demonstrated in the section 4.1.6.1. Furthermore, A23187 treated retinas presented an increase in p-S6 protein level, which implicate an autophagy blockade (**figure 4.22**). These results demonstrated that A23187 treatment induced autophagy blockade, in agreement to the Rd10 mouse model phenotype.

4.1.5.3 Lysosomal leackage in A23187-treated wild-type retinas

To address if the A23187 treatment in the wild-type retinas was inducing LMP we next assessed cathepsin B activity. Wild-type retinas were treated with A23187 for 24 hours. After the treatment, retinas were stained with Magic Red, mounted and studied in confocal microscopy.

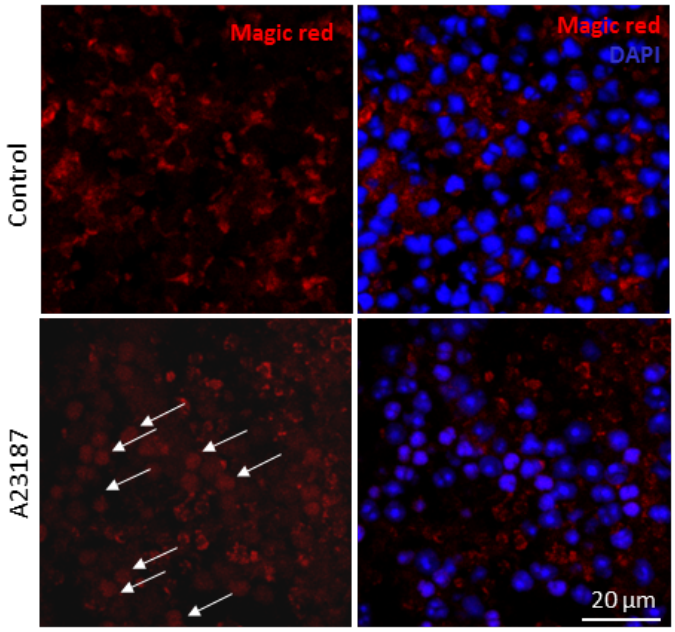

Figure 4.23. Study of the cathepsin B activity in A23187 treated retinas. Images from confocal microscopy from wild-type retinas after 24 hours of A23187 treatment stained with Magic Red (red) and DAPI (blue). White narrows indicate cytoplasmic magic red staining. Bar scale 20 µm.

A23187 treatment in wild-type retinas induced a nuclear Magic Red staining (**figure 4.23**). The cathepsin B activity was observed in the whole cell and not exclusively in the lysosomes, as in the control condition. These results suggested that A23187 treatment was inducing LMP in the wild-type retinas.

4.1.5.4 Autophagy modulation in A23187-treated wild-type retina

The A23187 treatment was a worthy model to try to find cell death inhibitors. To investigate the role of autophagy in the photoreceptor cell death, wild-type retinas were treated at the same time with A23187 in the absence or the presence of protease, using calpain inhibitor (ALLN) or cathepsin inhibitors (E64-d or L/P).

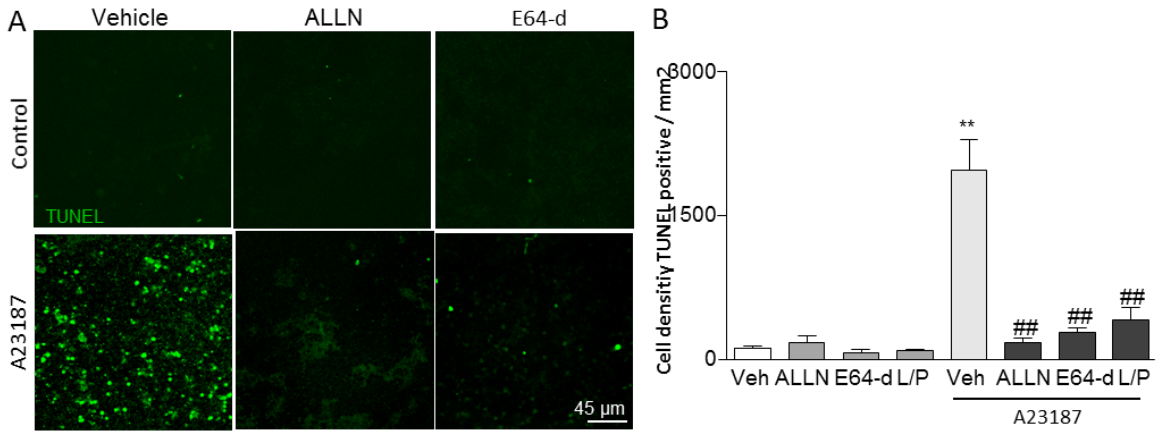

Figure 4.24 Calpain and cathepsin inhibition rescued from the A23187-induced cell death. (A) TUNEL staining in wild-type cultured retinas after 24 hours of A23187 in the presence or absence of calpain inhibitor (ALLN), cathepsin B, L and H inhibitor (E64-d) and the combination of cathepsin inhibitors (Leupeptin A and Pepstatin A). **(B)** Quantification of TUNEL-positive cells. Mean ± SEM of three independent experiments is shown. (** p<0.001 to the control; ## p<0,001 referred to the vehicle of A23187).

Interestingly, after 24 hours of treatment with A23187 in presence of protease and calpain inhibitors, the level of cell death was rescue in comparison with the same treatment in the absence of protease or calpains inhibitors (**Figure 4.24A** and **4.24B**). Similarly, wild-type retinas were treated in combination with A23187, the autophagy inductor rapamycin, in combination with protease inhibitor; and the autophagy inhibitor wortmanin. Staining of TUNEL positive cells was carried out after 24 hours of treatment of A23187 in presence or absence of rapamycin or wortmanin.

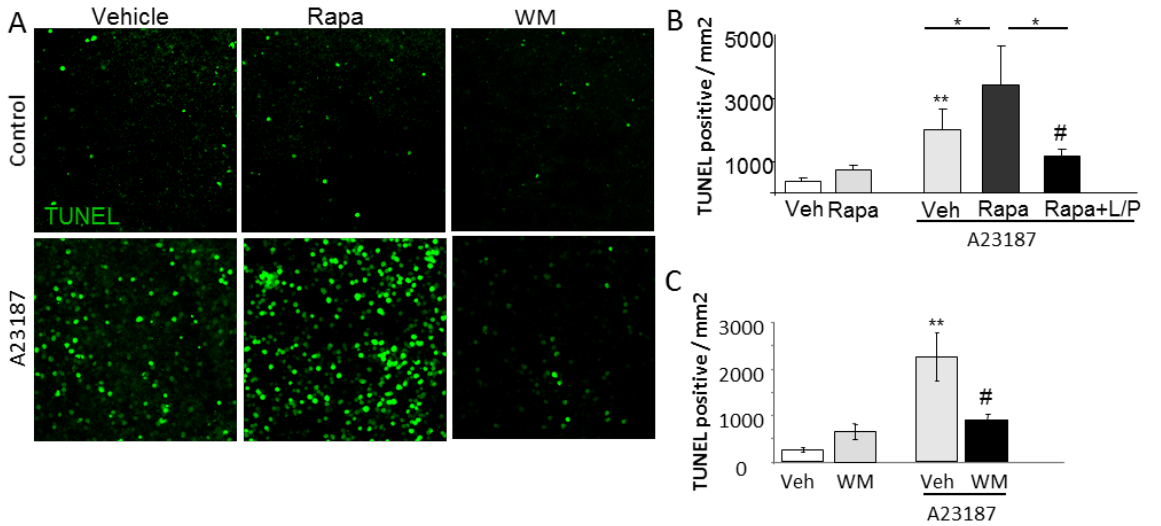

Figure 4.25. Autophagy modulation after A23187-induced cell death. (A) TUNEL staining of wild-type retinas after 24 hours of treatment with A23187, rapamycin, rapamycin, Leupeptin A and Pepstatin A, and wortmanin. **(B)** Quantification of TUNEL positive cells for the treatment of A23187 and rapamycin combination. **(C)** Quantification of TUNEL positive cells after 24 hours of treatment of A23187 and wortmanin. Mean ± SEM represented.

Remarkably, autophagy induction was detrimental in the A23187-treated model. The activation of autophagy with rapamycin in the A23187 model was increasing the photoreceptor cell death (**figure 4.25A** and **4.25B**). More interestingly, the presence of protease inhibitors (Leupeptin A and Pepstatin A) was able to prevent the induction of cell death after rapamycin and A23187 treatment (**figure 4.25B**). Whereas, inhibition of autophagy with wortmanin was rescuing from the cell death induced by A23187 (**figure 4.25C**).

Together, these data suggest that increasing autophagy by rapamycin treatment in the A23187 model was increasing cell death levels. However, autophagy blockade by using wortmanin was decreasing cell death levels. Additionally, the increase in cell death with rapamycin was block by using cathepsin inhibitors (L/P).

4.1.6 Autophagy induction increase photoreceptor cell death

4.1.6.1 Autophagy induction by rapamycin

Due to the results observed in the modulation of autophagy in the A23187-treated wild-type retinas, Rd10 retinas were treated *in vivo* with rapamycin. For that aim, animals from postnatal day P13 were injected with intraperitoneal injections for 7 days with rapamycin (10 mg/kg). When the animals were at postnatal day P23, they were sacrificed, retinas isolated and TUNEL reaction was done.

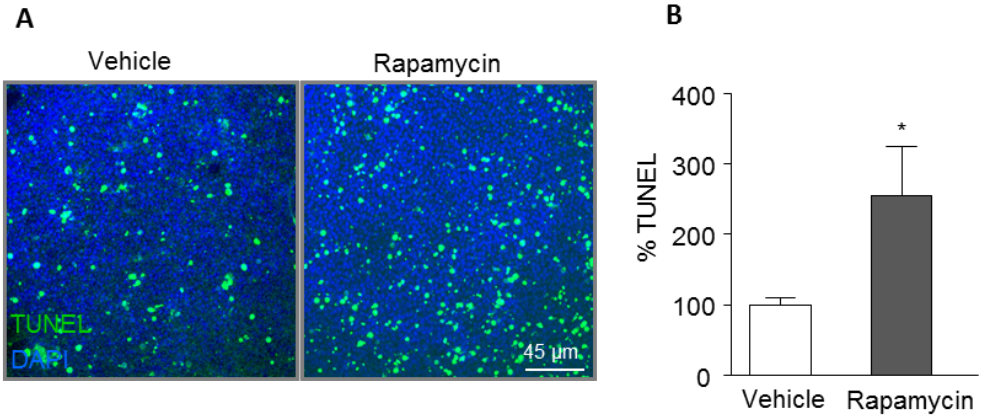

Figure 4.26. Autophagy activation increased TUNEL in Rd10 retinas. (A) TUNEL staining of Rd10 retinas after 10 days of rapamycin treatment. **(B)** Quantification of the percent of TUNEL positive cells. Mean ± SEM represented. (* $p < 0.05$).

Interestingly, autophagy induction with rapamycin treatment was increasing the cell death in the Rd10 mouse model (**figure 4.26A** and **4.26B**). To avoid the response due to the inhibition of mTOR with the rapamycin treatment, Rd10 animals were injected intravitreously with trehalose, an mTOR-independent autophagy inductor. Sucrose was injected as control. For that experiment, Rd10 animals from postnatal day P20 were injected with trehalose and sacrificed at P22. Retinas were isolated and TUNEL reaction was carried out.

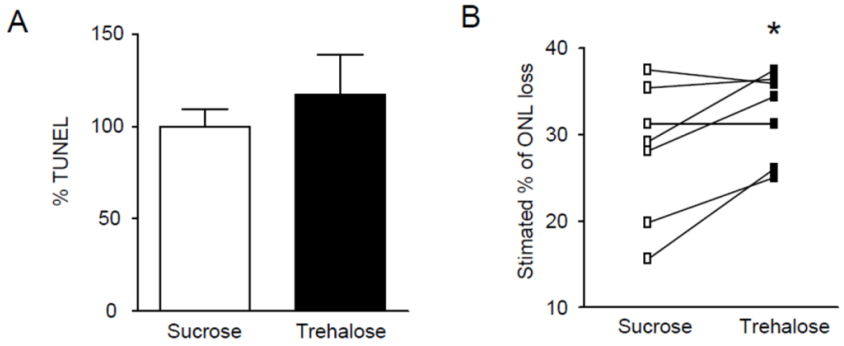

Figure 4.27. Autophagy induction did not increased TUNEL, but increase ONL loss in Rd10 retinas. (A) Quantification of the percent of TUNEL positive cells. Mean ± SEM represented. **(B)** Representation of the percent of ONL loss in the retinas. Mean of every retina represented. (* $p<0.05$). 7 animals used in 2 independent experiments. Contralateral eyes were treated with each drug.

The percent of TUNEL was not rescue but the percent of the ONL loss was higher after the trehalose injections (**figure 4.27A** and **4.27B**). In summary, Rd10 retinas were more sensible to the effects of autophagy induction and these effects were mTOR independent.

4.1.6.2 Autophagy blockade with lysosomal inhibition treatment

To address that the autophagy was being detrimental in the Rd10 retinas, autophagy inhibition was studied in the Rd10 mouse model. For that aim, intreavitreal injections with 80 µM ALLN and 400 µM Leupeptin A and 40 µg/ml Pepstatin A were carried out.

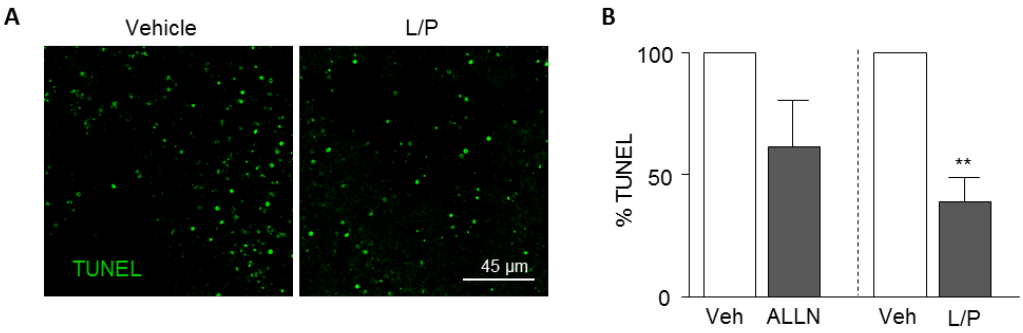

Figure 4.28. Autophagy inhibition decreased cell death in Rd10 retinas. (A) TUNEL staining of Rd10 retinas after Leupeptin A and Pepstatin A treatment. **(B)** Quantification of the percent of TUNEL positive cells. Mean ± SEM represented. (** $p<0.01$).

Finally, Rd10 retinas presented an ameliorated phenotype after the ALLN and Leupeptin A and Pepstatin A treatment *in vivo* (**Figure 4.28)**. In conclusion, these data suggest that blocking cathepsin activity was rescuing from photoreceptor cell death. We hypothethized that it is late for calpain inhibition to rescue cell death.

4.1.7 HDAC inhibition as a new therapy for *Retinitis pigmentosa*

4.1.7.1 Modulation of deacetylates: Trichostatin A

The relation between histone deacetylases (HDAC) and autophagy is under current investigation (Li and Zhu, 2014). To address if the modulation and inhibition of deacetylases was affecting to the Rd10 photoreceptor cell death, viability of wild-type retinas after 24 hours of treatment with A23187 in presence or absence of the deacetylase inhibitor Trichostatin A (TSA) was studied. For that aim, TUNEL staining was done after the treatment and the TUNEL-positive cell was quantified.

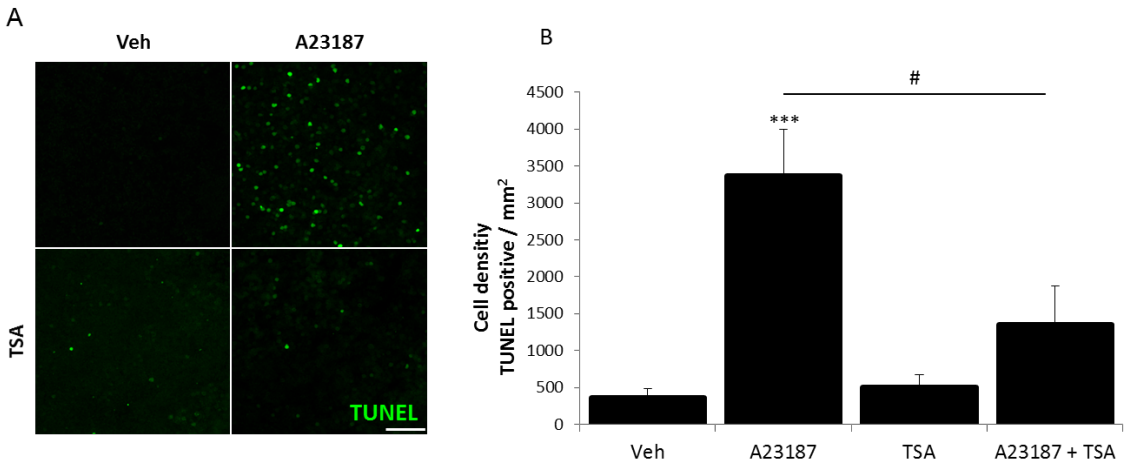

Figure 4.29 HDAC inhibition rescued from the A23187-induced cell death. (A) Representative confocal images from the ONL layer for TUNEL (green). Scale 50 µm. **(B)** Quantification of cell density of TUNEL positive cell. N=8 each condition, Student´s test (*** p<0.0001; # p<0.01).

TSA treatment rescued from the A23187 induced cell death in wild-type retinas (**figure 4.29**). So therefore, TSA was able to inhibit the cell induced by the calcium entrance to the photoreceptor. To solve if this rescue of the A23187-induced cell death was due to the modulation of autophagy, wild-type retinas after the combined treatment were studied by western blot technique.

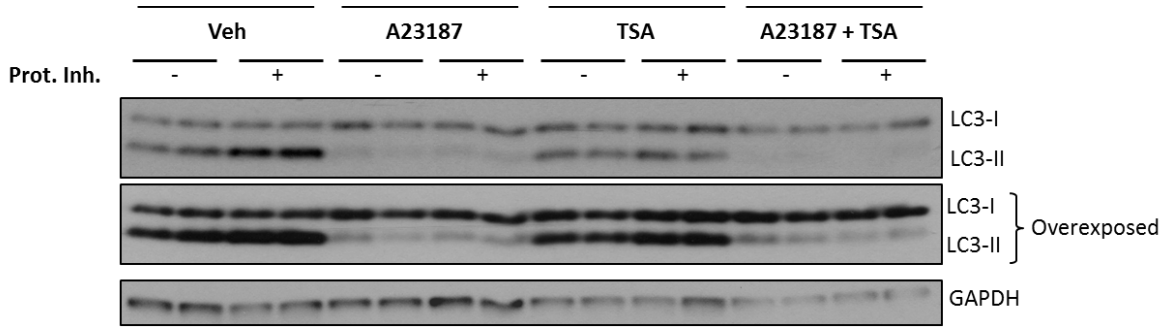

Figure 4.30 TSA do not restore the autophagy basal, neither autophagic flux levels after A23187-induced cell death. Immunoblots from retinal extracts after 24 hours of A23187 in presence or absence of TSA.

Interestingly, TSA was not triggering autophagy in the wild-type retinas. Indeed, TSA was decreasing the formation of LC3-II in wild-type retinas after proteases inhibitors (**figure 4.30**). This result agreed with the improvement of the Rd10 retinas when autophagy flux was blocked. In addition, retinas from Rd10 animals at postnatal day P20 were treated with TSA for 24 hours. After the culture, retinas were fixed and TUNEL staining was carried out.

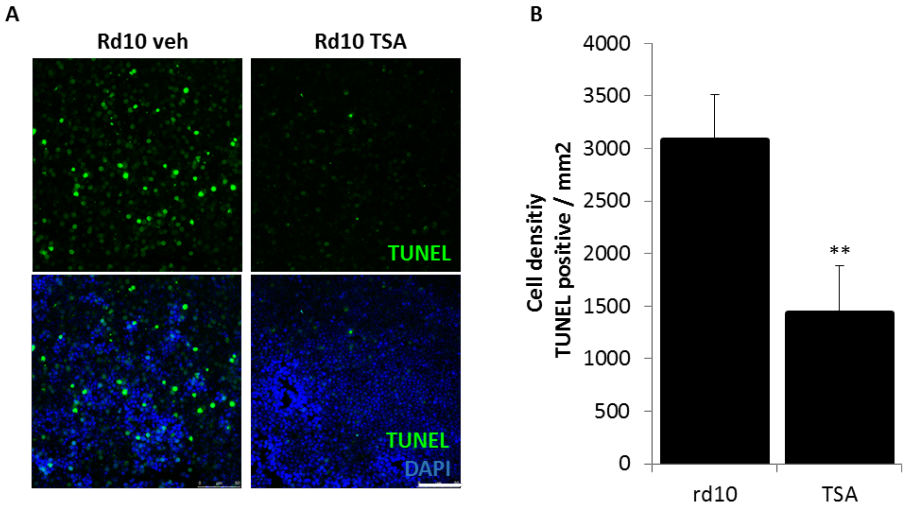

Figure 4.31 HDAC inhibition is rescuing from the photoreceptor cell death in Rd10 mouse model. (A) Representative confocal images from the ONL layer for TUNEL (green). Scale 50 µm. **(B)** Quantification of cell density of TUNEL positive cell. N=8 each condition, Student´s test (*** $p<0.0001$; # $p<0.01$).

Interestingly, photoreceptor cell death was lower after the treatment with TSA (**figure 4.31**). After these results, study of the mayor autophagy-related proteins was done. For that goal, Rd10 retinas of post-natal day P20 were treated with TSA for 24 hours and an immunoblotting was carried out from the retinal extracts.

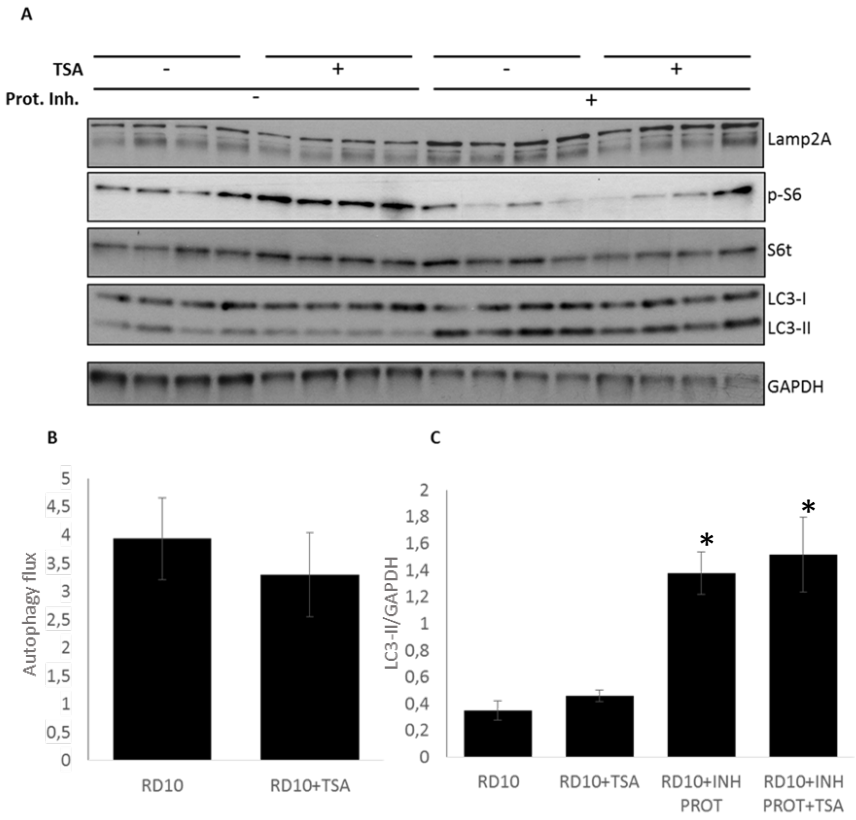

Figure 4.32 Study of the basal autophagy and autophagy flux in Rd10 retinas after TSA treamtn. (A) Immunoblots from Rd10 retinal extracts after 24 hours of TSA. **(B)** Quantification of autophagy flux after the treatment with TSA. Autophagy flux was studied by dividing LC3-II/GADPH and then the sample with protease inhibitor divided by the control sample. **(C)** Study of the LC3-II protein levels after the treatment with TSA. Mean ± SEM of two independent experiments is shown. T-Student, * p-value < 0.05.

After 24 hours of inhibition of HDAC in the Rd10 retinas, no changes in the autophagy-related proteins was observed (**figure 4.32A**). Moreover, no differences were observed in the autophagy flux between vehicle and TSA treatment (**figure 4.32B**), and no differences in the LC3-II protein levels (**figure 4.32C**).

Additionally, we treated the animals with TSA *in vivo*. Rd10 animals were injected intravitreously at postnatal day P20. Animals were sacrified at postnatal day P22 and retinas were isolated. After fixing, TUNEL reaction was done and images were taken with confocal microscopy.

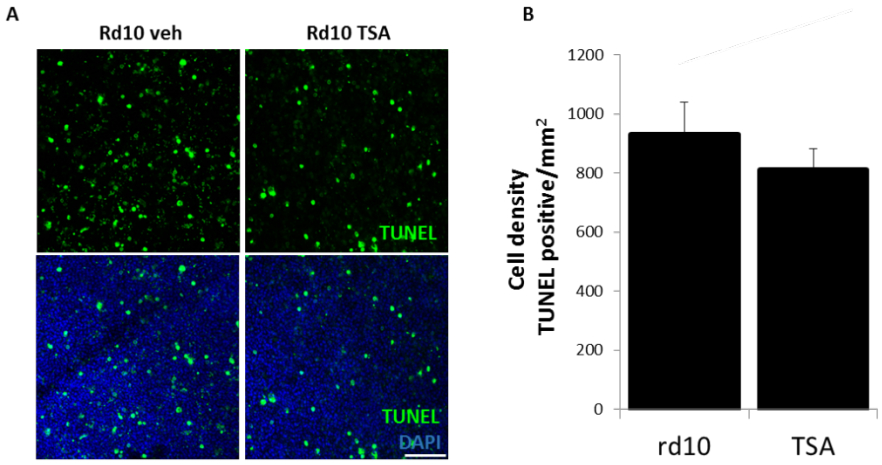

Figure 4.33 HDAC inhibition do not rescue from cell death in Rd10 retinas. Rd10 animals were injected with TSA and vehicle. After two days, retinas were isolated. **(A)** Representative images of TUNEL staining from ONL layer of TUNEL (green) and nuclei (blue). Scale bar 50 µm. **(B)** Quantification of TUNEL positive cells**.** Nine animals each condition in total.

No differences in the photoreceptor cell death were observed after the intravitreous injection with TSA (**figure 4.33A and 4.33B**). TSA was able to rescue in the explants *ex vivo* but no in the animals *in vivo*. This could be explained due to the difficulties of the intravitreous injections.

4.2 PHARMACOLOGICAL LYSOSOME-DEPENDENT CELL DEATH

Due to the induction of cell death in the Rd10 mouse model photoreceptors when the animals were treated with rapamycin and trehalose, and the fact that autophagy was blocked before neurodegeneration, the molecular relation between autophagy and lysosomal damage was further studied. For that aim, lysosomal damage and lysosome-dependent cell death was studied *in vitro* in autophagy-deficienct cell lines. Cationic amphiphilic drugs (CADs) were used as a model to trigger lysosomal damage and LMP. CAD treatment promotes the release of the acid sphingomyelinase (ASM) from the internal lysosomal membrane to the lysosomal lumen, inducing ASM degradation of the acid sphingomyelinase. This degradation sensitizes lysosomes to be more instable, inducing LMP (Petersen et al., 2013).

4.2.1 Cationic amphiphilic drugs (CADs) as a model of lysosomal damage

4.2.1.1 CADs induce cell death in mouse embryonic fibroblasts (MEFs)

Several CADs were used to determine cell death in mouse embryonic fibroblast (MEFs). We used: desloratadine, ebastine, loratadine, siramesine and terfeneadine. The detergent Leu-Leu methyl ester hydrobromide (LLOMe) and hydrogen peroxide, t-butyl peroxide were used as positive controls for cell death. Cells were seeded in 96-well plates, the day after the cells were treated with the different compounds at the indicated doses and propidium iodide incorporation was assesed after 16 hours. The plate was run in Celigo machine and percent of propidium iodide positive cells was graphed.

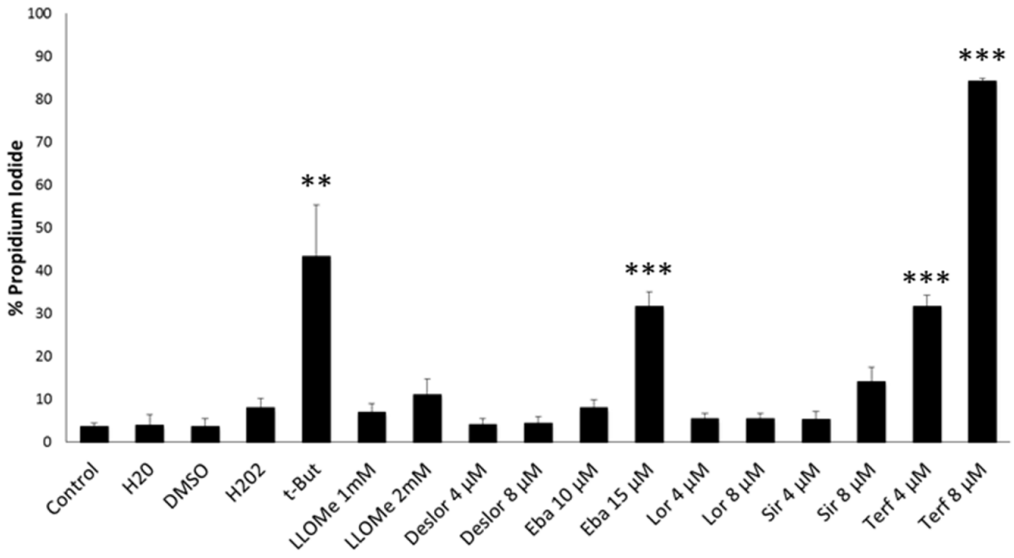

Figure 4.34. MEFs were used to evaluate cell death after CADs treatment. MEFs were seeded and treated for 16 hours with several CADs. Cells were stained with propidium iodide and Celigo analyze was

carried out. Four independent experiments were included in this graph. Deslor: desloratadine; Eba: ebastine; Lor: Loratadine; Sir: siramesine; Terf: terfenadine. T-Student. (** p-value<0.01; ***<p-value <0.001).

Several antihistamines were able to induce cell death after 16 hours, such as ebastine 15µM, siramesine 8µM, terfenadine 4µM and terfenadine 8µM (**figure 4.34**). Additionally, t-butyl peroxide 150µM was able to induce almost 50% of cell death. Interestingly, LLOMe was not able to induce cell death in MEFs after 16 hours.

4.2.1.2 Tefernadine triggers lysosomal permeabilization in MEFs

We selected terfenadine 8µM for subsequent studies as it induces moderate levels of cell death. To study the lysosomal damage leaded by terfenadine, galectin-3 immunofluorescence was carried out as described by Dra. Jäättelä's group (Aits et al., 2015). For that aim, MEFs were seeded in coverslips and treated with terfenadine 8 µM for 3, 6, 18 and 24 hours. After that, immunofluorescence of galectin-3 was carried out. Percentage of cells with galectin-3 puncta was quantified and ploted.

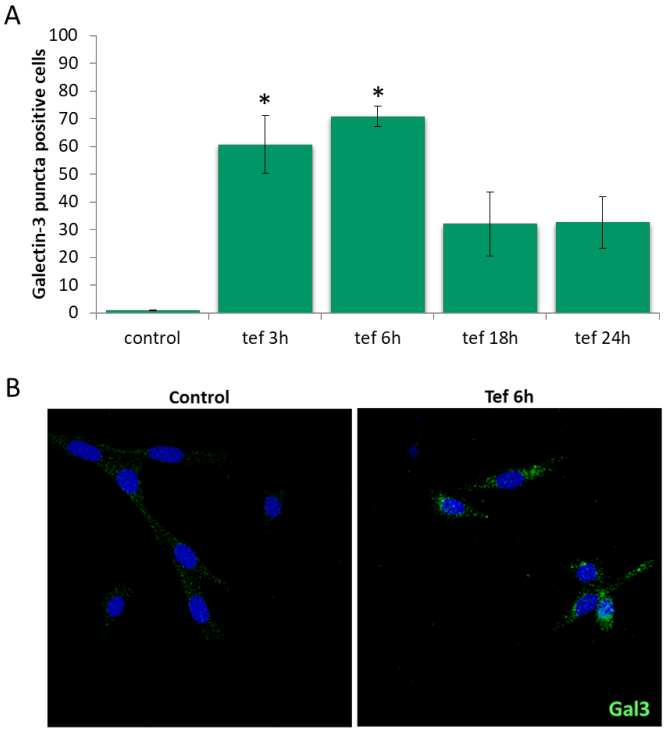

Figure 4.35. Terfenadine induces galectin-3 puncta in MEFs. (A) The graph represents the quantification of the percent of positive galectin-3 puncta cells. Three independent experiments. At least 200 cells per experiment were quantified. (B) Representative confocal images of galectin-3 immunofluorescence after 6 hours of terfenadine treatment. Tef: terfenadine. T-Student test. * p-value<0.05.

Quantification of galectin-3 puncta positive cells demonstrated a time-dependent response during terfenadine treatment. The staining with galectin-3 was higher in the first three hours of terfenadine treatment. Interestingly, this response decreased during long time of

terfenadine treatment (**figure 4.35A**). Representative images of galectin-3 are showed in **figure 4.35B**. Untreated cells present diffuse galectin-3 staining in the whole cytoplasm, while after 6 hours of terfenadine, galectin-3 was observed in bright puncta in the cytoplasm of cells.

4.2.1.3 Terfenadine induces cathepsin B release in MEFs

After LMP, cathepsin B can translocate to the cytoplasm and its diffuse staining can be used as a marker of LMP. The percentage of diffuse cathepsin B (outside lysosomes) was studied after terfenadine treatment. MEFs were seeded in coverslips and treated with terfenadine 8 μM for 3, 6, 18 and 24 hours. After that, immunofluorescence of cathepsin B was carried out and the percentage of cells with diffuse cathepsin B was quantified.

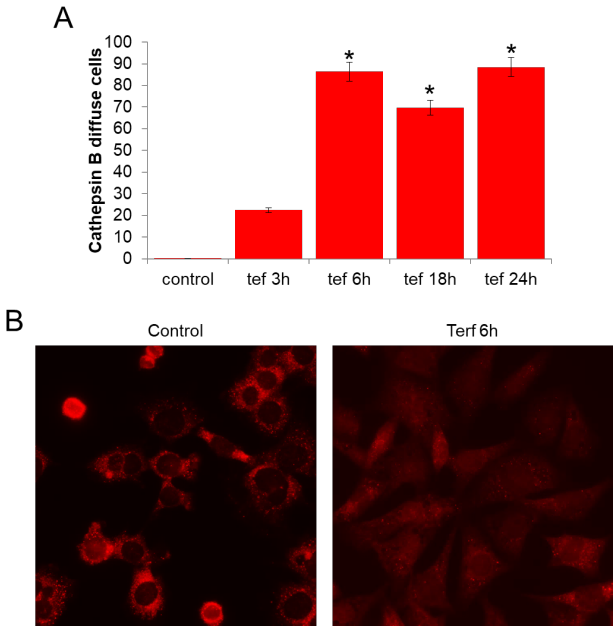

Figure 4.36. Terfenadine induces cathepsin B release in MEFs. (A) Percentage of cells with cathepsin B diffuse staining. The graph was done with three independent experiments. At least 200 cells per experiment were quantified. **(B)** Representative images of immunofluorescence of cathepsin B. In control condition, cathepsin B is observed in puncta (lysosomes) and the black hole of the nuclei can be observed; after 6 hours of terfenadine, most of cathepsin is observed in the whole cell, including nuclei. Tef: terfenadine. T-Student test. * p-value<0.05.

As it is observed in **figure 4.36A**, terfenadine treatment induced cathepsin B release in 80% of the cells after 6 hours. Moreover, 18 hours of terfenadine treatment showed a slight decrease in the percent of cells with cathepsin B release, but this percent increased after 24 hours of terfenadine. This result could suggest that cells are trying to recover from the cathepsin B release after terfenadine treatment. It could indicate that there are two waves of lysosomal damage. Moreover, cathepsin B can be observed in puncta in the control

cells, while the cells treated with terfenadine for 6 hours presented diffuse cathepsin B (**figure 4.36B).** This results demonstrate that terfenadine induce cathepsin B release, indicating lysosomal damage and LMP.

4.2.1.4 Terfenadine induces cell death in MEFs

In addition, quantification of nuclei was carried out to detect the effect of terfenadine treatment in cell viability. The same approach as section 4.2.1.1 and 4.2.1.2 was carried out. After the treatment, cells were stained with DAPI and number of rounded and non-fragmented nuclei was quantified.

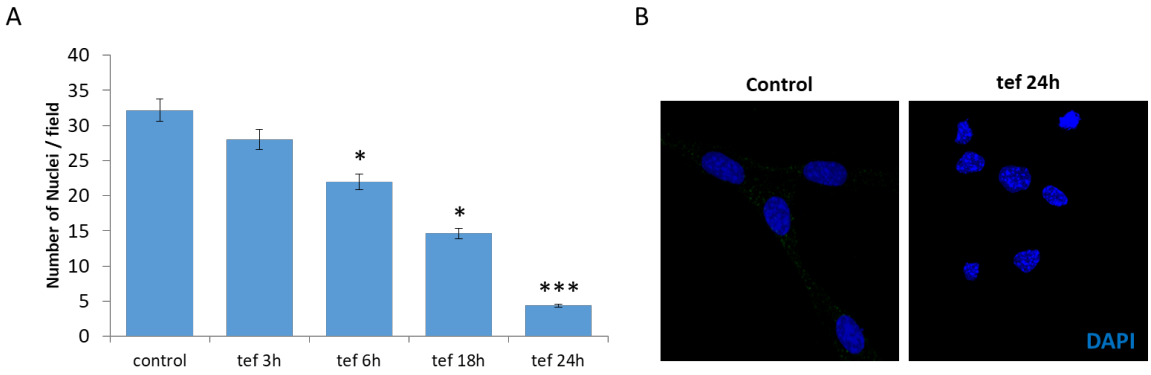

Figure 4.37. Terfenadine treatment induced cell death in MEFs. (A) Number of rounded nuclei per field. The graph was done with three independent experiments. At least 200 cells per experiment were quantified. **(B)** Representative images of DAPI in control condition and after 24 hours of terfenadine treatment. Tef: terfenadine. T-Student test. * p-value<0.05.

As it is observed in **figure 4.37A**, terfenadine treatment induced a decrease in the number of nuclei per field. This decline began after 3 hours of treatment and it diminished with time. After 24 hours of treatment, nuclei lost their contour and chromatin appeared fragmented, indicating instable chromatin in MEFs (**figure 4.37B**).

4.2.2 Autophagy-deficiency cell lines present lower lysosomal damage

4.2.2.1 MEFs Atg7-/- are more resistant after CAD treatment

After the develop of the techniques to study LMP in MEFs, the role of autophagy was studied after lysosomal damage with CAD treatment. For that aim, MEFs Atg7+/+ and Atg7 -/- were used to study viability after CAD treatment. First of all, we studied the autophagy induction after terfenadine treatment, to observe autophagy blockade in the

MEFs Atg7-/- and the accumulation of LC3-II due to the terfenadine-induced lysosomal inactivation.

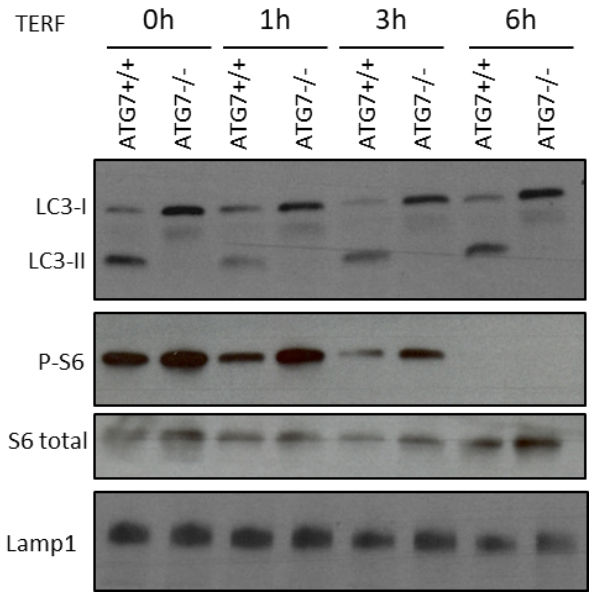

Figure 4.38. MEFs Atg7$^{-/-}$ do not present LC3-II. Western blot of MEFs Atg7 +/+ and Atg7-/- after 1, 3 and 6 hours of terfenadine.

As it shown in the **figure 4.38**, MEFs Atg7-/- did not present LC3-II in control situation as after terfenadine treatment. Interestingly, MEFs Atg7-/- presented unprocessed LC3, which was observed between LC3-I and LC3-II. MEFs Atg7+/+ presented a decrease of LC3-II after 1 and 3 hours of terfenadine treatment, which could suggest that autophagosomes are being degraded. Interestingly, an increase of LC3-II after 6 hours of terfenadine was observed, indicating autophagy blockade after that time. Both cell lines presented a decrease in the phosphorylation of S6 after 3 and 6 hours of terfenadine, suggesting an induction of autophagy. In conclusion, MEFs Atg7 -/- were not able to induce autophagy and terfenadine was blocking autophagy in MEFs Atg7-/- after 3 hours.

To study viability of MEFs cells after CAD treatment, 3000 cells per well were seeded in 96-well plates. The day after, treatment was carried out and propidium iodide was added to the cells after the treatments. The percent of cells with positive propidium iodide staining was quantified by Celigo and graphed.

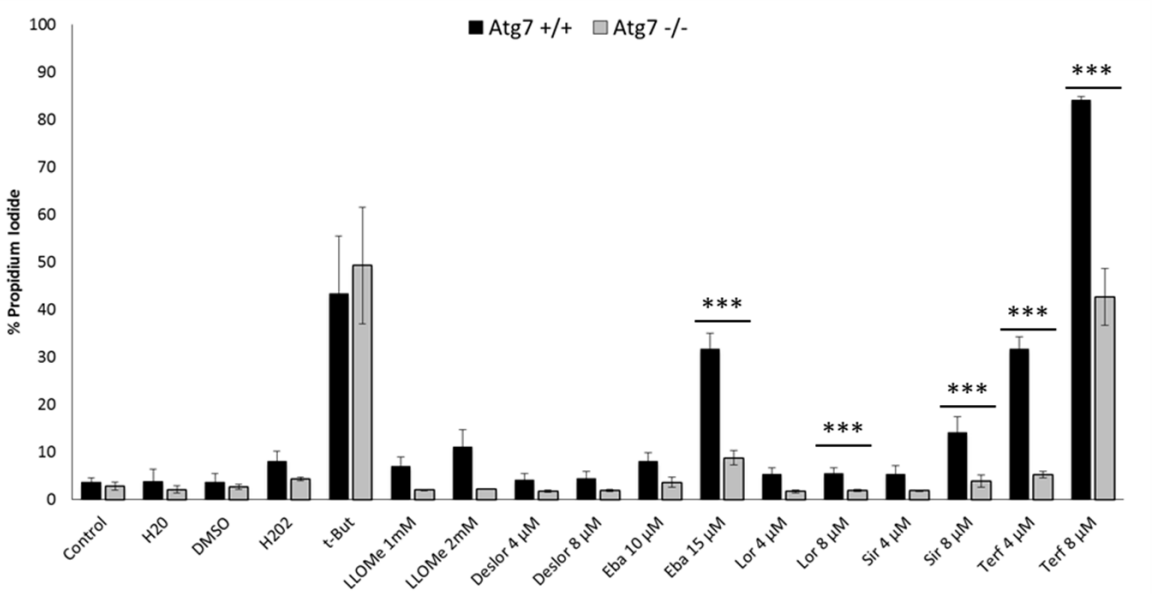

Figure 4.39. MEFs Atg7-/- are more resistant to CAD treatment. MEFs were seeded and treated for 16 hours with the indicated doses of CADs. Cells were then stained with propidium iodide and Celigo analyze was carried out. Four independent experiments were included in this graph. Deslor: desloratadine; Eba: ebastine; Lor: Loratadine; Sir: siramesine; Terf: terfenadine. T-Student test. *** p-value<0.001.

MEFs Atg7-/- presented higher viability after the treatment with ebastine 15µM, loratadine 8µM, siramesine 8µM and terfenadine 4 and 8 µM than MEFs Atg7+/+ (**figure 4.39**). Interestingly, the response with t-butyl peroxide was similar between both cell lines, which suggested that the differences observed in other treatment were not due to autophagy.

4.2.2.2 MEFs Atg7-/- presented less lysosomal damage

Next, MEFs Atg7 -/- were treated with terfenadine 8µM to understand how autophagy deficiency impacts the lysosomal damage. For that aim, MEFs Atg7-/- cells were treated and analyzed for galectin-3 immunofluorescence.

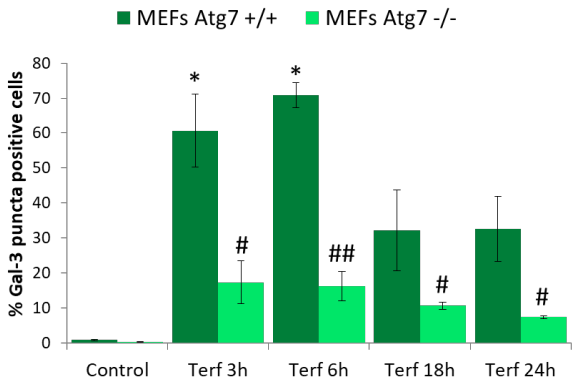

Figure 4.40. MEFs Atg7 -/- present less galectin-3 puncta positive cells than MEFs Atg7 +/+. Quantification of the percent of positive galectin-3 puncta cells. Three independent experiments. At least 200 cells per experiment were quantified. Terf: terfenadine. T-Student test. *, # p-value<0.05. #: refers to the comparation between MEFs Atg7+/+ and Atg7-/-.

Interestingly, MEFs Atg7 -/- presented a low percent of galectin-3 puncta positive cells in all the treatments studied in comparison with MEFs Atg7 +/+ (**figure 4.40**).

4.2.2.3 LMP and cathepsin B release in MEFs Atg7-/-

Similarly to the experiments of section 4.2.1.3, MEFs Atg7 -/- were compared with the MEFs Atg7 +/+ to observed differences in cathepsin B staining. For that aim, both MEF cell lines were seeded, treated with terfenadine at different times and cathepsin B immunofluorescence was carried out. Coverslips were observed under microscope and percent of cells with diffuse cathepsin B was counted.

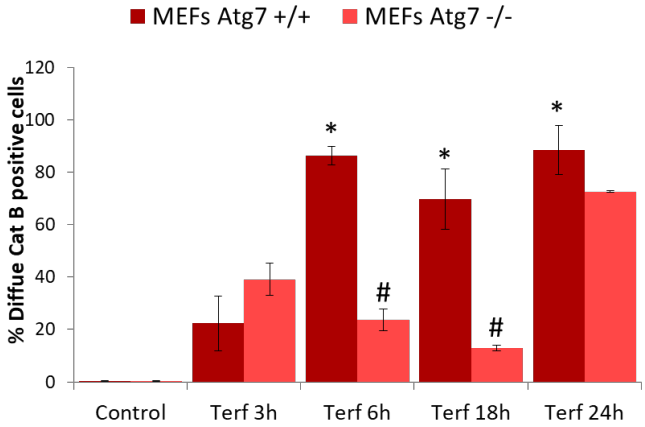

Figure 4.41. MEFs Atg7-/- present less cathepsin B release than MEFs Atg7 +/+. Percent of cells with cathepsin B diffuse staining. The graph was done with three independent experiments. At least 200 cells per experiment were quantified. Terf: terfenadine. T-Student test. *, # p-value<0.05. #: refers to the comparation between MEFs Atg7+/+ and Atg7-/-.

Surprinsinlgy, MEFs Atg7+/+ display lower percent of diffuse cathepsin B cells in comparison with MEFs Atg7-/- after 3 hours of terfenadine. At later time points, Atg7-/-

deficient cells displayed reduced diffuse cathepsin B staining in comparision to wt cells. (**figure 4.41)**. These results demonstrated that autophagy is implicated in the response of the cells against lysosomal damage, suggesting that autophagy is aggravating the situation after CAD treatment.

4.2.2.4 Viability with nuclei quantification after CAD treatment in MEFs

Finally, DAPI quantification was carried out after terfenadine treatment in MEFs Atg7 -/-. For that goal, same experiment as described in the appart 4.2.1.4 was carried out for the same hours. Nuclei quantification was completed.

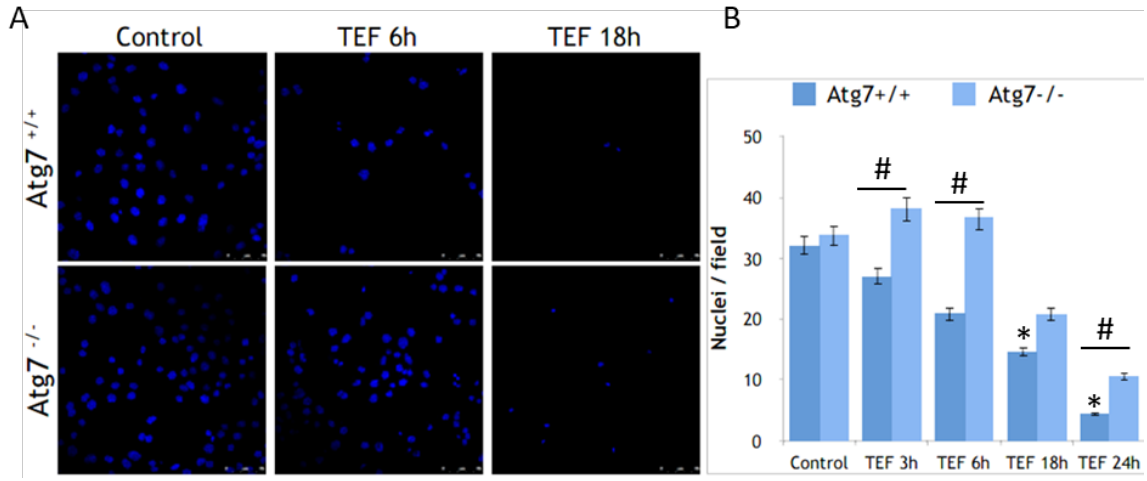

Figure 4.42. MEFs Atg7 -/- present delay cell death in comparison with MEFs Atg7 +/+. (A) Representative confocal images of nuclei after 6 and 18 hours of terfenadine treatment in MEFs Atg7 +/+ and Atg7 -/-. **(B)** Number of rounded nuclei per field. The graph was done with three independent experiments. At least 200 cells per experiment were quantified. Tef: terfenadine. T-Student test. *, # p-value<0.05.

Remarkably, MEFs Atg7 -/- presented more nuclei per field in comparison with MEFs Atg7 +/+ (**figure 4.42**). However, MEFs Atg7-/- presented a decrease in the number of nuclei/ field after 18 hours of terfenadine treatment, suggesting that MEFs Atg7-/- presented delay cell death.

4.2.2.5 Autophagy induction after terfenadine treatment

Additionally, autophagy was studied in both MEF cell lines after 16 hours of terfenadine treatment. For that aim, MEFs Atg7+/+ and Atg7-/- were seeded in coverslips. The day after, the cells were treated with terfenadine 8 µM. After 16 hours, coverslips were fixed and immunofluorescence of LC3 was carried out. Pictures were taken at confocal microscopy.

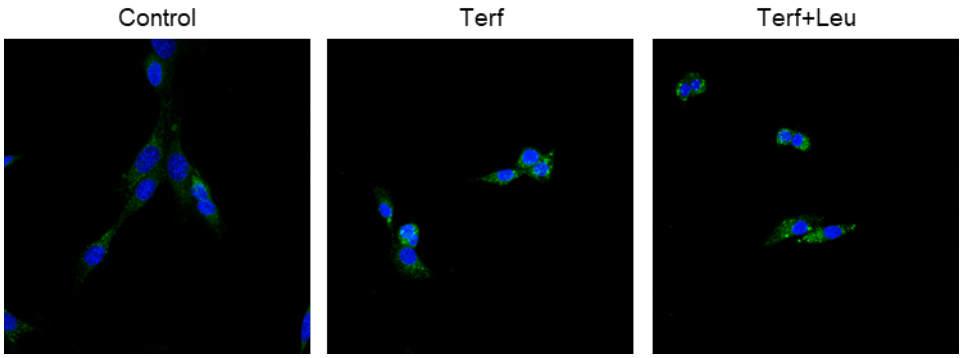

Figure 4.43. Terfenadine induced LC3 puncta in MEFs. Representative confocal images from MEFs treated with terfenadine for 16 hours. Scale 25 µm.

After 9 hours of terfenadine, MEFs Atg7+/+ presented LC3 puncta, suggesting autophagy activation (**figure 4.43**). Moreover, with the combined treatment of terfenadine and leupeptin, no increase of LC3 was observed, suggesting that terfenadine is activating autophagy but the autophagosomes are not being degraded.

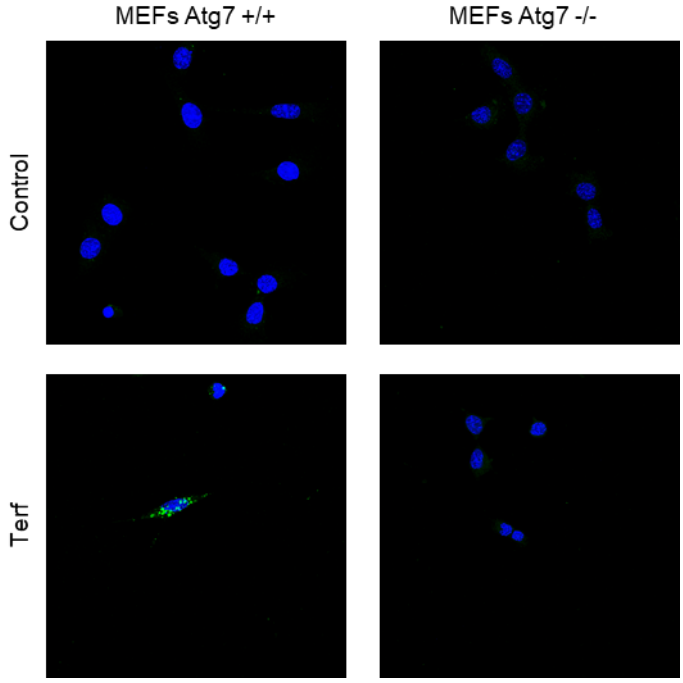

Figure 4.44. Terfenadine induced LC3 puncta in MEFs Atg7+/+, but not in MEFs Atg7-/-. Representative confocal images from MEFs treated with terfenadine for 16 hours. Scale 25 µm.

After 16 hours of terfenadine, MEFs Atg7+/+ presented LC3 puncta, suggesting autophagy activation (**figure 4.44**). As it was expected, MEFs Atg7-/- did not present LC3 accumulation due to the impossibility of autophagy induction due to the Atg7 deficiency.

4.2.2.6 Viability of cell lines deficient in MEFs Atg5-/-

To gain insight on the cytoprotective effect of Atg7-deficience after lysosomal damage, other autophagy-deficient MEFs was studied. MEFs Atg5-/- were seeded and treated with the CADs to study lysosomal damage. After that, propidium iodide was added to the wells and the plates were studied by Celigo. Percent of propidium iodide positive cells was represented.

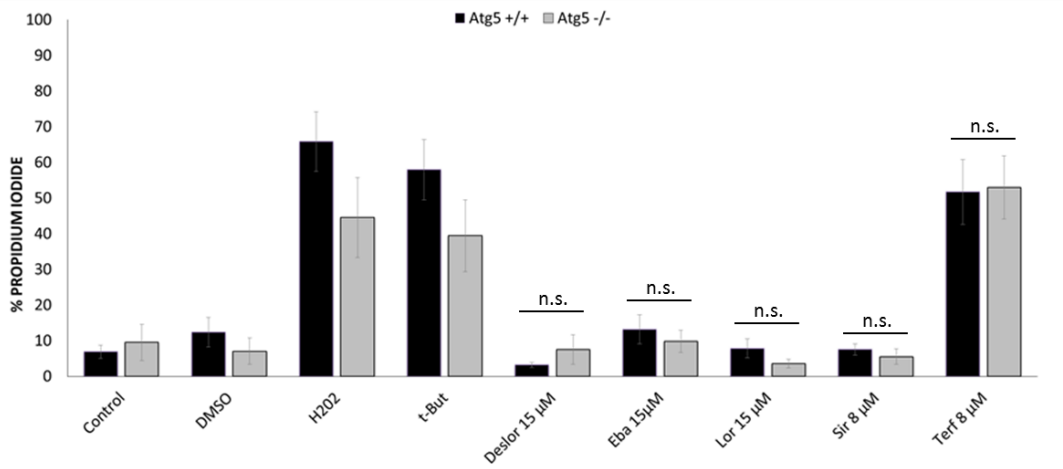

Figure 4.45. MEFs Atg5 -/- present similar viability in comparison with Atg5 +/+ after CAD treatment. MEFs were seeded and treated for 16 hours with several CADs. Cells were stained with propidium iodide and Celigo analyze was carried out. Five independent experiments were included in this graph. Deslor: desloratadine; Eba: ebastine; Lor: Loratadine; Sir: siramesine; Terf: terfenadine.

Surprisingly, the percentage of propidium iodide between MEFs Atg5+/+ and MEFs Atg5-/- was similar after the lysosomal damage (**figure 4.45**). These results could suggest that Atg7 deficiency could have a novel cytoprotective role during lysosome-dependent cell death.

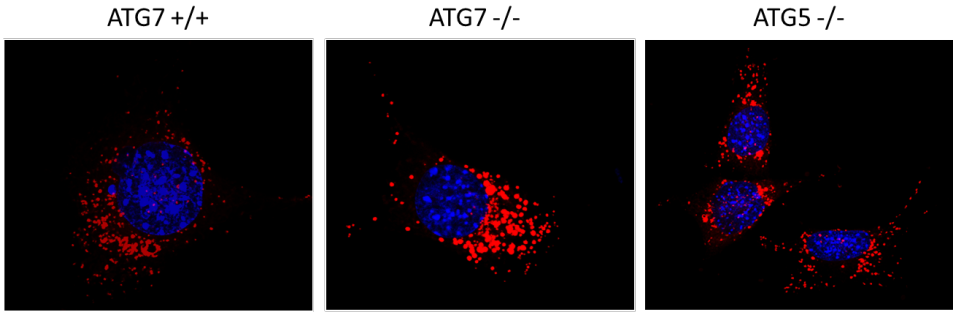

Figure 4.46. MEFs Atg5 -/- present LTR staining as MEFs wild-type. MEFs were seeded and staing with LTR. Pictures of MEFs Atg7+/+, MEFs Atg7-/- and Mefs Atg5-/- were taken. Scale 10 µm.

We decided to study lysosomal acidification in MEFs Atg5-/- to identify differences in lysosomal acification and localization. Interestingly, no differences were observed in comparison with MEFs wild-type (**figure 4.46)**. But, interestingly, MEFs Atg7-/- presented an increase in the staining in comparison with the other two cell lines.

4.2.3 ATG7-deficient cell lines presented differences in lysosomal characteristics

4.2.3.1 MEFs Atg7-/- present ultrastructural differences

Ultrastructural studies of MEFs were carried out to observe lysosomes. For that aim, cells were seeded in 6-well plates. Cells were fixed and observation of cells was carried out.

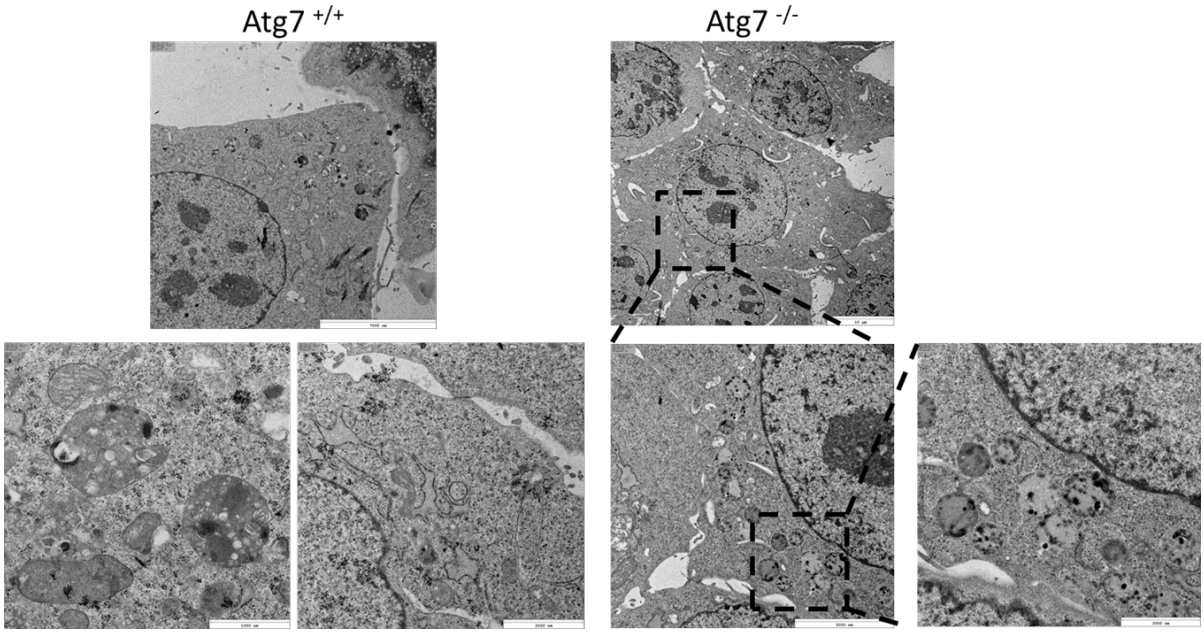

Figure 4.47. Electronic microscopy from MEFs Atg7 +/+ and Atg7 -/-. Magnification from the cytoplasm of both cell lines showing vacuoles.

The electronic microscopy observation suggest that MEFs Atg7-/- presented several vacuoles with electro-dense particles (**figure 4.47)**. Interestingly, these particles were not observed in MEFs Atg7+/+.

4.2.3.2 MEFs Atg7-/- present diffent lysosomal characteristics

To understand the possible role of Atg7 to induce cell death after CAD treatment, we first assessed lysosomal acidity staining the cells with lysotracker red in both MEFs Atg7 +/+ and MEFs Atg7 -/- under basal conditions. Moreover, lamp1 immunofluorescence was done to study lysosomal protein.

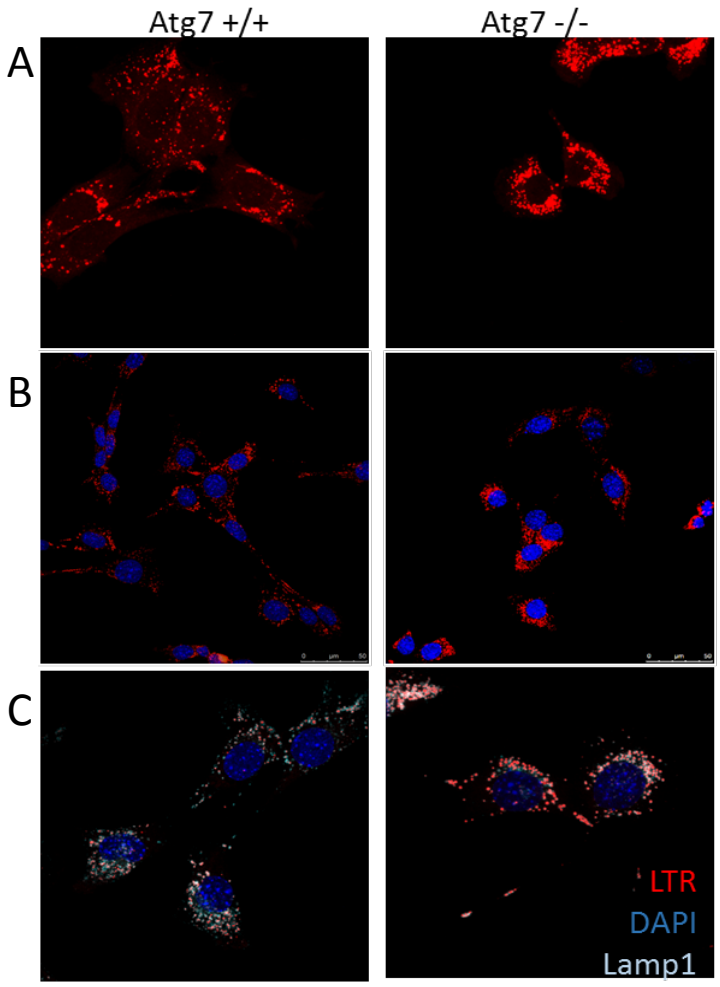

Figure 4.48. MEFs Atg7 -/- presented differential lysosomal characteristics. Lysotracker staining **(A and B)** and Lamp1 **(C)** immunofluorescence of MEFs Atg7 +/+ and Atg7 -/-. Representative confocal images. A and C, scale 10 µm. B, scale 25 µm.

Interestingly, lysosomes from MEFs Atg7 -/- appear to be closer to the nucleus. Additionally, lysotracker presented stronger staining in comparison with the MEFs Atg7+/+. More importantly, when lamp1 was studied in both cell lines, no differences were observed (**figure 4.48)**.

Then, lysotracker was studied after terfenadine treatment at different times in both cells lines. MEFs were seeded and treated with terfenadine 8 µM for 3, 6, 9, 18 and 24 hours. After those hours, lysotracker was added to the wells to stain the acidic lysosomes. Coverslips were fixed and cells were observed at confocal microscopy. For this approach, lysotracker was added to the well after terfenadine treatment.

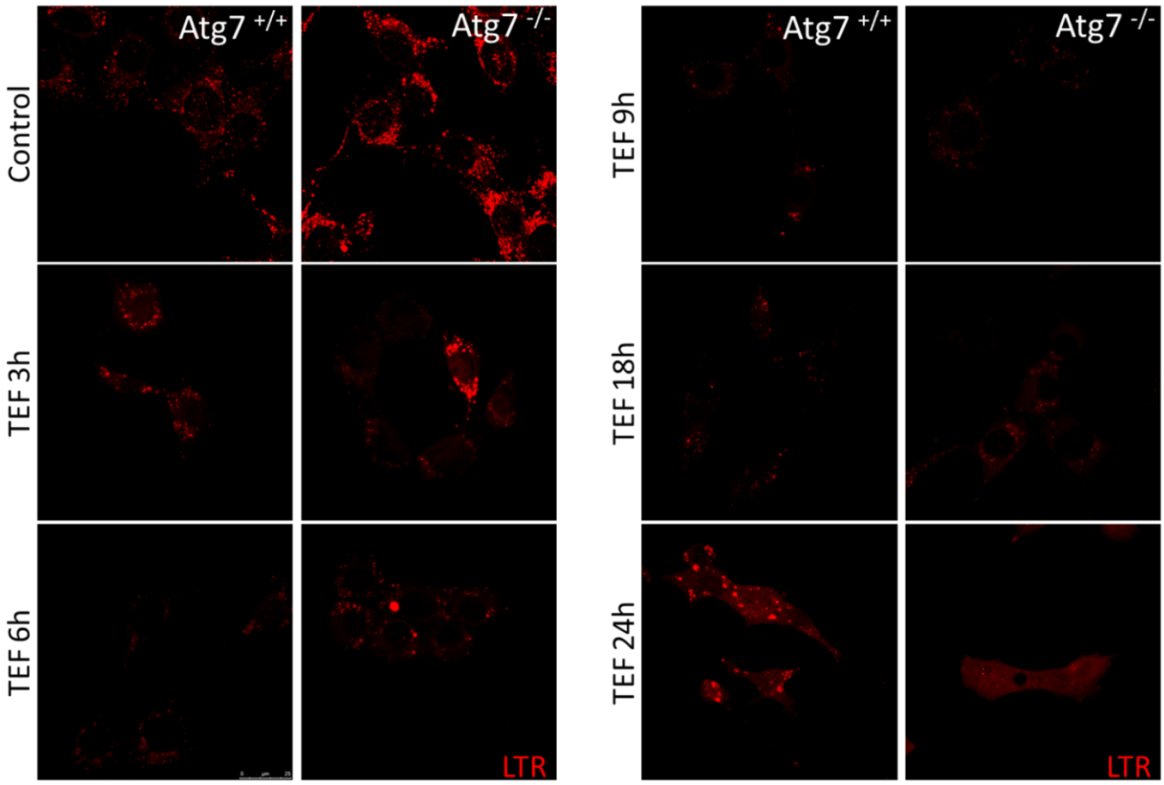

Figure 4.49. MEFs Atg7+/+ and Atg7-/- presented differential lysosomal pH after terfenadine treatment. MEFs were seeded and treated with terfenadine 8 µM for 3, 6, 9, 18 and 24 hours. After those hours, lysotracker was added to the wells to stain the acidic lysosomes. Representative images of three different experiments are shown.

Remarkably, lysotracker staining was stronger in MEFs Atg7-/- during more time than in MEFs Atg7+/+, at least, 6 hours after the treatment (**figure 4.49**). Interestingly, MEFs Atg7+/+ cell line was able to present lysotracker 24 hours after the treatment, although the lysotracker was missed at shorter times of terfenadine treatment. This result promoted a novel question: whether the MEFs Atg7+/+ are able to induce lysosomal biogenesis after terfenadine treatment? To resolve this question, lysotracker was added at the beginning of terfenadine treatment. Additionally, lamp1 immunofluorescence was done in the same coverslips. With this experimental approach, the lysosomes that maintain the acidic pH would be there during the complete treatment, while the novel lysosomes would be observed in red in the previous experiment. Additionally, the novel lysosomes would be stained with Lamp1.

A

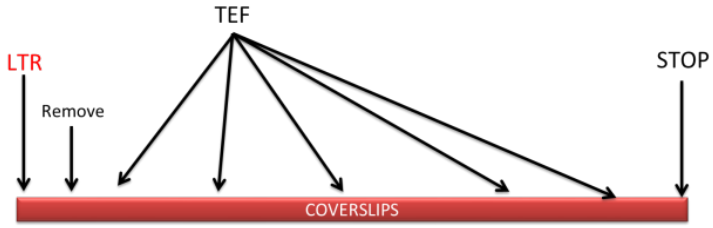
TEF
LTR
Remove
STOP
COVERSLIPS

B

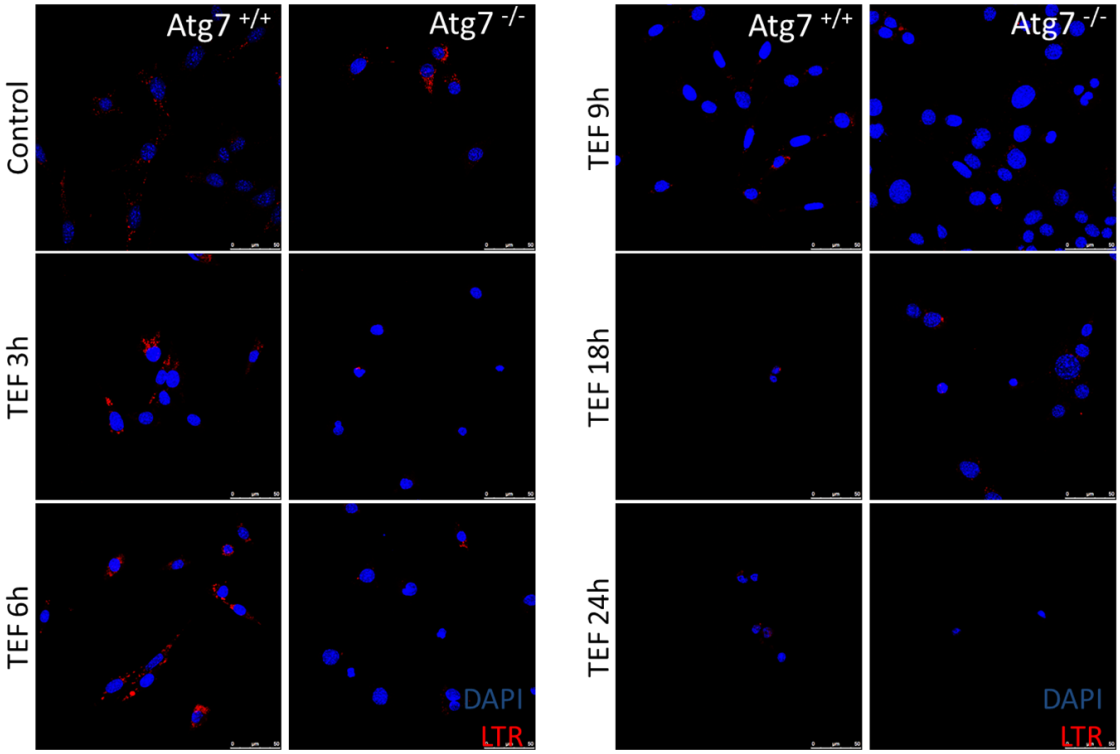
Atg7 +/+
Atg7 -/-
Atg7 +/+
Atg7 -/-
Control
TEF 3h
TEF 6h
TEF 9h
TEF 18h
TEF 24h
DAPI
LTR
DAPI
LTR

C

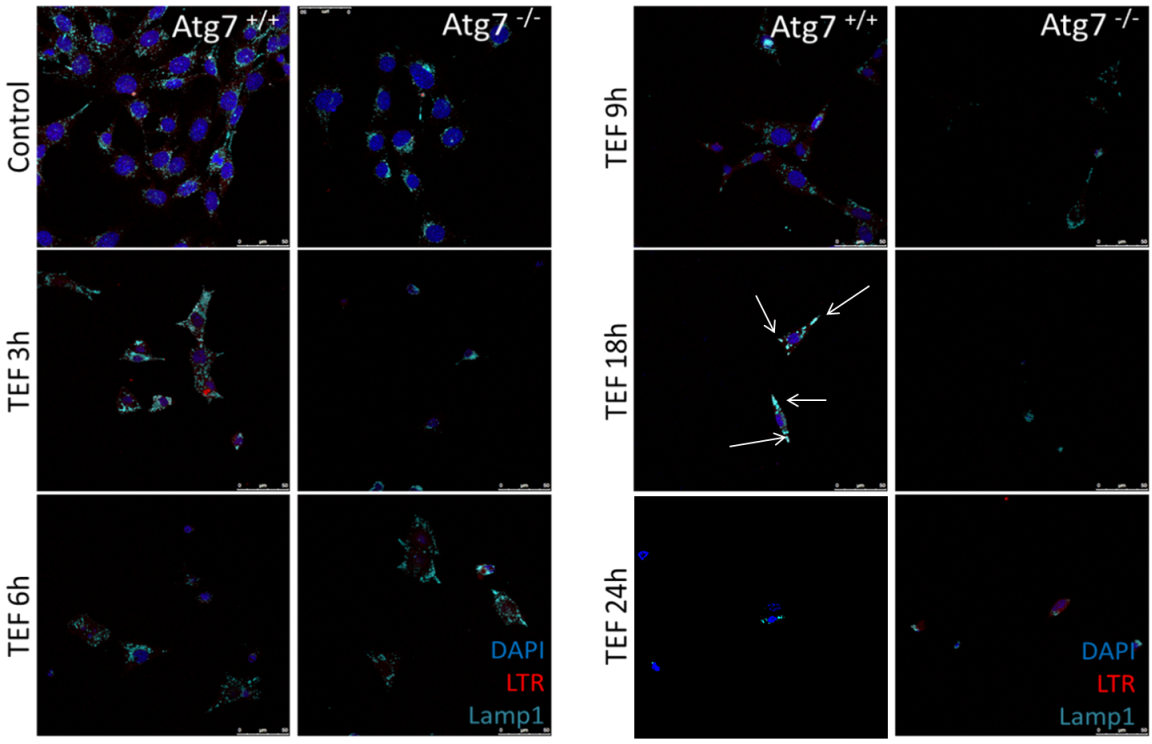

Figure 4.50. Lysosomal biogenesis in MEFs Atg7 +/+ after long time terfenadine treatment. (A) MEFs were seeded in coverslips. Lysotracker was added before the terfenadine treatment. After the different time points, coverslips were fixed and observed. **(B)** Lysotracker was added before terfenadine treatment. **(C)** After the corresponding time of terfenadine treatment, coverslips were fixed and immonufluorescence of lamp1 was carried out. Two independent experiments. Representative images.

Interestingly, MEFs Atg7+/+ lost the acidity of lysosomes after 3 hours of terfenadine treatment when we stain lysosomes at the end of the treatment. Interestingly, after 24 hours, the survival cells present LTR staining. When we stained the lysosomes at the beginning of the treatment, LTR disappeared after 9 hours in the MEFs Atg7+/+, meaning that the residual lysosomes lost their acidity or that they are broken **(figure 4.50B)**. However, when we stain the coverslips with Lamp1, we can observe Lamp1 lysosomes in puncta after 18 hours of terfenadine **(figure 4.50C)**. These results could suggest that lysosomal biogenesis is happening after terfenadine treatment. Interestingly, MEFs Atg7-/- do not present these novel lysosomes; suggesting that may Atg7 is crutial to induce lysosomal biogenesis.

4.2.3.3 Genes expression after terfenadine treatment

Due to the possible lysosomal biogenesis observed with the LTR staining, we decided to carry out a qPCR. For that aim, MEFs Atg7+/+ and Atg7-/- were seeded and treated with

terfenadine. Then, cells were stopped and RNA extracted at different points: 3, 6, 9, 16 and 24 hours. RNA extraction and qPCR were carried out as described in the section 3.2.6.

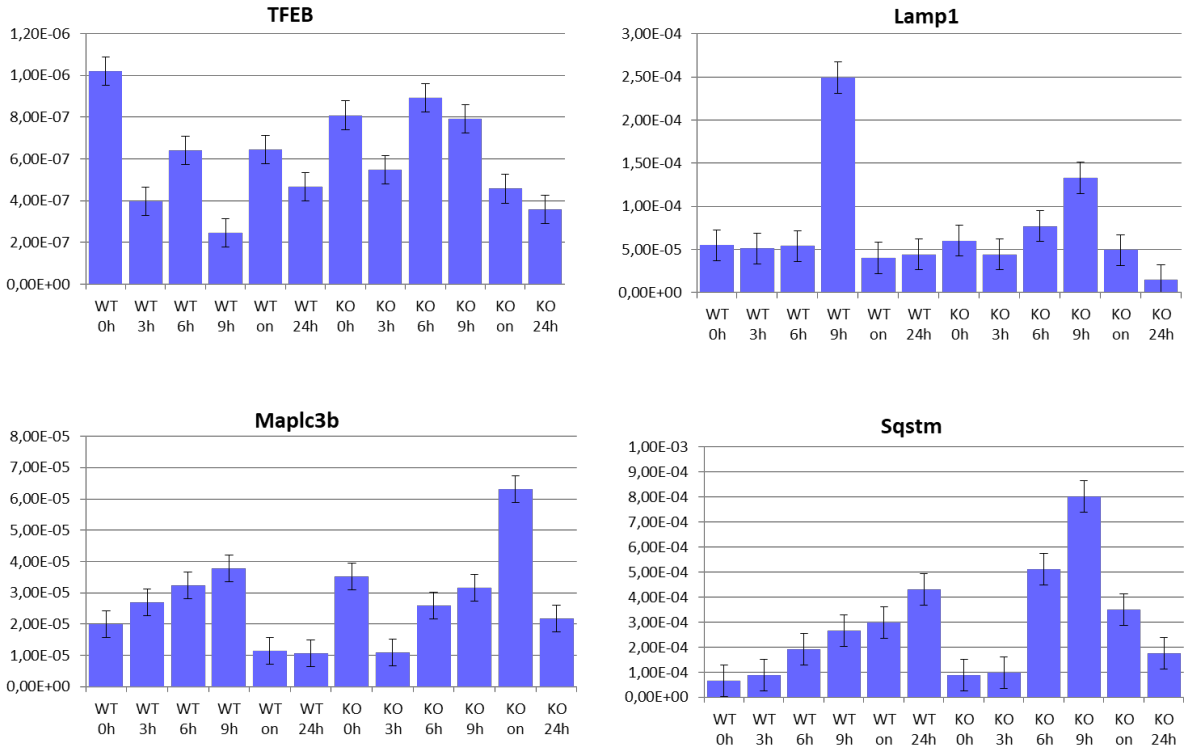

Figure 4.51. Gene expression of autophagy and lysosomes related proteins in MEFs Atg7 +/+ and Atg7 -/- after terfenadine time-course. qPCR analyze after 0, 3, 6, 9, 16 (on) and 24 hours of terfenadine. Two independent experiments.

As is shown in the **figure 4.51**, TFEB decreased the expression after terfenadine treatment. However, TFEB is a protein able to translocate to the nucleus when lysosomal biogenesis is needed. Nevertheless, lamp1 increased its expression after 9 hours of terfenadine in MEFs Atg7+/+, which could indicate an overexpression of the CLEAR genes. Interestingly, Maplc3b and Sqstm showed an increase in the MEFs Atg7-/- after 9 hours. In conclusion, MEFs Atg7+/+ could increase the lysosomal biogenesis, but further experiments need to be done to highlight whether TFEB is translocated to the nucleus.

4.2.4 ATG7 as a protein implicated in cell death

Due to these differences in viability after lysosomal damage, more cell lines were compared. For this aim, Hela and MCF7 were used to compare response after antihistamines treatment in Atg7-deficiency.

4.2.4.1 Viability of Hela ATG7CRISPr after CAD treatment

Hela cell line was used to compare the response of Atg7 after lysosomal damage. For this aim, Hela wild-type, Hela CRISPr control and Atg7 CRIPSr cell lines were used. Characterization of these cell lines was carried out by a western blot to detect Atg7 levels and LC3 after autophagy induction by rapamycin and inhibition by concanamicin A. For the viability assay, same approach was carried out: 3000 cells per well were seeded in a 96-well plate. Treatment was done the day after and Celigo was run after the propidium iodide staining.

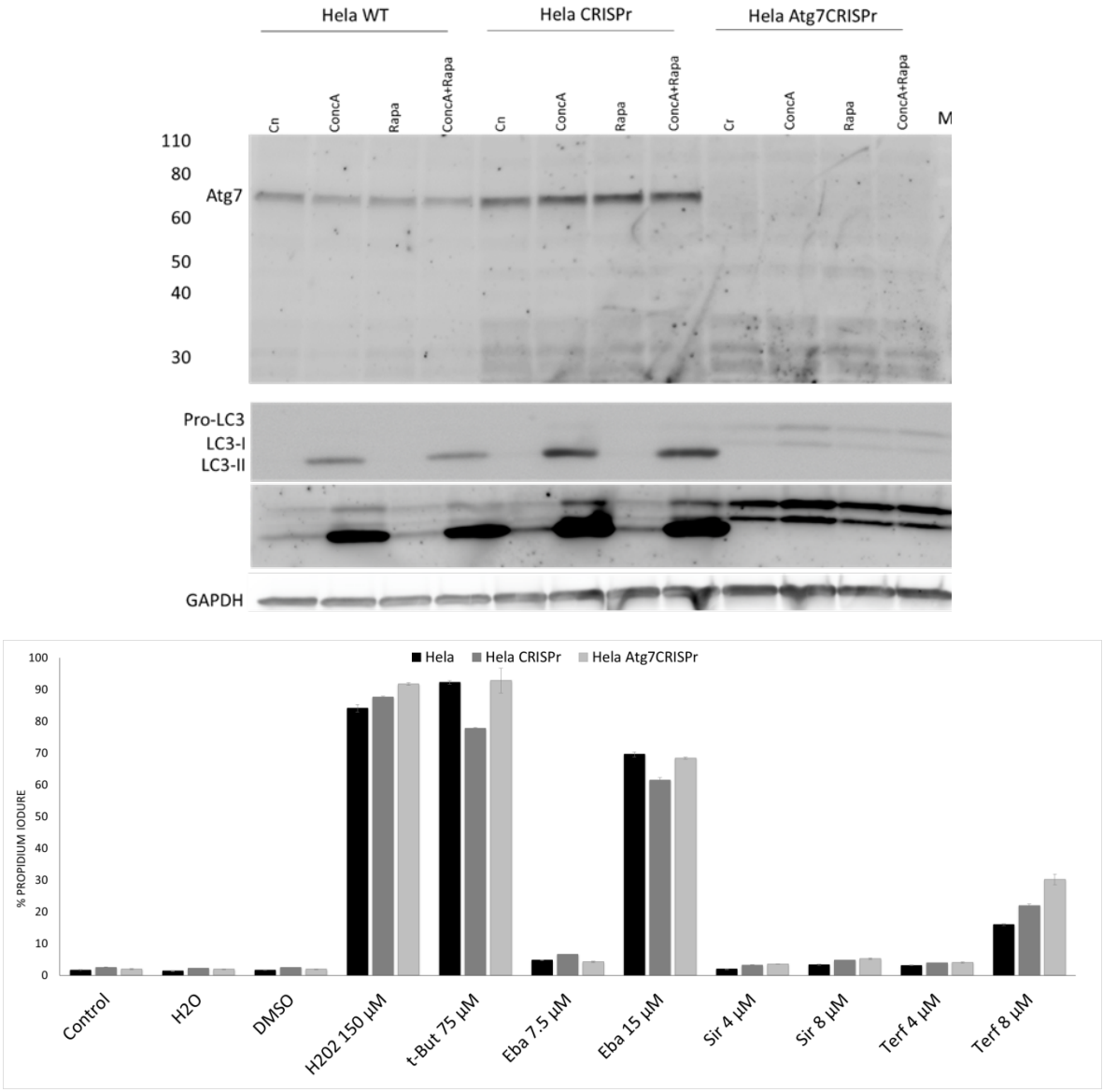

Figure 4.51. Hela Atg7 CRIPSr cells do not present higher viability response after CAD treatment. (A) Hela wild-type, Hela CRIPSr control and Atg7 CRIPSr were seeded and treated overnight with rapamycin and concanamicin A. Protein extraction was carried out and study of proteins by western blot was done. **(B)** Hela wild-type, Hela CRIPSr control and Atg7 CRIPSr were seeded and treated for 24 hours with several CADs. Cells were stained with propidium iodide and Celigo analyze was carried out. Three independent experiments were included in this graph. Eba: ebastine; Lor: Loratadine; Sir: siramesine; Terf: terfenadine.

First of all, Hela CRISPr was working correctly, due Atg7 was disappeared in the Hela Atg7 CRISPr cell line (**figure 4.51**). Additionally, no autophagy was induced after rapamycin or concanamicin treatment. However, HeLa cell lines presented similar resistance to the CAD treatment, except to ebastine 15 µM, so it was complicated to induce cell death and compare with the previous results with no triggering other pathways. Fascinatingly, the Atg7 CRISPr cell line presented even more cell death than Hela wild-type after terfenadine treatment.

4.2.4.2 Viability of MCF7 shRNA

To confirm this result, same approach was carried out in the MCF7 cell line. Dr. Jäättelä's laboratory gave us gently two clones Atg7-deficiency by shRNA done in MCF7 cell line. Parental MCF7 was used as control. First, western blot was carried out to determine the deficiency of Atg7.

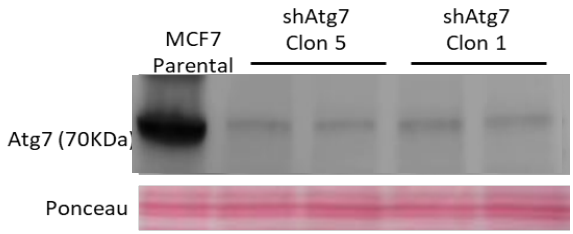

Figure 4.52. Atg7 protein levels in parental and shAtg7 clones in MCF7 cell line. Western blot to study Atg7 in shRNA MCF7. Parental MCF7 was used as a control.

After confirming the deficiency of Atg7 in the shAtg7 clones (**figure 4.52)**, viability of parental MCF7 and shAtg7 clones was studied after CAD treatment. Due to the higher resistant of the MCF7 cell line to CAD treatment, cells were seeded and treated for 48 hours. After the treatment, propidium iodide was added to the wells and the percent of cells propidium iodide positive was graphed.

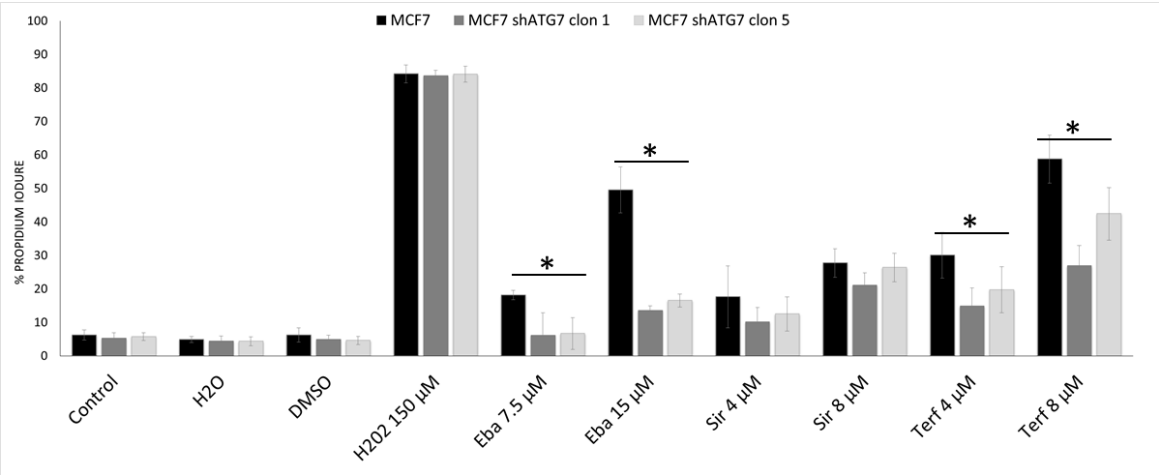

Figure 4.53. MCF7 shAtg7 present less cell death than parental MCF7 after 48 hours of CAD treatment. Parental MCF7 and shAtg7 were seeded and treated for 24 hours with several CADs. Cells were stained with propidium iodide and Celigo analyze was carried out. Three independent experiments were included in this graph. Eba: ebastine; Lor: Loratadine; Sir: siramesine; Terf: terfenadine. (* p-value <0.05).

Remarkably, both clones of Atg7 presented lower cell death response after ebastine, siramesine and terfenadine treatment (**figure 4.53**). Additionally, the cell death rate was similar after hydrogen peroxide, but not after t-butyl peroxide. These results, with the results from the MEFs, suggest that Atg7 is aggravating the cell survival response after lysosomal damage.

4.2.4.3 Reintroduction of ATG7 in the ATG7-deficient cell lines

To demonstrate that Atg7 could present a novel role in lysosome-dependent cell death, we decided to reintroduce Atg7 in the Atg7-deficient cell lines. For that aim, Atg7-GFP was transfected to the shAtg7 clones of MCF7. First, the concentration of the plasmid was set up. After that study, the viability assay was carried out in both clones. For that aim, transfection was carried out and after 48 hours, cells were seeded and treated with the lysosomal damage inductors. GFP plasmid was used as a control.

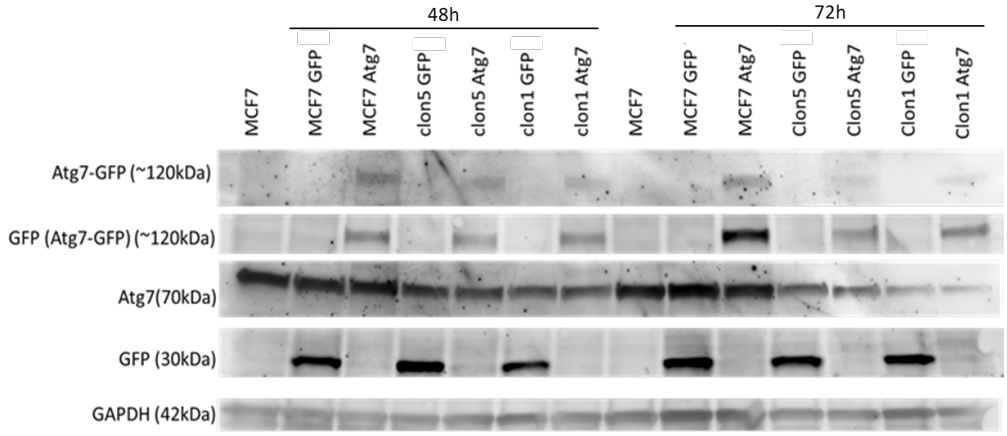

Figure 4.54. Western blot after the transfection of Atg7-GFP and GFP. Transfection of Atg7-GFP was detected by western blotting.

The transfection of 0.5 µg of DNA was enough to not affect cellular viability and to have protein levels quite similar to the endogenous Atg7 (**figure 4.54**). After the detection of Atg7 transfection, we decided to transfect the cells for 48 hours and then proceed to do the viability assay with ebastine 15 µM and terfenadine 8 µM for other 48 hours.

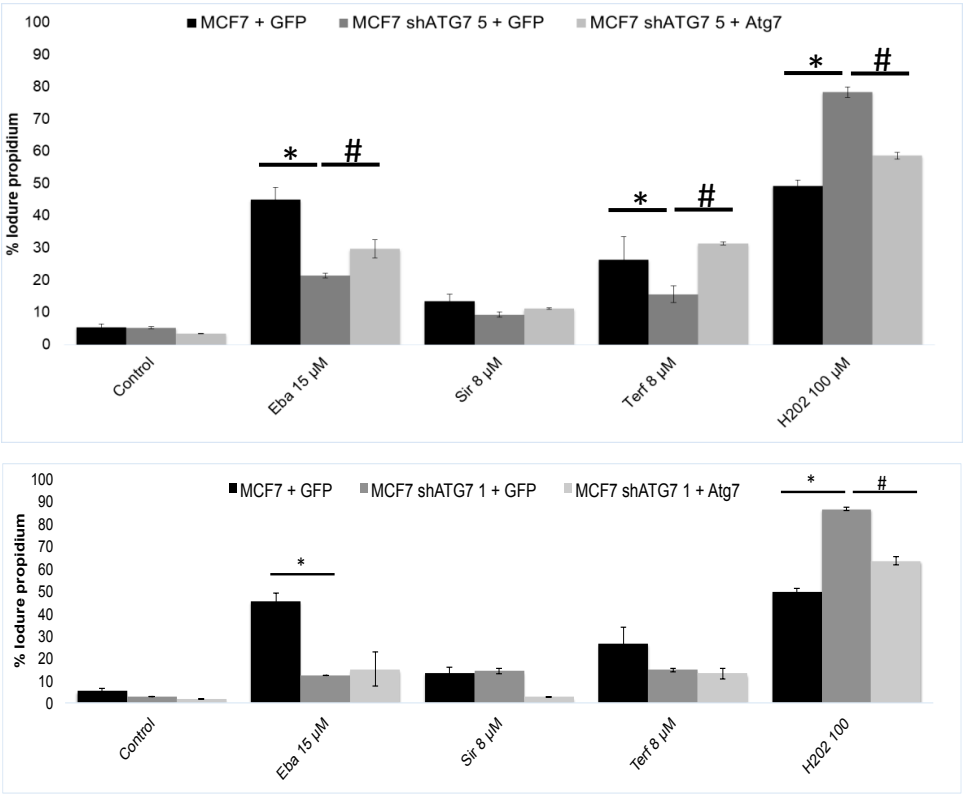

Figure 4.55. Reintroduce Atg7 was able to rescue the phenotype in the clon 5 after terfenadine treatment. (A) Viability assay by celigo of parental MCF7 with GFP, and shAtg7 clon 5 with GFP and Atg7-GFP transfection after 48 hours CAD treatment. **(B)** Viability assay by celigo of parental MCF7 with GFP, and shAtg7 clon 1 with GFP and Atg7-GFP transfection after 48 hours CAD treatment. Three independent experiments were carried out. (* p-value <0.05).

The viability in the clon 5 after the transfection and the CAD treatment showed that we were able to rescue the phenotype after terfenadine treatment. Additionally, an increase in the cell death was observed after the ebastine treatment in the Atg7-GFP transfected cells (**figure 4.55A**). However, the results obtained after the transfection in the clon 1 were different. There were no differences between the cells transfected with GFP or with Atg7-GFP in any of the treatments (**figure 4.55B**).

4.2.5 Lipidomic studies in MCF7 cell line

Due to the differences in lysosomal characteristics observed in MEFs Atg7+/+ and MEFs Atg7-/-, we decided to study lipids, due to the response of the cell after CAD treatment and the relation with the lipids change in lysosomes.

Study of lipidomic profile was carried out in MCF7 cells. For that aim, cells were counted and lipids were extracted as in the appart 3.2.8. After the lipid extraction, lipidomic facility

from Danish Cancer Society Research Center was in charge of the study of the lipids. Three individual experiments with duplicate extractions were done for every cell line.

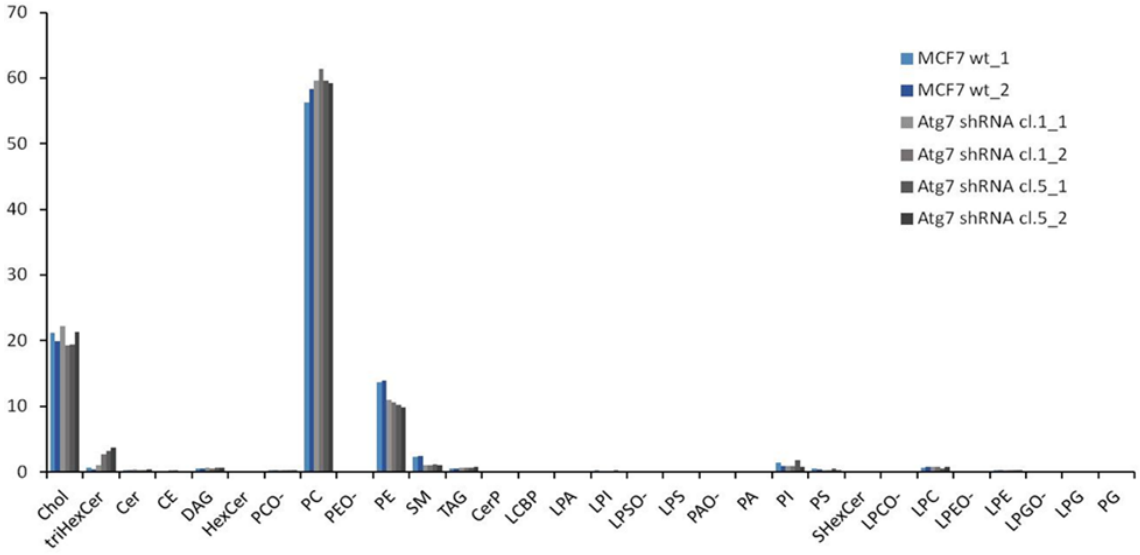

Figure 4.56. Lipidomic profile of all the lipids species. Data is representative of three independent experiments with duplicates.

Interestingly, the lipidic profile is different between Atg7-deficient and MCF7 parental cell line (**figure 4.56**). We decided to focus on sphingomyelin and ceramide, two types of lipids well-known to participate in lysosomal stability.

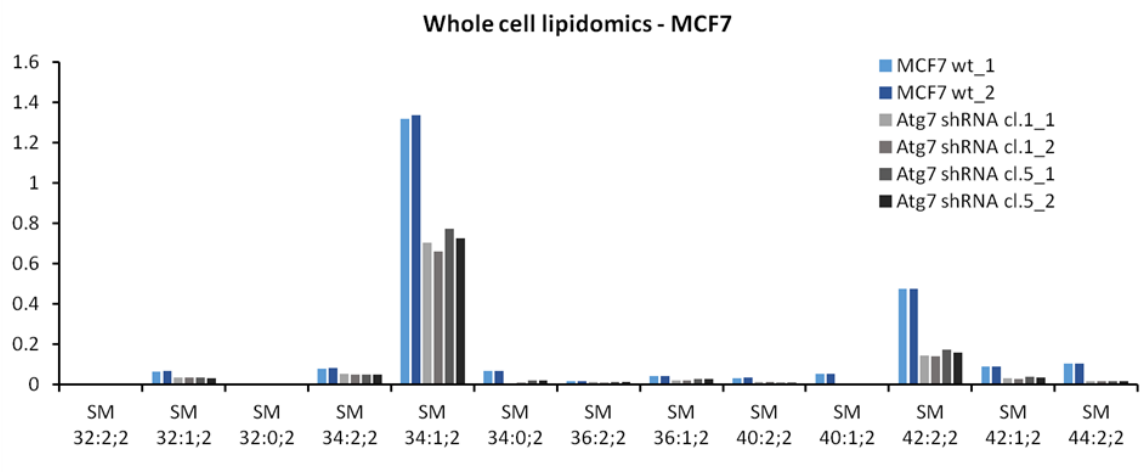

Figure 4.57. Sphingomyelin species in parental MCF7 and shAtg7 clones. Two independent experiments.

More interestingly, differences in sphingomyelinase species (SM) were observed between the parental cell line and both Atg7 knock-down clones (**figure 4.57**), for example, both clones presented less amount of SM 32:1;2, 34;1;2 or 42:2;2 in comparison with the

parental cell line. This result could suggest that the shAtg7 cell lines were more resistant due to the less amount of SM that the cells present by themselves.

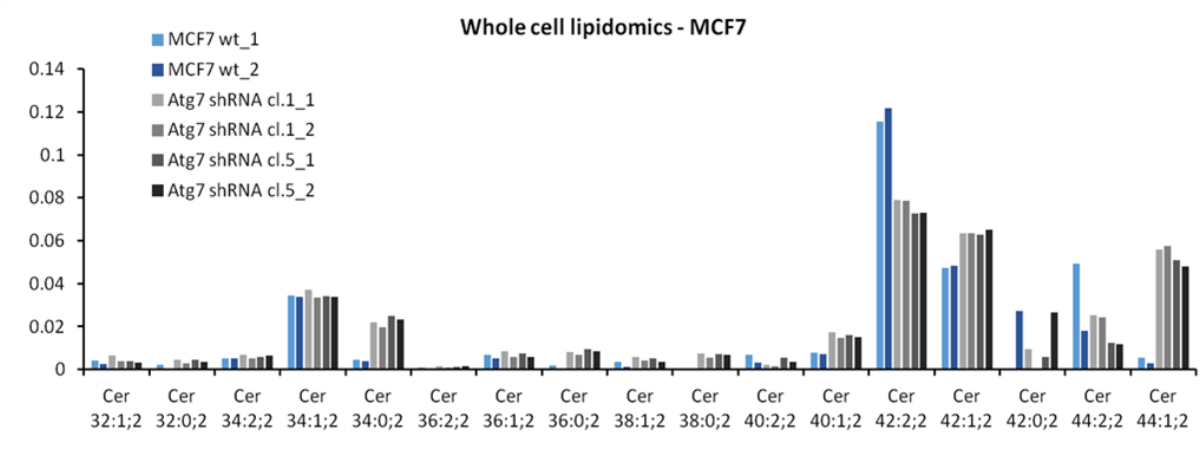

Figure 4.58. Ceramide species in parental MCF7 and shAtg7 clones. Two independent experiments.

The ASM is in charge of modifying SM to synthetize ceramide. Ceramide was studied carefully due to the differences in the SM species levels (**figure 4.58**). The lipidomic study demonstrated that ceramide levels were higher in certain species, such as Cer 34;0;2, Cer 40:1;2, Cer 44:1;2. Further investigation needs to be done to understand whether this lipidic imbalance is the mechanism which could explain the resistance of the Atg7-deficient cell lines.

DISCUSSION

5. DISCUSSION

5.1 RD10 MOUSE RETINA DISPLAYS A BLOCK IN AUTOPHAGIC FLUX

Several experiments in this thesis aimed to elucidate autophagic processes in a mouse model of *Retinitis pigmentosa*. These experiments demonstrated that the Rd10 retinas display lower LC3 and Ambra1 levels by immunofluorescence. In addition, our data show that the rd10 mice present less lipidated form of the autophagosomal marker LC3-II than the wild-type mice before neurodegeneration. The fact that most photoreceptors have been lost by P60 in the Rd10 retinas, and that the levels of LC3-II were almost imperceptible at this stage, could indicate that most of the autophagy activity comes from photoreceptors. Also he phosphorylation of S6 was observed in the western blot, according to the fact that autophagy is blocked in the Rd10 retinas. Moreover, when we blocked the autophagy flux by using lysosomal inhibitors, no increase of LC3-II was observed in the Rd10 retinas. As the levels of the protein p62 were increased in the basal stage in the Rd10 retinas, these data confirm the existence of an autophagy block in the rd10 retina.

Interestingly, when we treated the Rd10 mice with rapamycin *in vivo* or using the mTOR independent activator trehalose, photoreceptor cell death was increased in the retina. More importantly, downregulation of autophagy by using leupeptin and pepstatin A rescued form the photoreceptor cell death. This entire batch of experiments demonstrated that autophagy was detrimental in the Rd10 retinas. Several studies demonstrated that autophagy was detrimental in other models of retinal disease. This was observed, for example, in another model of *retinitis pigmentosa* caused by the mutation P23H in the opsin gene that induce conformational alterations of the protein that results in photoreceptor degeneration (Bogea et al., 2015). In 2015, a group used one model of *Xenopus laevis*, where the tadpoles express the bovine mutated P23H opsin in photoreceptors. When these tadpoles were exposed to 12 hours of light and 12 hours of dark, they displayed autophagy induction and photoreceptor cell death. The authors proposed that autophagy was implicated in the photoreceptor cell death, but they did not demonstrate an increase of autophagosomes or autophagy flux when they administrated the

photoreceptor cell death inductor AP20187 to the animals (Bogea et al., 2015). In retinal for example, in 2007, a study demonstrated that autophagy was only present in degenerated photoreceptor (Kunchithapautham and Rohrer, 2007).

Detrimental autophagy is also found in other tissues, not only in retina. In cortical neurons, after deprivation of glucose and reintroduction of glucose, the authors demonstrated that during the reintroduction, calpains are activated, leading to LMP and cell death. They proposed that during the glucose reintroduction, autophagy changes from an adaptive process to a defective autophagy pathway, which contributes to neuronal death (Gerónimo-Olvera et al., 2017). On the other hand, several studies have demonstrated that autophagy is beneficial in retinal neurodegeneration. In 2011, Kunchithapautham and colleagues demonstrated that rapamycin protected photoreceptors after light damage in Balb and GFP-LC3 mice as the consequence of autophagy induction in cones (Kunchithapautham et al., 2011). Others authors demonstrated that treating the 661w cell line with rapamycin after light damage was increasing cell viability (Li et al., 2014). Moreover, in Kaushal's thesis (Kaushal, 2006) the expression of the mutated P23H opsin in HEK293 cells was inducing autophagy, and this effect was stronger after rapamycin or amino acid depletion. Aggregates of P23H were being degraded specifically after autophagy induction. In summary, they concluded that autophagy was beneficial in this model (Kaushal, 2006). In conclusion, it seems that increasing autophagy appears to be cytoprotective in models that are associated to accumulation of misfolded proteins.

Autophagy is also detrimental in other models of degeneration. For example, during ischemic reperfusion, several tissues, such as cardiac muscle (Ma et al., 2015), liver (Cursio et al., 2015) or cerebral neurons (Zhang et al., 2013) enhance autophagy after ischemic reperfusion, but the role of autophagy remains still under debate. Studies in autophagy-deficient models have been used to understand the role of autophagy in retina. For example, the Atg5 (flox/flox) Nestina-cre is a mouse model of Atg5 deficiency in the neuronal precursors. This model presents photoreceptor degeneration. Interesintlgy, authopagy deficiency leads to an increase in CMA, indicating a cross-talk between both catabolic pathways during retinal degeneration (Rodríguez-Muela et al., 2013). Furthermore, after optic nerve axotomy, a model of glaucoma, which promotes the cell death of retinal ganglion cells, the Atg5 (flox/flox) or Atg4B knockout mouse models present less survival of the ganglion cells, while autophagy induction increases the numer

of surviving cells (Rodriguez-Muela et al., 2012). Additionally, other study demonstrated that animals $Atg5^{ARPE}$ and $Atg7^{ARPE}$, which are animals deficient in Atg5 or Atg7 in the RPE specifically, presented a reduction of the photoreceptor layer (Zhang et al., 2017). All these data together demonstrate the importance of autophagy in the retina and more specifically, in photoreceptors, but why under some conditions autophagy is detrimental or beneficial needs to be further elucidated.

With the batch of data from this thesis, we concluded that autophagy was detrimental in the Rd10 mouse model. Several models commented previously present autophagy as a cytoprotective mechanism in models with protein accumulation. Interestingly, when we block lysosomal function, we observed an increase in the survival cells. It seems that increased autophagy is deleterious when lysosomal damage in involved; on the other hand, when the cells present proteic aggregates, increased autophagy could help to the survival of the cells, suggesting a dual role for autophagy in the retinal homeostasis.

5. 2 THE RD10 MOUSE MODEL DISPLAY LYSOSOMAL MEMBRANE PERMEABILIZATION

The Rd10 mouse model presents a deficiency in the phosphodisterase Pde6b. As described in the introduction, this mutation leads to a calcium increase inside the cells. A calcium input in the cells can have several implications, such as triggering calpain activation (Sahara and Yamashima, 2010); In this thesis, we have analysed the relation between calpains and photoreceptor cell death, which has been described previously in other mouse models of *Retinitis pigmentosa* (Sancho-Pelluz et al., 2008; Łopatniuk and Witkowski, 2011). We demonstrated that calpain-2 (also known as m-calpain) appeared in the cleaved form from postnatal day P15 to postnatal day P25. Conversely calpain-1 (also known as μ-calpain) is not cleaved in this model.

As calpains have been implicated in lysosomal membrane destabilization and autophagy blockade (reviewed in Serrano-Puebla and Boya, 2016; Serrano-Puebla and Boya, 2018), we decided to study lysosomal integrity in the Rd10 retinas. First of all, our experiments demonstrated that cathepsin B and Lamp1 were not colocalizing in the

lysosomes, suggesting the release of cathepsin B outside lysosomes. Additionally, the retinas were stained with the fluorogenic Cathepsin B substrated called Magic Red. This staining appeared in photoreceptor cytoplasms in the rd10 retinas, but it is restricted in lysosomes in the wild type retinas. These results demonstrated that the Rd10 retinas present cathepsin B activity in the whole photoreceptor cytoplasm. These experiments suggested that Rd10 retinas presented an increase of calcium – caused by the mutation-, leading to calpain activation and LMP.

Several publications have demonstrated the relation between calpains and lysosomal membrane destabilization. In the first place, in an *in vitro* model in rat brain demonstrated that calpain-1 is able to cleave Lamp2, a lysosomal membrane protein essential for the lysosomal stability (Villapando and Torriglia, 2014). In the second place, during the mammary gland involution, calpain activation has been related to lysosomal destabilization (Kreuzaler e tal., 2011). Finally, some other authors proposed that calpains can present a role during LMP (Luke and Silverman, 2010; Kreuzaler et al., 2011). Further experiments should be done to analyze if calpains are implicated in the lysosomal damage in that model. During retinal degeneration in a rat model of P23H RHO, researchers discovered that calpain-1 and 2 were not overexpressed, but they found increased levels of caspase-12 protein compared to the wild-type animals. Interestingly, they observed an increase in the expression of apoptotic-related proteins, such as Bax, Bcl2 or Puma. In addition, they demonstrated mTOR inhibition in the P23H rats with rapamycin injections increased the visual function (Sizova et al., 2014). Interestingly, this model presented an increase in calpains in photoreceptors but, in this case, the autophagy induction increased cell viability. One of the differences between this model and Rd10 is the increase of apoptotic proteins. In our laboratory, we did not observe induction of apoptotic proteins in the Rd10 retinas (data not shown). It would be interesting to elucidate if autophagy is detrimental or beneficial depending on the apoptosis activation.

The relation between autophagy and LMP needs to be understood. Most of the studies demonstrate an autophagy block when lysosomes are damaged, for example in lysosomal storage disorders (LSD) (Settembre et al., 2008; Gabandé-Rodríguez et al., 2014), in neurodegenerative diseases, as in Alzheimer's Disease (Vila et al., 2011) or under administration of certain chemotherapies (Kanzawa et al., 2004). Interestingly, we observed that autophagy is blocked at P16 but we observed LMP at P20. It is really

important to understand why autophagy is blocked before LMP induction. More interestingly, autophagy was detrimental in the photoreceptor survival when we triggered it with rapamycin or trehalose. LMP has been shown to induce autophagy blockade in a wide range of diseases, such as in pancreatic cancer (Liu et al., 2017), Parkinson disease (Bové et al., 2014) or renal injuries (Song et al., 2017). In conclusion, we hypothesize that autophagy was increasing the damage triggered by LMP.

Understanding the circumstances that activate LMP are necessary to try to find ways to block them. For example, iron chelation can attenuate LMP and cell death in vitro (Berndt et al., 2010). Another strategy to protect cells from LMP is the overexpression of Hsp70 (Kirkegaard et al., 2010). For example, N-Methyl-N-nitrosourea (MNU) toxicity, an *in vitro* model of photoreceptor cell death, present a less harmful phenotype when the animals are treated with valproic acid, which induces Hsp70 expression (Mitton et al., 2014). Hsp70 is a chaperone that connects with Lamp2A to stabilize lysosomes (Bandyopadhyay et al., 2008). Interestingly, Lamp2A is a protein which is increased in the Rd10 retinas, suggesting an attemp to ameliorate lysosomal function.

Moreover, LMP has been related to apoptosis. Both pathways are quite related, but we did not observe caspase activation in the photoreceptors (data not shown). After all of these experiments, we wondered the mechanism how photoreceptors are dying in the Rd10 mouse model. Due to the fact that there is no caspase activity in the Rd10 mouse model and the LMP was confirmed with the experiments from this thesis, we hypothesize that lysosome-dependent cell death is happening in the photoreceptors of the Rd10 mice. This model could be a model to study the direction of lysosome-dependent cell death with no relation with caspase-dependent apoptosis.

5. 3 CIRCADIAN VARIATION OF AUTOPHAGY IN RETINA

We had some difficulties to conclude some of the experiments related to study autophagy due to the variability observed in the levels of LC3-II. In 2014, Yao and colleagues (Yao et al., 2014) demonstrated that autophagy oscillate throughout the day and it is quite related to the circadian cycle. For example, 1 hour after the shift from light to dark or from dark to light, there was a decrease in the LC3-II/LC3-I ratio. After

understanding the point that autophagy is changing almost every hour in the retina, we decided to sacrifice the animals for experiments always at the same hour.

The link between circadian rhythm and autophagy has been demonstrated in more neuronal models, besides retina. For example, in hippocampus, autophagy proteins appear decreased during sleep fragmentation (He et al., 2016). Moreover, in brain, melatonin, the hormone released during sleeping time, activates autophagy to delay ageing phenotype (Jenwitheesuk et al., 2014). Also, several studies demonstrated that the loss of circadian rhythm leads to an increase in the incidences of several diseases, such as Alzheimer and Parkinson, suggesting the possible relation between resting and autophagy. In these cases, autophagy regulation plays an important role to ameliorate the diseases (Maiese, 2017). This effect has been observed in other tissues, not only neuronal. In liver, it has been demonstrated that autophagy has a role in glucose metabolism during diurnal hours (Li and Lin, 2015). Additionally, it has been demonstrated that Atg14 is playing an essential role in lipid metabolism in pancreas, according to the circadian rhythm (Xiong et al., 2012). In conclusion, all of these novel finding suggest the relation and importance of autophagy and circadian rhythm.

5.4 THE DEACETYLASE INHIBITOR TRICHOSTATIN A RESCUES FROM THE RD10 RETINA CELL DEATH

HDAC classes I/II seems to precede photoreceptor degeneration in the rd1 model (Sancho-Pelluz et al., 2010). Furthermore, other studies have reported that some HDACs are implicated in autophagy process (Iwata et al., 2005; Lee et al., 2008). Thus, we decided to study Rd10 photoreceptor degeneration after treatment with HDAC inhibitor TSA. Our results show that *in vitro* model with the calcium ionophore A23187 presented lower cell death rate after treatment with TSA. In addition, treatment with TSA rescued Rd10 photoreceptor cell death *ex vivo,* but this was not observed *in vivo*. In addition, previous studies show the rescue in rd1 mouse model inhibiting HDAC (Sancho-Pelluz and Paquet-Durand, 2012). The authors of this research proposed a model: the elevated calcium accumulation causes HDAC overactivation, which could reduce transcription factor CREB activity, implicated in reactive oxidative species (ROS) protection. These ROS could cause DNA damage and therefore activation of PARP; with subsequent energy depletion and

translocation of apoptosis factors to the nucleus. This hypothesis could explain the rescue with the treatment of TSA in Rd1 mouse model as well as in the Rd10. Although we have observed rescue with TSA in both models, the Rd10 and wild-type retinas treated with A23187, we have not observed a significant rescue in Rd10 treatment *in vivo*. One explanation could be the difficult of the intravitreous injections, due to the small size of the mice eyes. Anyway, as a tendency was also observed *in vivo*, further experiments will clarify whether TSA could be a cytoprotetive agent in the retinitis pigmentosa mouse models *in vivo*.

However, *in vitro* experiments show contradictory results in cell viability after HDAC inhibition. For example, in bladder cancer cells induces cell death via intrinsic apoptosis (Wang et al., 2017), in lung cancer cells TSA induces cell death through Akt inhibition (Yang et al., 2017). In 2003 a study demonstrated that HDACs induce cell death act via death receptor pathway (extrinsic) or mitochondrial pathway (intrinsic) to activate caspases (Rosato et al., 2003). For instance, HDAC inhibition protect against the pyruvate dehydrogenase dysfunction in Huntington's Disease (Naia et al., 2017); moreover, other studies reported that treatment of cerebellar granule neurons with HDAC inhibitors induce apoptosis (Morrison et al., 2006). The opposite effects of HDAC inhibition could be explained by the tissue and stage-specific expression of different classes of HDAC. Finally, taking into account the importance of HDAC6 in autophagosomes degradation (Iwata et al., 2005) and the implication of this protein in multiple neurodegenerative disorders (Du and Jiao, 2011), it would be interesting to test a specific HDAC6 inhibitor in the Rd10 retinas and support the importance of autophagy fas a new therapeutic target for *Retinitis pigmentosa*.

To further investigate the role of autophagy in TSA rescue, autophagy flux was studied in retinas treated with A23187 and TSA. Although our results displayed a rescue of the cell death, there was no increase in autophagy flux. An autophagy block was observed, according to our previous hypothesis that autophagy is detrimental in the Rd10 model. As commented previously, autophagy inhibition appears to be beneficial for the photoreceptor survival in certain scenarios. Actually, in cultured rat cardiomiocytes, the HDAC inhibition with TSA results in the inhibition of cardiac hypertrophy by autophagy suppression (Cao et al., 2011). However, the activation of autophagy with HDACs inhibitors seems to be tissue-dependent. Fascinatingly, and contrary to our results, a study demonstrated that

autophagy is enhanced by deacetylase inhibitors in a FOXO-dependent manner in MEFs (Zhang et al., 2015). Recently it has been demonstrated that TSA enhances autophagy after subarachnoid hemorrhage in rats and that this induction ameliorates the phenotype (Shao et al., 2016). We observed an improvement of cell survival in the Rd10 retinas, but may due to the autophagy block that TSA induces in the retina. Interestingly, in a Parkinson model it has been demonstrated that HDAC inhibition potentiates the model of neuronal cell death. Interestingly, in this model, the inhibition of autophagy leads to improve the phenotype (Park et al., 2016). However, in cancer cell lines, it has been demonstrated that TSA is able to induce cell death through with ROS increase (Sun et al., 2014).

In order to conclude the implication and importance of autophagy in retinal dytrofies and, in particular, in the Rd10 mouse model, further studies need to be performed.

5.5 THE TREATMENT WITH CADs INDUCES LYSOSOMAL DAMAGE AND CELL DEATH IN MOUSE EMBRYONIC FIBROBLASTS

In the second part of this thesis, we have tried to understand the processes triggered by lysosomal damage, LMP and lysosome-dependent cell death and their relation with autophagy. MEFs were used to study these links at molecular level. Several lysosomal damage agents were used in this thesis: anti-histamines with CAD properties; LLOMe as a detergent; and the ROS inducers, hydrogen peroxide and t-butyl-peroxide. Our results showed that two of the anti-histamine drugs were inducing cell death in MEFs: ebastine and terfenadine, but no cell death was observed after loratadine and desloratadine. Curiously, siramesine was not inducing significant levels of cell death; however, t-butyl-peroxide was inducing cell death in MEFs. The differences observed between the different lysosomal damage inductors represent the complexity of LMP; every LMP inductors induce different cascade of signaling to –maybe- induce cell death. Siramesine was not able to induce cell death in our system, but previously, siramesine was described as lysosomal damage inductor able to trigger cell death through caspase-independent pathway in MCF7 cells (Ostenfeld et al., 2005), but we were not able to reproduce this results in our system. However, the processes triggered by siramesine are not completely elucidated yet. Interestingly, a recent publication demonstrated that siramesine induces cell death first

through mitochondrial membrane permeabilization (MMP), which triggers LMP afterwards (Česen et al., 2013). More experiments should be done in our model to understand why cell death is not triggered in MEFs after siramesine treatment. LLOMe is a detergent that induces LMP, but requires cathepsin C to be active (Jacobson et al., 2013). The fact that the cells lines used in this thesis do not have big amount of cathepsin C could be a reason why LLOMe is neither inducing cell death, nor galectin-3 puncta (data not shown). However, it has been described recently that Hela cells die after LLOMe treatment through proteolytic signaling. The authors hypothetized that the reason is the absence of cathepsin B or L in the cytosol (Repnik et al., 2017). In our system, his could be an explanation why we did not observe cathepsin B release in our model (data not shown), but this do not explain why we did not observe galectin-3 after LLOMe in MEFs.

The mechanisms of action of the anti-histamines are poorly understood to date. It has been described that most of them induce cell death through lysosomal destabilization in cancer cell lines, such as non-small cell lung cancer cell lines, prostate cancer cell line and breast cancer (Ellegard et al., 2016). More interestingly, the authors demonstrated that loratadine and astemizole had a low effect in cell death *in vitro*, but in a clinical trial with patients with lung cancer treated with these two anti-histamines, they presented the lowest mortality in comparison with patients administred other anti-histamines more effective *in vitro*. The authors proposed that the tissue distribution of loratadine and astemizole is higher comparing with others anti-histamines, such as terfenadine, which is a potent killer, but may present less efficient tissue distribution. These data demonstrated the specificity and differences of action between every CAD.

Our results demonstrated that MEFs Atg7-/- display decreased cell death after CADs treatment. As commented in the introduction, autophagy-dependent cell death (ADCD) and lysosomal-dependent cell death (LDCD) are processes highly related which difficult the differentiation from one type of cell death to other. We wondered whether (ADCD) could be occuring in MEFs Atg7+/+ after CAD treament. ADCD and lysosome-dependent cell death are two processes highly related. Some authors proposed that ADCD is characterized by an enhanced autophagic flux (Fulda and Kögel, 2015; Mariño et al., 2014). The circumstances when autophagy inhibitors do not block cell death, although an increase of LC3 or p62 decrease is visible, should not be considered ADCD. In our studies, we did not observe rescue from terfenadine-induced cell death after combined the

treatment with wortmanin. In the same way, the common condition for LDCD is the cathepsins release. Additionally, the use of cathepsin inhibitors should prevent the cell death. In fact, the cathepsin B inhibitor CA-074 can block most of the LDCD (Montaser et al., 2002). Furthermore, E64-d or z-VAD, a well-known apoptotic inhibitor that also inhibit the lysosomal cysteine cathepsins (Schote et al., 1999). In our model, autophagy is induced after one hour of terfenadine treatment due to the reduction of phospho-S6, but we concluded that at that point, autophagy flux was not efficient due to the fact that LC3-II was not increased after terfenadine treatment. However, our model display cathepsin release from lysosomes, but the treatment with cathepsin inhibitor, like E64d and Pepstatin A, was not blocking cell death (data not shown). To prevent the precise moment when cathepsin release is inducing cell death is quite complicated due to the differences in the dynamism of cathepsin release in both cell lines. We concluded that in our system it is LDCD (and not ADCD) what is happening during the cell death because we did not observe autophagy flux increase. Further experiments have to be done to try to rescue from terfenadine-induced cell death with cathepsin inhibitors.

Lysosome-dependent cell death triggered after CAD is poorly understood. The experiments carried out to assess cathepsin B activity aimed to understand whether the cells presented LMP after the treatment with terfenadine. New questions appeared when we used MEFs Atg7-/-. The experiments presented two different responses between MEFs Atg7 +/+ and MEFs Atg7 -/-. At 3 hours, both cell lines presented similar percentage of cells with diffuse cathepsin B (close to 30%); but after 6 hours, MEFs Atg7 +/+ displayed an increase of the number of cells with diffuse cathepsin B (± 80 %), while MEFs Atg7-/- presented a reduction (± 20 %). This difference is observed at 16 hours. But, after 24 hours, the effect was similar in Atg7-/- than wild-type MEFs. This experiment suggested that autophagy is contributing to lysosome-dependent cell death, at least at the early time points after CAD treatment.

At what point are LDCD and ADCD interacting? It is not the first time that it is described that lysosomal damage is less detrimental in autophagy-deficient models. For example, the treatment with tetrahydrocannabinol (THC) in cancer cell lines is inducing cell death through endoplasmic reticulum stress, autophagy induction and LMP (Salazar et al., 2009; Hernández-Tiedra, et al., 2016). In this publication, the authors demonstrated that the genetic deficiency of Atg5 and Atg7 prevented from the THC-induced cell death.

In this thesis, we hypothesize that there are two waves of cathepsin B release due to the different responses between MEFs Atg7+/+ and Atg7-/- during the terfenadine time-course. The first wave would need autophagy-related proteins to act. In fact, it has been demonstrated that Atg7 overexpression induced an increase in cathepsin B expression in INS-1 cells exposed to fatty acids (Li et al., 2013), triggering the proinflammatory and apoptotic response. This result shows the relation between autophagy-related proteins and cathepsin B. The second wave would be autophagy-independent, triggering the cell death pathway.

Additionally, the experiments carried out with galectin-3 demonstrated that terfenadine is inducing galectin-3 puncta formation in MEFs after 3 hours of treatment. After 6 hours the number of cells with galectin-3 dots is almost the 70% in MEFs wild-type, but after long-time treatment, such as 18 hours or 24 hours, the percent of cells with galectin-3 dots decreased. This protein can be used as a marker for LMP (Aits et al., 2015), but recently it has been described a novel function for galectin-3. Chauhan and colleagues proposed that TRIM family proteins interact with galectins to guide autophagy to target damaged lysosomal membranes after LLOMe treatment (Chauhan et al., 2016). This result proposes galectin protein family as lysophagy receptors (Maejima et al., 2013). Considering this point, galectin-3 could be a signal for damaged endolysosomal membranes, and not only for LMP. When MEFs Atg7-/- were treated with terfenadine in a time-course experiment and then the galectin-3 was studied, the percent of cells with galectin-3 dots was always lower in comparison with MEFs Atg7+/+. Considering the two possible options of galectin-3 staining, our experiments could suggest two things: firstly, MEFs Atg7-/- displayed reduced lysosome damage and LMP after terfenadine treatment; secondly, MEFs Atg7-/- do not trigger the receptors for lysophagy after this treatment, but it would be interesting to determine whether the lack of Atg proteins induces a fail in the receptors signaling. To discuss both options, we can study cathepsin B release after terfenadine treatment. After 3 hours of terfenadine treatment MEFs Atg7-/- presented more of cells with cathepsin B release than MEFs Atg7+/+. This result could suggest that lysosomal damage and LMP are happening in both cell lines, but Atg7 is not inducing galectin-3 signal as a lysophagy receptor. Additional experiments should be done to understand why Atg7 lack promotes defects in the autophagy-receptor signaling.

5.6 ATG7-DEFICIENT CELLS PRESENT A DECREASE IN LYSOSOMAL DAMAGE AND CELL DEATH

In this thesis, it has been described the differences in viability between MEFs Atg7+/+ and MEFs Atg7-/-, being Atg7 deficiency a beneficial situation after lysosomal damage treatment. Additionally, two clones of shAtg7 MCF7 breast cancer cells were used to corroborate the hypothesis that Atg7 is inducing the cell death after CAD treatment. To test whether Atg7 could have a role related to lysosomal damage, Atg7 was reintroduced in MCF7 shAtg7. The rescue was observed in one of the clones after terfenadine and ebastine treatment, suggesting that Atg7 could present a role in lysosomal damage, but it may depend on the protein levels of every cell line. Surprisingly, HeLa ATG7 CRISPr did not present any differences in cell viability in comparison with HeLa wild-type. One explanation could be that whether autophagy is activated and is involved in LCDC. But this reason is not enough to explain the results. Firstly, because viability of MEFs Atg5-/- is similar to MEFs Atg5+/+ after CAD treatment. This result indicates that autophagy *perse* is not implicated in lysosome-dependent cell death. If autophagy would be implicated in cell death, Atg5-deficiency cell line would be also resistant to lysosomal damage induction. Second, because there is autophagy flux blockade after terfenadine treatment, suggesting that autophagosome-dependent cell death is not being induced. Additionally, the differences observed in MEFs Atg7-/-, such as the stronger LTR staining in comparison with MEFs Atg7+/+, or the differences observed in the lipid profile (that this book will discuss later), or the different dynamic for cathepsin B release, response found in MEFs Atg7-/- but not in MEFs Atg7 +/+, suggest that Atg7 has a role autophagy-independent and related to lysosomes.

As commented in the introduction, it is not the first time that autophagy-related proteins present novel autophagy-independent functions. In fact, Atg7 has been related to an increase in cell death after lysosomal damage previously. In 2012, Kessel and colleagues demonstrated that shRNA knock-down of Atg7 in murine hepatoma cell line lclc7 increased the resistance to photodamage, a classic lysosomal damage inductor (Kessel et al., 2012). This model induces caspase activation, which is suppressed in the Atg7-deficiency cells. Similar results were demonstrated in 2010, when Walls and colleagues demonstrated that cultured neural precursor cells treated with chloroquine or

bafilomycin A1 caused blockade of autophagic flux and apoptosis. An Atg7 knock-down suppressed the apoptosis induced by chloroquine and bafilomycin A1, compounds that affect to the lysosomal stability (Walls et al., 2010). These authors proposed that Atg7 is necessary for the p53 phosphorylation-induced after lysosomal damage. Further experiments should be done to extrapolate this model to the system presented in this thesis.

Furthermore, another research demonstrated that Atg7 knock-down repressed the apoptosis induced by TGF-β in human hepatocarnoma cell line. In addition, the Atg7-deficiency cell line was able to jump the cycle arrest induced by TGF-β. In conclusion, the authors proposed that autophagy inhibition in TGF-β-mediated cell death was attributable to the apoptosis induction and cell cycle arrest (Kiyono et al., 2009). Several other publications have demonstrated additional roles for Atg7 related to cell cycle and cell death (Xiong, 2015). For example, in 2012, Atg7 was described as necessary to survive during starvation due to its interaction with p53 in MEFs. This interaction promoted the expression of p21 during starvation. Atg7-deficient cells did not express p21, promoting a fail in the cell cycle arrest, thus increasing the damage DNA (Lee et al., 2011). This relation between Atg7 and p53 is quite important, due to the importance of p53 during cell cycle; and suggests that Atg7 is participating in cell cycle control. Additionally, it has been described that p53 is a protein which can trigger LMP. For example in myeloid leukemia cells, the activation of p53 can induce LMP (Yuan et al., 2002); other publication demonstrated that in fibrosarcoma cells, phosphorylated p53 translocates to the lysosomes through the interaction with a protein called LAPF, triggering apoptosis (Li et al., 2007). The mechanism of action of p53 in the lysosomal membrane remains unknown. It could be interesting to understand if Atg7 interaction with p53 is affecting to the lysosomal stability in our model.

The relation between Atg7 and p53 is not the only one proposed as additional function of Atg7. In RAW264.7, a mouse macrophague cell line, Atg7 and Beclin1 are participating in the cell death induced by the pan-caspacase inhibitor zVAD, in fact, Atg7 and Beclin1 knock-out cell lines presented a reduced cell death after the treatment (Yu et al., 2004). They proposed that Atg7 and Beclin1 were implicated in autophagic cell death, being this process activated when caspase 8 is inhibited with zVAD.

In several human tissues, Atg7 has been described as a tumor suppressor, increasing cell death. This could be in agreement with our hypothesis. For example, Atg7 increases the cell death rate, faciliting antitumor actions of obatoclax in lung cancer (McCoy et al., 2010). In addition, in breast cancer cell line MCF7, the deficiency of Atg7 reduces the cell death induced by photodynamic therapy (Xue et al., 2010). Interestingly, photodynamic therapy induces lysosomal damage, but the authors justify the resistance of Atg7-deficient cells to autophagy, although they did not study lysosomal impact. Furthermore, Atg7 has been described as a tumor suppressor in liver after tetrandine treatment, by increasing Atg7 expression and enhancing autophagy, leading to ADCD (Gong et al., 2012). However, several publications have demonstrated that Atg7 has a role as an oncogene. For example, to block the Atg7-mediated autophagy augments the sensitivity of human prostate cancer cells (Zhu et al., 2010). Moreover, Atg7 inhibit caspase-9-dependent apoptosis in human colon and cervical cancer (Han et al., 2014).

These findings show the diverse roles of Atg7 in different situations. Xiong attributed these processes due to the selective Atg7-dependent autophagy (Xiong et al., 2015), and the response will depend on the tissue and damage. More in-depth studies are necessary to understand the diverse roles of Atg7. With this batch of experiments, and the previous experiments that show Atg7 presents a double role in cellular viability, always after lysosomal damage, for example after THC treatment or photodynamic therapy, we concluded that Atg7 may promote cell death when lysosomal function is compromised.

5.7 LIPIDIC IMPLICATION IN LYSOSOME-DEPENDENT CELL DEATH

Due to the inhibition caused by the CADs in the acid sphingomyelinase, we decided to study the lipid profile in the breast cancer cell line MCF7 in the parental cell line and in both shRNA clones knock-down for Atg7. The analysis of the lipid profile demonstrated several differencences in the lipid profile between the parental and the Atg7-deficient cell lines. More specific studies showed that Atg7-deficient cell lines presented lower amount of sphingomyelin species. Additionally, ceramide levels appeared to be decrease in Atg7-deficient cell lines, except the specie Ceramide 44:1;2.

ASM is a water-soluble glycoprotein in charge of sphingomyeline degradation to ceramide. Sphingomyeline and ceramides are lipids able to influence cell survival, but the processes are still poorly understood. Several researchers have demonstrated that an increase in sphingomyelin leads to cell death. For example, during the treatment with camptothecin and doxorubicin of thyroid carcinoma showed a critical role of ceramide during cell death (Taniguchi and Okazaki, 2014). Additionally, it has been described that acid sphingomyelinase deficiency increases the cell death due to the lysosomal instability in Niemann Pick Disease (Smith and Schuchman, 2008). Interestingly, the gene encoding ASM, *SMPD1*, is decreased in gastrointestinal, hepatocellular, salivary gland, renal and head and neck carcinomas (Kallunki et al., 2013), suggesting the anti-apoptotic role of this protein. It is well known that a decrease in sphingomyelin, or a default in the acid sphingomyelinase reduces the lysosomal membrane stability (Pedersen et al., 2013). In 2013, Pedersen et al., demonstrated that the acid sphingomyelinase (ASM) inhibition is able to destabilize cancer cell lysosomes, leading to cell death. They used siramesine and ASM inhibitors and observed that the interference of ASM with bis(monoscylglycero)phosphate (BMP) was inducing the lysosomal destability (Pedersen et al., 2013). The lack of ASM induces an accumulation of sphingomyelin because it is not transformed to ceramide. It is not the first time that the increase with sphingomyelin is related to cell death. For example, in Niemann Pick type A it has been described that an increase in sphingomyelin induced LMP and cell death (Gabandé-Rodríguez et al., 2014). The treatment with THC in cancer cell lines is inducing cell death and LMP due to the increment of dihydroceramide: ceramide ratio in the endoplasmic reticulum, leading to autophagosomes and triggering lysosomal membrane permeabilization (Hernández-Tiedra, et al., 2016) For example, ceramide is able to form rafts in the plasma membrane able to increase apoptosis induction (Carpinteiro et al., 2008). However, sphingomyelinase and ceramides are lipids able to regulate cell survival, but the processes are remaining unclear.

In conclusion, we hypothethize that Atg7 could present a role related to ASM inhibition. In this case, cells with Atg7 would present an increase in sphingomyeline, promoting a sensibilization of the cells to CAD treatment. On the other hand, Atg7-deficient cell lines would present an increase in ceramide species and a decrease in sphingomyeline. As commented previously, an increase in shpingomyelin species could display lysosomal membrane destabilization. This could explain why Atg7-deficient cell lines are more resistant after CAD treatment.

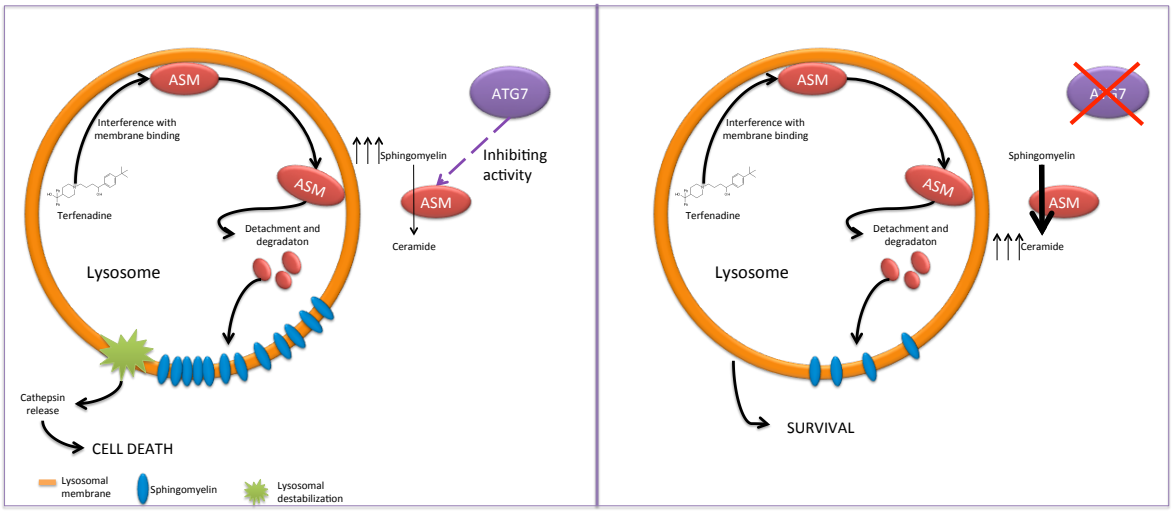

Model of Atg7 could be related to the ASM to change the lipidic profile in the lysosomes. Atg7 could be inhibiting the ASM activity. In that case, the amount of sphingomyelins would be higher, leading to lysosomal destability. When there is a deficiency of Atg7, the ASM would be increasing the levels of ceramide in the lysosomes, improving the lysosomal stability.

CONCLUSIONS

6. CONCLUSIONS

1. The Rd10 mouse model presents calcium influx increase and calpain cleavage. This activation leads to lysosomal membrane permeabilization. Inhibition of lysosomal protease activity in vitro and in vivo prevents photoreceptor cell death.

2. The Rd10 mice display autophagy blockade and autophagy flux block before neurodegeneration. Photoreceptors are the cells in the retina that present higher autophagy activity.

3. The calcium ionophore A23187 is a suitable in vitro model to mimetize Retinitis pigmentosa. A23187 treatment in wild-type retinas induces intracellular calcium increase, autophagy blockade, lysosomal membrane permeabilization and photoreceptor cell death. A23187-induced cell death was rescued by blocking lysosomal activity.

4. Autophagy induction with rapamycin or trehalose increases the levels of photoreceptor cell death in Rd10 mice. Activation of autophagy seems to be detrimental when lysosomal membranes are damaged. Autophagy inhibition ex vivo delays cell death.

5. The cationic amphiphilic drugs ebastine, siramesine and terfenadine induce cell death in mouse embryonic fibroblasts. They induce cathepsin B release from lysosomes and lysosomal galectin-3 staining, indicative of lysosome membrane permeabilozation.

6. Atg7-deficient mouse embryonic fibroblasts are more resistant to cationic amphiphilic drug treatment and display reduced cathepsin B release from the lysosomes to the cytosol compared to wild-type fibroblasts.

7. Atg7-deficient mouse embryonic fibroblasts present more acidic lysosomes with perinuclear localization. By electronic microscopy, Atg7-deficient mouse embryonic fibroblasts present more electrodense particles.

8. Knock-down shAtg7 in MCF7 cells present more resistance than its parental cell line and overexpression of Atg7 sensitizes to cell death.

9. Lipidomic analysis shows that Atg7-deficient cell lines presented fewer amounts of sphingomyeline species, lipids that decrease lysosome stability.

REFERENCES

7. REFERENCES

Ahuja S, Ahuja-Jensen P, Johnson LE, Caffé AR, Abrahamson M, Ekström PA, van Veen T. rd1 Mouse retina shows an imbalance in the activity of cysteine protease cathepsins and their endogenous inhibitor cystatin C. Invest Ophthalmol Vis Sci. 2008 Mar;49(3):1089-96.

Aita VM, Liang XH, Murty VV, Pincus DL, Yu W, Cayanis E, Kalachikov S, Gilliam TC, Levine B. Cloning and genomic organization of beclin 1, a candidate tumor suppressor gene on chromosome 17q21. Genomics. 1999 Jul 1;59(1):59-65.

Aits S, Kricker J, Liu B, Ellegaard AM, Hämälistö S, Tvingsholm S, Corcelle-Termeau E, Høgh S, Farkas T, Holm Jonassen A, Gromova I, Mortensen M, Jäättelä M. Sensitive detection of lysosomal membrane permeabilization by lysosomal galectin puncta assay. Autophagy. 2015;11(8):1408-24.

Aits S, Jäättelä M. Lysosomal cell death at a glance. J Cell Sci. 2013 May 1;126(Pt 9):1905-12.

Anding AL, Baehrecke EH. Cleaning House: Selective Autophagy of Organelles. Dev Cell. 2017 Apr 10;41(1):10-22.

Araújo Couto L, Sampaio Narciso M, Hokoç JN, Blanco Martinez AM. Calpain inhibitor 2 prevents axonal degeneration of opossum optic nerve fibers. J Neurosci Res. 2004 Aug 1;77(3):410-9.

Arroba AI, Alvarez-Lindo N, van Rooijen N, de la Rosa EJ. Microglia-mediated IGF-I neuroprotection in the rd10 mouse model of retinitis pigmentosa. Invest Ophthalmol Vis Sci. 2011 Nov 25;52(12):9124-30.

Arnandis T, Ferrer-Vicens I, García-Trevijano ER, Miralles VJ, García C, Torres L, Viña JR, Zaragozá R. Calpains mediate epithelial-cell death during mammary gland involution: mitochondria and lysosomal destabilization. Cell Death Differ. 2012 Sep;19(9):1536-48.

Azarian SM, King AJ, Hallett MA, Williams DS. Selective proteolysis of arrestin by calpain. Molecular characteristics and its effect on rhodopsin dephosphorylation. J Biol Chem. 1995 Oct 13;270(41):24375-84.

Baehrecke EH. Autophagic programmed cell death in Drosophila. Cell Death Differ. 2003 Sep;10(9):940-5.

Baerga R, Zhang Y, Chen PH, Goldman S, Jin S. Targeted deletion of autophagy-related 5 (atg5) impairs adipogenesis in a cellular model and in mice. Autophagy. 2009 Nov;5(8):1118-30.

Bandyopadhyay U, Kaushik S, Varticovski L, Cuervo AM. The chaperone-mediated autophagy receptor organizes in dynamic protein complexes at the lysosomal membrane. Mol Cell Biol. 2008 Sep;28(18):5747-63.

Bánréti A1, Sass M, Graba Y. The emerging role of acetylation in the regulation of autophagy. Autophagy. 2013 Jun 1;9(6):819-29.

Barhoum R, Martínez-Navarrete G, Corrochano S, Germain F, Fernandez-Sanchez L, de la Rosa EJ, de la Villa P, Cuenca N. Functional and structural modifications during retinal degeneration in the rd10 mouse. Neuroscience. 2008 Aug 26;155(3):698-713.

Barondes SH, Castronovo V, Cooper DN, Cummings RD, Drickamer K, Feizi T, Gitt MA, Hirabayashi J, Hughes C, Kasai K, et al. Galectins: a family of animal beta-galactoside-binding lectins. Cell 1994; 76:597-8.

Barone I, Novelli E, Piano I, Gargini C, Strettoi E. Environmental enrichment extends photoreceptor survival and visual function in a mouse model of retinitis pigmentosa. PLoS One. 2012;7(11):e50726.

Behrends C, Sowa ME, Gygi SP, Harper JW. Network organization of the human autophagy system. Nature. 2010 Jul 1;466(7302):68-76.

Benato F, Skobo T, Gioacchini G, Moro I, Ciccosanti F, Piacentini M, Fimia GM, Carnevali O, Dalla Valle L. Ambra1 knockdown in zebrafish leads to incomplete development due to severe defects in organogenesis. Autophagy. 2013 Apr;9(4):476-95.

Berger Z, Ravikumar B, Menzies FM, Oroz LG, Underwood BR, Pangalos MN, Schmitt I, Wullner U, Evert BO, O'Kane CJ, Rubinsztein DC. Rapamycin alleviates toxicity of different aggregate-prone proteins. Hum Mol Genet. 2006 Feb 1;15(3):433-42.

Berndt C, Kurz T, Selenius M, Fernandes AP, Edgren MR, Brunk UT. Chelation of lysosomal iron protects against ionizing radiation. Biochem J. 2010 Dec 1;432(2):295-301.

Bewley MA, Naughton M, Preston J, Mitchell A, Holmes A, Marriott HM, Read RC, Mitchell TJ, Whyte MK, Dockrell DH. Pneumolysin activates macrophage lysosomal membrane permeabilization and executes apoptosis by distinct mechanisms without membrane pore formation. MBio. 2014 Oct 7;5(5):e01710-14.

Bewley MA, Marriott HM, Tulone C, Francis SE, Mitchell TJ, Read RC, Chain B, Kroemer G, Whyte MK, Dockrell DH. A cardinal role for cathepsin d in co-ordinating the host-mediated apoptosis of macrophages and killing of pneumococci. PLoS Pathog. 2011 Jan 27;7(1):e1001262.

Bogéa TH, Wen RH, Moritz OL. Light Induces Ultrastructural Changes in Rod Outer and Inner Segments, Including Autophagy, in a Transgenic Xenopus laevis P23H Rhodopsin Model of Retinitis Pigmentosa. Invest Ophthalmol Vis Sci. 2015 Dec;56(13):7947-55

Bové J, Martínez-Vicente M, Dehay B, Perier C, Recasens A, Bombrun A, Antonsson B, Vila M. BAX channel activity mediates lysosomal disruption linked to Parkinson disease. Autophagy. 2014 May;10(5):889-900.

Bowes C, Li T, Danciger M, Baxter LC, Applebury ML, Farber DB. Retinal degeneration in the rd mouse is caused by a defect in the beta subunit of rod cGMP-phosphodiesterase. Nature. 1990 Oct 18;347(6294):677-80.

Boya P, Esteban-Martínez L, Serrano-Puebla A, Gómez-Sintes R, Villarejo-Zori B. Autophagy in the eye: Development, degeneration, and aging. Prog Retin Eye Res. 2016 Nov;55:206-245.

Boya P, Reggiori F, Codogno P. Emerging regulation and functions of autophagy. Nat Cell Biol. 2013 Jul;15(7):713-20.

Boya P. Lysosomal function and dysfunction: mechanism and disease. Antioxid Redox Signal. 2012 Sep 1;17(5):766-74.

Boya P, Andreau K, Poncet D, Zamzami N, Perfettini JL, Metivier D, Ojcius DM, Jäättelä M, Kroemer G. Lysosomal membrane permeabilization induces cell death in a mitochondrion-dependent fashion. J Exp Med. 2003 May 19;197(10):1323-34.

Brady J, Bolen JB, Radonovich M, Salzman N, Khoury G. Stimulation of simian virus 40 late gene expression by simian virus 40 tumor antigen. Proc Natl Acad Sci U S A. 1984 Apr;81(7):2040-4.

Brennan MA, Cookson BT. Salmonella induces macrophage death by caspase-1-dependent necrosis. Mol Microbiol 2000; 38: 31–40.

Brunk UT, Ericsson JL. Cytochemical evidence for the leakage of acid phosphatase through ultrastructurally intact lysosomal membranes. Histochem J. 1972 Nov;4(6):479-91.

Buki KG, Bauer PI, Kun E. Isolation and identification of a proteinase from calf thymus that cleaves poly(ADP-ribose) polymerase and histone H1. Biochim Biophys Acta. 1997 Mar 7;1338(1):100-6.

Caffé AR, Ahuja P, Holmqvist B, Azadi S, Forsell J, Holmqvist I, Söderpalm AK, van Veen T. Mouse retina explants after long-term culture in serum free medium. J Chem Neuroanat. 2001 Nov;22(4):263-73.

Cao, DJ, Wang, ZV, Battiprolu, PK, Jiang, N, Morales, C R., Kong, Y, Rothermel, BA, Gillete, T. G., Hill, J. A. Histone deacetylase (HDAC) inhibitors attenuate cardiac hypertrophy by suppressing autophagy. Proc Natl Acad Sci USA 2011; 108 (10): 4123-4128.

Carpinteiro A, Dumitru C, Schenck M, Gulbins E. Ceramide-induced cell death in malignant cells. Cancer Lett. 2008 Jun 8;264(1):1-10.

Cataldo AM, Peterhoff CM, Schmidt SD, Terio NB, Duff K, Beard M, Mathews PM, Nixon RA. Presenilin mutations in familial Alzheimer disease and transgenic mouse models accelerate neuronal lysosomal pathology. J Neuropathol Exp Neurol. 2004 Aug;63(8):821-30.

Česen MH, Repnik U, Turk V, Turk B. Siramesine triggers cell death through destabilisation of mitochondria, but not lysosomes. Cell Death Dis. 2013 Oct 3;4:e818.

Chang GQ, Hao Y, Wong F. Apoptosis: final common pathway of photoreceptor death in rd, rds, and rhodopsin mutant mice. Neuron. 1993 Oct;11(4):595-605.

Chauhan S, Kumar S, Jain A, Ponpuak M, Mudd MH, Kimura T, Choi SW, Peters R, Mandell M, Bruun JA, Johansen T, Deretic V. TRIMs and Galectins Globally Cooperate and TRIM16 and Galectin-3 Co-direct Autophagy in Endomembrane Damage Homeostasis. Dev Cell. 2016 Oct 10;39(1):13-27.

Chen H, Chan AY, Stone, Mandal NA. Beyond the cherry-red spot: Ocular manifestations of sphingolipid-mediated neurodegenerative and inflammatory disorders. Surv Ophthalmol. 2014 Jan-Feb;59(1):64-76.

Chen S, Wang C, Yeo S, Liang CC, Okamoto T, Sun S, Wen J, Guan JL. Distinct roles of autophagy-dependent and -independent functions of FIP200 revealed by generation and analysis of a mutant knock-in mouse model. Genes Dev. 2016 Apr 1;30(7):856-69.

Chen Y, Sawada O, Kohno H, Le YZ, Subauste C, Maeda T, Maeda A. Autophagy protects the retina from light-induced degeneration. J Biol Chem. 2013 Mar 15;288(11):7506-18.

Chinskey ND, Zheng QD, Zacks DN. Control of photoreceptor autophagy after retinal detachment: the switch from survival to death. Invest Ophthalmol Vis Sci. 2014 Feb 4;55(2):688-95.

Chu YP, Hung YH, Chang HY, Yang WY. Assays to Monitor Lysophagy. Methods Enzymol. 2017;588:231-244.

Claudepierre T, Paques M, Simonutti M, Buard I, Sahel J, Maue RA, Picaud S, Pfrieger FW. Lack of Niemann-Pick type C1 induces age-related degeneration in the mouse retina. Mol. Cell Neurosci. 2010 43, 164e176.

Clowes DD. A randomized trial of vitamin A and vitamin E supplementation for retinitis pigmentosa. Arch Ophthalmol. 1993 Nov;111(11):1461-2; author reply 1462-5.

Corrochano S, Barhoum R, Boya P, Arroba AI, Rodríguez-Muela N, Gómez-Vicente V, Bosch F, de Pablo F, de la Villa P, de la Rosa EJ. Attenuation of vision loss and delay in apoptosis of photoreceptors induced by proinsulin in a mouse model of retinitis pigmentosa. Invest Ophthalmol Vis Sci. 2008 Sep;49(9):4188-94.

Crooke A, Huete-Toral F, Colligris B, Pintor J. The role and therapeutic potential of melatonin in age-related ocular diseases. J Pineal Res. 2017 Sep;63(2).

Cuervo AM, Dice JF. A receptor for the selective uptake and degradation of proteins by lysosomes. Science. 1996 Jul 26;273(5274):501-3.

Cursio R, Colosetti P, Gugenheim J. Autophagy and liver ischemia-reperfusion injury. Biomed Res Int. 2015;2015:417590

De Duve C, Wattiaux R. Functions of lysosomes. Annu Rev Physiol. 1966;28:435-92.

De Duve C, Pressman Bc, Gianetto R, Wattiaux R, Appelmans F. Tissue fractionation studies. 6. Intracellular distribution patterns of enzymes in rat-liver tissue. Biochem J. 1955 Aug;60(4):604-17.

De Haan CA, Reggiori F. Are nidoviruses hijacking the autophagy machinery? Autophagy. 2008 Apr;4(3):276-9.

Degenhardt K, Mathew R, Beaudoin B, Bray K, Anderson D, Chen G, Mukherjee C, Shi Y, Gélinas C, Fan Y, Nelson DA, Jin S, White E. Autophagy promotes tumor cell survival and restricts necrosis, inflammation, and tumorigenesis. Cancer Cell. 2006 Jul;10(1):51-64.

Dehay B, Bové J, Rodríguez-Muela N, Perier C, Recasens A, Boya P, Vila M. Pathogenic lysosomal depletion in Parkinson's disease. J Neurosci. 2010 Sep 15;30(37):12535-44.

Denny CA, Alroy J, Pawlyk BS, Sandberg MA, d'Azzo A, Seyfried TN. Neurochemical, morphological, and neurophysiological abnormalities in retinas of Sandhoff and GM1 gangliosidosis mice. J Neurochem. 2007 Jun;101(5):1294-302.

DeSelm CJ, Miller BC, Zou W, Beatty WL, van Meel E, Takahata Y, Klumperman J, Tooze SA, Teitelbaum SL, Virgin HW. Autophagy proteins regulate the secretory component of osteoclastic bone resorption. Dev Cell. 2011 Nov 15;21(5):966-74.

Domenech M, Marrero-Berrios I, Torres-Lugo M, Rinaldi C. Lysosomal membrane permeabilization by targeted magnetic nanoparticles in alternating magnetic fields. ACS Nano. 2013 Jun 25;7(6):5091-101.

Doonan F, Donovan M, Cotter TG. Caspase-independent photoreceptor apoptosis in mouse models of retinal degeneration. J Neurosci. 2003 Jul 2;23(13):5723-31.

Du, G., Jiao, R. To prevent neurodegeneration: HDAC6 uses different strategies for different challenges. Commun Integr Biol. 2011;4: 139-42.

Duewell P, Kono H, Rayner KJ, Sirois CM, Vladimer G, Bauernfeind FG, Abela GS, Franchi L, Nuñez G, Schnurr M, Espevik T, Lien E, Fitzgerald KA, Rock KL, Moore KJ, Wright SD, Hornung V, Latz E. NLRP3 inflammasomes are required for atherogenesis and activated by cholesterol crystals. Nature. 2010 Apr 29;464(7293):1357-61.

Eiyama A, Okamoto K. PINK1/Parkin-mediated mitophagy in mammalian cells. Curr Opin Cell Biol. 2015 Apr;33:95-101. d

Ellegaard AM, Dehlendorff C, Vind AC, Anand A, Cederkvist L, Petersen NH, Nylandsted J, Stenvang J, Mellemgaard A, Østerlind K, Friis S, Jäättelä M. Repurposing Cationic Amphiphilic Antihistamines for Cancer Treatment. EBioMedicine. 2016 Jul;9:130-9.

Eno CO, Zhao G, Venkatanarayan A, Wang B, Flores ER, Li C. Noxa couples lysosomal membrane permeabilization and apoptosis during oxidative stress. Free Radic Biol Med. 2013 Dec;65:26-37.

Eriksson I, Nath S, Bornefall P, Giraldo AM, Öllinger K. Impact of high cholesterol in a Parkinson's disease model: Prevention of lysosomal leakage versus stimulation of α-synuclein aggregation. Eur J Cell Biol. 2017 Mar;96(2):99-109.

Esteban-Martínez L, Sierra-Filardi E, McGreal RS, Salazar-Roa M, Mariño G, Seco E, Durand S, Enot D, Graña O, Malumbres M, Cvekl A, Cuervo AM, Kroemer G. Boya P.

Programmed mitophagy is essential for the glycolytic switch during cell differentiation. EMBO J. 2017 May 2.

Fagerberg L, Hallström BM, Oksvold P, Kampf C, Djureinovic D, Odeberg J, Habuka M, Tahmasebpoor S, Danielsson A, Edlund K, Asplund A, Sjöstedt E, Lundberg E, Szigyarto CA, Skogs M, Takanen JO, Berling H, Tegel H, Mulder J, Nilsson P, Schwenk JM, Lindskog C, Danielsson F, Mardinoglu A, Sivertsson A, von Feilitzen K, Forsberg M, Zwahlen M, Olsson I, Navani S, Huss M, Nielsen J, Ponten F, Uhlén M. Analysis of the human tissue-specific expression by genome-wide integration of transcriptomics and antibody-based proteomics. Mol Cell Proteomics. 2014 Feb;13(2):397-406.

Farré JC, Krick R, Subramani S, Thumm M. Turnover of organelles by autophagy in yeast. Curr Opin Cell Biol. 2009 Aug;21(4):522-30.

Feng Y, He D, Yao Z, Klionsky DJ. The machinery of macroautophagy. Cell Res. 2014 Jan;24(1):24-41.

Fiscus RR. Involvement of cyclic GMP and protein kinase G in the regulation of apoptosis and survival in neural cells. Neurosignals. 2002 Jul-Aug;11(4):175-90.

Frasson M, Sahel JA, Fabre M, Simonutti M, Dreyfus H, Picaud S. Retinitis pigmentosa: rod photoreceptor rescue by a calcium-channel blocker in the rd mouse. Nat Med. 1999 Oct;5(10):1183-7.

Fulda S, Kögel D. Cell death by autophagy: emerging molecular mechanisms and implications for cancer therapy. Oncogene. 2015 Oct 1;34(40):5105-13.

Füllgrabe J, Klionsky DJ, Joseph B. Histone post-translational modifications regulate autophagy flux and outcome. Autophagy. 2013 Oct;9(10):1621-3.

Gabandé-Rodríguez E, Boya P, Labrador V, Dotti CG, Ledesma MD. High sphingomyelin levels induce lysosomal damage and autophagy dysfunction in Niemann Pick disease type A. Cell Death Differ. 2014 Jun;21(6):864-75.

Galluzi L et al., Molecular mechanisms of cell death: Recommendations of the Nomenclature Committee on Cell Death 2018. *Manucript in preparation.*

Galluzzi L, Baehrecke EH, Ballabio A, Boya P, Bravo-San Pedro JM, Cecconi F, Choi AM, Chu CT, Codogno P, Colombo MI, Cuervo AM, Debnath J, Deretic V, Dikic I, Eskelinen EL, Fimia GM, Fulda S, Gewirtz DA, Green DR, Hansen M, Harper JW, Jäättelä M, Johansen T, Juhasz G, Kimmelman AC, Kraft C, Ktistakis NT, Kumar S, Levine B, Lopez-Otin C, Madeo F, Martens S, Martinez J, Melendez A, Mizushima N, Münz C, Murphy LO, Penninger JM, Piacentini M, Reggiori F, Rubinsztein DC, Ryan KM, Santambrogio L, Scorrano L, Simon AK, Simon HU, Simonsen A, Tavernarakis N, Tooze SA, Yoshimori T, Yuan J, Yue Z, Zhong Q, Kroemer G. Molecular definitions of autophagy and related processes. EMBO J. 2017 Jul 3;36(13):1811-1836.

Galluzzi L, Vitale I, Abrams JM, Alnemri ES, Baehrecke EH, Blagosklonny MV, Dawson TM, Dawson VL, El-Deiry WS, Fulda S, Gottlieb E, Green DR, Hengartner MO, Kepp O, Knight RA, Kumar S, Lipton SA, Lu X, Madeo F, Malorni W, Mehlen P, Nuñez G, Peter ME, Piacentini M, Rubinsztein DC, Shi Y, Simon HU, Vandenabeele P, White E, Yuan J, Zhivotovsky B, Melino G, Kroemer G. Molecular definitions of cell death subroutines: recommendations of the Nomenclature Committee on Cell Death 2012. Cell Death Differ. 2012 Jan;19(1):107-20.

Gargini C, Terzibasi E, Mazzoni F, Strettoi E. Retinal organization in the retinal degeneration 10 (rd10) mutant mouse: a morphological and ERG study. J Comp Neurol. 2007 Jan 10;500(2):222-38.

Gegg ME, Cooper JM, Chau KY, Rojo M, Schapira AH, Taanman JW. Mitofusin 1 and mitofusin 2 are ubiquitinated in a PINK1/parkin-dependent manner upon induction of mitophagy. Hum Mol Genet. 2010 Dec 15;19(24):4861-70.

Guerini D, Coletto L, Carafoli E. Exporting calcium from cells. Cell Calcium. 2005 Sep-Oct;38(3-4):281-9.

Gerónimo-Olvera C, Montiel T, Rincon-Heredia R, Castro-Obregón S, Massieu L. Autophagy fails to prevent glucose deprivation/glucose reintroduction-induced neuronal death due to calpain-mediated lysosomal dysfunction in cortical neurons. Cell Death Dis. 2017 Jun 29;8(6):e2911.

Gong K, Chen C, Zhan Y, Chen Y, Huang Z, Li W. Autophagy-related gene 7 (ATG7) and reactive oxygen species/extracellular signal-regulated kinase regulate tetrandrine-induced autophagy in human hepatocellular carcinoma. J Biol Chem. 2012 Oct 12;287(42):35576-88.

Guo JY, Chen HY, Mathew R, Fan J, Strohecker AM, Karsli-Uzunbas G, Kamphorst JJ, Chen G, Lemons JM, Karantza V, Coller HA, Dipaola RS, Gelinas C, Rabinowitz JD, White E. Activated Ras requires autophagy to maintain oxidative metabolism and tumorigenesis. Genes Dev. 2011 Mar 1;25(5):460-70.

Gutierrez EM, Seebacher NA, Arzuman L, Kovacevic Z, Lane DJ, Richardson V, Merlot AM, Lok H, Kalinowski DS, Sahni S, Jansson PJ, Richardson DR. Lysosomal membrane stability plays a major role in the cytotoxic activity of the anti-proliferative agent, di-2-pyridylketone 4,4-dimethyl-3-thiosemicarbazone (Dp44mT). Biochim Biophys Acta. 2016 Jul;1863(7 Pt A):1665-81.

Halle A, Hornung V, Petzold GC, Stewart CR, Monks BG, Reinheckel T, Fitzgerald KA, Latz E, Moore KJ, Golenbock DT. The NALP3 inflammasome is involved in the innate immune response to amyloid-beta. Nat Immunol. 2008 Aug;9(8):857-65.

Han J, Hou W, Goldstein LA, Stolz DB, Watkins SC, Rabinowich H. A Complex between Atg7 and Caspase-9: a novel mechanism of cross-regulation between autophagy and apoptosis. J Biol Chem. 2014 Mar 7;289(10):6485-97.

Hara T, Nakamura K, Matsui M, Yamamoto A, Nakahara Y, Suzuki-Migishima R, Yokoyama M, Mishima K, Saito I, Okano H, Mizushima N. Suppression of basal autophagy in neural cells causes neurodegenerative disease in mice. Nature. 2006 Jun 15;441(7095):885-9.

Hara T, Takamura A, Kishi C, Iemura S, Natsume T, Guan JL, Mizushima N. FIP200, a ULK-interacting protein, is required for autophagosome formation in mammalian cells. J Cell Biol. 2008 May 5;181(3):497-510.

Hasegawa J, Maejima I, Iwamoto R, Yoshimori T. Selective autophagy: lysophagy. Methods. 2015 Mar;75:128-32.

He Y, Cornelissen-Guillaume GG, He J, Kastin AJ4, Harrison LM, Pan W. Circadian rhythm of autophagy proteins in hippocampus is blunted by sleep fragmentation. Chronobiol Int. 2016;33(5):553-60.

Hernández-Tiedra S, Fabriàs G, Dávila D, Salanueva ÍJ, Casas J, Montes LR, Antón Z, García-Taboada E, Salazar-Roa M, Lorente M, Nylandsted J, Armstrong J, López-Valero I, McKee CS, Serrano-Puebla A, García-López R, González-Martínez J, Abad JL, Hanada K, Boya P, Goñi F, Guzmán M, Lovat P, Jäättelä M, Alonso A, Velasco G. Dihydroceramide accumulation mediates cytotoxic autophagy of cancer cells via autolysosome destabilization. Autophagy. 2016 Nov;12(11):2213-2229.

Hockly, E, Richon, VM, Woodman, B, Smith, DL, Zhou, X, Rosa, E, Sathavisam, K, Ghazi-Noori, S, Mahal, A, Lowden, PA, Steffan, JS, Marsh, JL. Suberoylanilide

hydroxamic acid, a histone deacetylase inhibitor , ameliorates motor deficits in a mouse model of Huntington's disease. Proc Natl Acad Sci USA 2003;100: 2041-2046.

Hornung JP, Koppel H, Clarke PG. Endocytosis and autophagy in dying neurons: an ultrastructural study in chick embryos. J Comp Neurol. 1989 May 15;283(3):425-37.

Hung YH, Chen LM, Yang JY, Yang WY. Spatiotemporally controlled induction of autophagy-mediated lysosome turnover. Nat Commun. 2013;4:2111.

Ichimura Y, Komatsu M. Pathophysiological role of autophagy: lesson from autophagy-deficient mouse models. Exp Anim. 2011;60(4):329-45.

Ishibashi K, Uemura T, Waguri S, Fukuda M. secretion from PC12 cells independently of autophagic activity. Atg16L1, an essential factor for canonical autophagy, participates in hormone. Mol Biol Cell. 2012 Aug;23(16):3193-202.

Iwata, A., Riley, B. E., Jhonston, J. A., Kopito, R. R. HDAC6 and microtubules are required for autophagic degradation of aggregation Huntington. J Biol Chem 2005;280: 40282 – 40292.

Jacobson LS, Lima H Jr, Goldberg MF, Gocheva V, Tsiperson V, Sutterwala FS, Joyce JA, Gapp BV, Blomen VA, Chandran K, Brummelkamp TR, Diaz-Griffero F, Brojatsch J. Cathepsin-mediated necrosis controls the adaptive immune response by Th2 (T helper type 2)-associated adjuvants. J Biol Chem. 2013 Mar 15;288(11):7481-91.

Joussen AM, Poulaki V, Le ML, Koizumi K, Esser C, Janicki H, Schraermeyer U, Kociok N, Fauser S, Kirchhof B, Kern TS, Adamis AP. A central role for inflammation in the pathogenesis of diabetic retinopathy. FASEB J. 2004 Sep;18(12):1450-2.

Kabeya Y, Mizushima N, Ueno T, Yamamoto A, Kirisako T, Noda T, Kominami E, Ohsumi Y, Yoshimori T. LC3, a mammalian homologue of yeast Apg8p, is localized in autophagosome membranes after processing. EMBO J. 2000 Nov 1;19(21):5720-8.

Kågedal K, Zhao M, Svensson I, Brunk UT. Sphingosine-induced apoptosis is dependent on lysosomal proteases. Biochem J. 2001 Oct 15;359(Pt 2):335-43.

Kallunki T, Olsen OD, Jäättelä M. Cancer-associated lysosomal changes: friends or foes? Oncogene. 2013 Apr 18;32(16):1995-2004

Kaushal S. Effect of rapamycin on the fate of P23H opsin associated with retinitis pigmentosa (an American Ophthalmological Society thesis). Trans Am Ophthalmol Soc. 2006;104:517-29.

Kanzawa T, Germano IM, Komata T, Ito H, Kondo Y, Kondo S. Role of autophagy in temozolomide-induced cytotoxicity for malignant glioma cells. Cell Death Differ. 2004 Apr;11(4):448-57.

Kessel DH, Price M, Reiners JJ Jr. ATG7 deficiency suppresses apoptosis and cell death induced by lysosomal photodamage. Autophagy. 2012 Sep;8(9):1333-41.

Kiyono K, Suzuki HI, Matsuyama H, Morishita Y, Komuro A, Kano MR, Sugimoto K, Miyazono K. Autophagy is activated by TGF-beta and potentiates TGF-beta-mediated growth inhibition in human hepatocellular carcinoma cells. Cancer Res. 2009 Dec 1;69(23):8844-52.

Kim J, Kundu M, Viollet B, Guan KL. AMPK and mTOR regulate autophagy through direct phosphorylation of Ulk1. Nat Cell Biol. 2011 Feb;13(2):132-41.

Kim J, Moon C, Ahn M, Joo HG, Jin JK, Shin T. Immunohistochemical localization of galectin-3 in the pig retina during postnatal development. Mol Vis. 2009 Sep 26;15:1971-6.

Kirkegaard T, Roth AG, Petersen NH, Mahalka AK, Olsen OD, Moilanen I, Zylicz A, Knudsen J, Sandhoff K, Arenz C, Kinnunen PK, Nylandsted J, Jäättelä M. Hsp70 stabilizes lysosomes and reverts Niemann-Pick disease-associated lysosomal pathology. Nature. 2010 Jan 28;463(7280):549-53.

Kolosova NG, Muraleva NA, Zhdankina AA, Stefanova NA, Fursova AZ, Blagosklonny MV. Prevention of age-related macular degeneration-like retinopathy by rapamycin in rats. Am J Pathol. 2012 Aug;181(2):472-7.

Krenn MA, Schürz M, Teufl B, Uchida K, Eckl PM, Bresgen N. Ferritin-stimulated lipid peroxidation, lysosomal leak, and macroautophagy promote lysosomal "metastability" in primary hepatocytes determining in vitro cell survival. Free Radic Biol Med. 2015 Mar;80:48-58.

Kreuzaler PA, Staniszewska AD, Li W, Omidvar N, Kedjouar B, Turkson J, Poli V, Flavell RA, Clarkson RW, Watson CJ. Stat3 controls lysosomal-mediated cell death in vivo. Nat Cell Biol. 2011 Mar;13(3):303-9.

Jenwitheesuk A, Nopparat C, Mukda S, Wongchitrat P, Govitrapong P. Melatonin regulates aging and neurodegeneration through energy metabolism, epigenetics, autophagy and circadian rhythm pathways. Int J Mol Sci. 2014 Sep 22;15(9):16848-84.

Jones BW, Kondo M, Terasaki H, Lin Y, McCall M, Marc RE. Retinal remodeling. Jpn J Ophthalmol. 2012 Jul;56(4):289-306.

Josh Morgan and Rachel Wong. Development of Cell Types and Synaptic Connections in the Retina. Webvision, 29. 2007.

Justin P. Kumar. Signalling pathways in Drosophila and vertebrate retinal development. Nat Rev Genet. 2001 Nov;2(11):846-57.

Kunchithapautham K, Coughlin B, Lemasters JJ, Rohrer B. Differential effects of rapamycin on rods and cones during light-induced stress in albino mice. Invest Ophthalmol Vis Sci. 2011 May 5;52(6):2967-75.

Kunchithapautham K, Rohrer B. Autophagy is one of the multiple mechanisms active in photoreceptor degeneration. Autophagy. 2007 Jan-Feb;3(1):65-6

Kurz T, Terman A, Gustafsson B, Brunk UT. Lysosomes in iron metabolism, ageing and apoptosis. Histochem Cell Biol. 2008a Apr;129(4):389-406.

Kurz T, Terman A, Gustafsson B, Brunk UT. Lysosomes and oxidative stress in aging and apoptosis. Biochim Biophys Acta. 2008b Nov;1780(11):1291-303.

Lage SL, Buzzo CL, Amaral EP, Matteucci KC, Massis LM, Icimoto MY, Carmona AK, D'Império Lima MR, Rodrigues MM, Ferreira LC, Amarante-Mendes GP, Bortoluci KR. Cytosolic flagellin-induced lysosomal pathway regulates inflammasome-dependent and -independent macrophage responses. Proc Natl Acad Sci U S A. 2013 Aug 27;110(35):E3321-30.

Langmann T. Microglia activation in retinal degeneration. J Leukoc Biol. 2007 Jun;81(6):1345-51.

Lazarou M, Sliter DA, Kane LA, Sarraf SA, Wang C, Burman JL, Sideris DP, Fogel AI, Youle RJ. The ubiquitin kinase PINK1 recruits autophagy receptors to induce mitophagy. Nature. 2015 Aug 20;524(7565):309-314.

Lee IH, Kawai Y, Fergusson MM, Rovira II, Bishop AJ, Motoyama N, Cao L, Finkel T. Atg7 modulates p53 activity to regulate cell cycle and survival during metabolic stress. Science. 2012 Apr 13;336(6078):225-8.

Lee, IH, Cao, L, Mostoslavsky, R, Lombard, DB, Liu, J, Bruns, NE, Tsokos, M, Alt, FW, Finkel, T. A role for the NAD-dependent deacetylase Sirt1 in the regulation of autophagy. Proc Natl Acad Sci USA 2008;105 (9): 3374-3379.

Lee JH, Yu WH, Kumar A, Lee S, Mohan PS, Peterhoff CM, Wolfe DM, Martinez-Vicente M, Massey AC, Sovak G, Uchiyama Y, Westaway D, Cuervo AM, Nixon RA. Lysosomal proteolysis and autophagy require presenilin 1 and are disrupted by Alzheimer-related PS1 mutations. Cell. 2010 Jun 25;141(7):1146-58.

Li GY, Fan B, Jiao YY. Rapamycin attenuates visible light-induced injury in retinal photoreceptor cells via inhibiting endoplasmic reticulum stress. Brain Res. 2014 May 14;1563:1-12.

Li N, Zheng Y, Chen W, Wang C, Liu X, He W, Xu H, Cao X. Adaptor protein LAPF recruits phosphorylated p53 to lysosomes and triggers lysosomal destabilization in apoptosis. Cancer Res. 2007 Dec 1;67(23):11176-85.

Li S, Lin JD. Transcriptional control of circadian metabolic rhythms in the liver. Diabetes Obes Metab. 2015 Sep;17 Suppl 1:33-8.

Li S, Du L, Zhang L, Hu Y, Xia W, Wu J, Zhu J, Chen L, Zhu F, Li C, Yang S. Cathepsin B contributes to autophagy-related 7 (Atg7)-induced nod-like receptor 3 (NLRP3)-dependent proinflammatory response and aggravates lipotoxicity in rat insulinoma cell line. J Biol Chem. 2013 Oct 18;288(42):30094-104.

Liang XH, Jackson S, Seaman M, Brown K, Kempkes B, Hibshoosh H, Levine B. Induction of autophagy and inhibition of tumorigenesis by beclin 1. Nature. 1999 Dec 9;402(6762):672-6.

Liu L, Zhang N, Dou Y, Mao G, Bi C, Pang W, Liu X, Song D, Deng H. Lysosomal dysfunction and autophagy blockade contribute to IMB-6G-induced apoptosis in pancreatic cancer cells. Sci Rep. 2017 Jan 31;7:41862.

Liu J, Xia H, Kim M, Xu L, Li Y, Zhang L, Cai Y, Norberg HV, Zhang T, Furuya T, Jin M, Zhu Z, Wang H, Yu J, Li Y, Hao Y, Choi A, Ke H, Ma D, Yuan J. Beclin1 controls the levels of p53 by regulating the deubiquitination activity of USP10 and USP13. Cell. 2011 Sep 30;147(1):223-34.

Little, GH, Bai, Y, Williams, T, Poizat, C. Nuclear calcium/calmodulin-dependent protein kinase II delta preferentially transmists signals to histone deacetylase 4 in cardiac cells. J Biol Chem 2007;282 (10): 7219-7231.

Loison F, Zhu H, Karatepe K, Kasorn A, Liu P, Ye K, Zhou J, Cao S, Gong H, Jenne DE, Remold-O'Donnell E, Xu Y, Luo HR. Proteinase 3-dependent caspase-3 cleavage modulates neutrophil death and inflammation. J Clin Invest. 2014 Oct;124(10):4445-58.

Lonskaya I, Hebron ML, Algarzae NK, Desforges N, Moussa CE. Decreased parkin solubility is associated with impairment of autophagy in the nigrostriatum of sporadic Parkinson's disease. Neuroscience. 2013 Mar 1;232:90-105.

Li Z, Zhu WG.Targeting histone deacetylases for cancer therapy: from molecular mechanisms to clinical implications. Int J Biol Sci. 2014 Jul 2;10(7):757-70.

Liu L, Liao JZ, He XX, Li PY. The role of autophagy in hepatocellular carcinoma: friend or foe. Oncotarget. 2017 Apr 18;8(34):57707-57722.

Liu X, Van Vleet T, Schnellmann RG. The role of calpain in oncotic cell death. Annu Rev Pharmacol Toxicol. 2004;44:349-70.

Łopatniuk P, Witkowski JM. Conventional calpains and programmed cell death. Acta Biochim Pol. 2011;58(3):287-96.

Luke CJ, Silverman GA. Necrotic cell death: harnessing the Dark side of the Force in mammary gland involution. Nat Cell Biol. 2011 Mar;13(3):197-9.

Ma S, Wang Y, Chen Y, Cao F. The role of the autophagy in myocardial ischemia/reperfusion injury. Biochim Biophys Acta. 2015 Feb;1852(2):271-6.

Maejima I, Takahashi A, Omori H, Kimura T, Takabatake Y, Saitoh T, Yamamoto A, Hamasaki M, Noda T, Isaka Y, Yoshimori T. Autophagy sequesters damaged lysosomes to control lysosomal biogenesis and kidney injury. EMBO J. 2013 Aug 28;32(17):2336-47.

Maiese K. Moving to the Rhythm with Clock (Circadian) Genes, Autophagy, mTOR, and SIRT1 in Degenerative Disease and Cancer. Curr Neurovasc Res. 2017;14(3):299-304.

Mannick JB, Schonhoff C, Papeta N, Ghafourifar P, Szibor M, Fang K, Gaston B. S-Nitrosylation of mitochondrial caspases. J Cell Biol. 2001 Sep 17;154(6):1111-6.

Mantamadiotis T, Lemberger T, Bleckmann SC, Kern H, Kretz O, Martin Villalba A, Tronche F, Kellendonk C, Gau D, Kapfhammer J, Otto C, Schmid W, Schütz G. Disruption of CREB function in brain leads to neurodegeneration. Nat Genet. 2002 May;31(1):47-54.

Mariño G, Niso-Santano M, Baehrecke EH, Kroemer G. Self-consumption: the interplay of autophagy and apoptosis. Nat Rev Mol Cell Biol. 2014 Feb;15(2):81-94.

Mariño G, Fernández AF, Cabrera S, Lundberg YW, Cabanillas R, Rodríguez F, Salvador-Montoliu N, Vega JA, Germanà A, Fueyo A, Freije JM, López-Otín C. Autophagy is essential for mouse sense of balance. J Clin Invest. 2010 Jul;120(7):2331-44.

Martinez-Lopez N, Athonvarangkul D, Singh R. Autophagy and aging. Adv Exp Med Biol. 2015;847:73-87.

Mauro-Lizcano M, Esteban-Martínez L, Seco E, Serrano-Puebla A, Garcia-Ledo L, Figueiredo-Pereira C, Vieira HL, Boya P. New method to assess mitophagy flux by flow cytometry. Autophagy. 2015;11(5):833-43.

McCoy F, Hurwitz J, McTavish N, Paul I, Barnes C, O'Hagan B, Odrzywol K, Murray J, Longley D, McKerr G, Fennell DA. Obatoclax induces Atg7-dependent autophagy independent of beclin-1 and BAX/BAK. Cell Death Dis. 2010 Dec 16;1:e108.

Mijaljica D, Prescott M, Devenish RJ. Microautophagy in mammalian cells: revisiting a 40-year-old conundrum. Autophagy. 2011 Jul;7(7):673-82.

Mikhaylova O, Stratton Y, Hall D, Kellner E, Ehmer B, Drew AF, Gallo CA, Plas DR, Biesiada J, Meller J, Czyzyk-Krzeska MF. VHL-regulated MiR-204 suppresses tumor growth through inhibition of LC3B-mediated autophagy in renal clear cell carcinoma. Cancer Cell. 2012 Apr 17;21(4):532-46.

Militante J, Lombardini JB. Age-related retinal degeneration in animal models of aging: possible involvement of taurine deficiency and oxidative stress. Neurochem Res. 2004 Jan;29(1):151-60.

Mitton KP, Guzman AE, Deshpande M, Byrd D, DeLooff C, Mkoyan K, Zlojutro P, Wallace A, Metcalf B, Laux K, Sotzen J, Tran T. Different effects of valproic acid on photoreceptor loss in Rd1 and Rd10 retinal degeneration mice. Mol Vis. 2014 Nov 4;20:1527-44.

Mitter SK, Song C, Qi X, Mao H, Rao H, Akin D, Lewin A, Grant M, Dunn W Jr, Ding J, Bowes Rickman C, Boulton M. Dysregulated autophagy in the RPE is associated with increased susceptibility to oxidative stress and AMD. Autophagy. 2014;10(11):1989-2005.

Mizushima N, Yoshimori T. How to interpret LC3 immunoblotting. Autophagy. 2007 Nov-Dec;3(6):542-5.

Mizushima N. Methods for monitoring autophagy. Int J Biochem Cell Biol. 2004 Dec;36(12):2491-502.

Mizushima N, Kuma A, Kobayashi Y, Yamamoto A, Matsubae M, Takao T, Natsume T, Ohsumi Y, Yoshimori T. Mouse Apg16L, a novel WD-repeat protein, targets to the autophagic isolation membrane with the Apg12-Apg5 conjugate. J Cell Sci. 2003 May 1;116(Pt 9):1679-88.

Mohand-Said S, Deudon-Combe A, Hicks D, Simonutti M, Forster V, Fintz AC, Léveillard T, Dreyfus H, Sahel JA. Normal retina releases a diffusible factor stimulating

cone survival in the retinal degeneration mouse. Proc Natl Acad Sci U S A. 1998 Jul 7;95(14):8357-62.

Montaser M, Lalmanach G, Mach L. CA-074, but not its methyl ester CA-074Me, is a selective inhibitor of cathepsin B within living cells. Biol Chem. 2002 Jul-Aug;383(7-8):1305-8.

Morrison, B. E., Majdzadeh, N., Zhang, X., Lyles, A., Bassel-Duby, R., Olson, E. N., D'Mello, S. R. Neuroprotection by histone deacetylase-related protein. Mol Cell Biol. 2006;26: 3350-3364.

Naia L, Cunha-Oliveira T, Rodrigues J, Rosenstock TR, Oliveira A, Ribeiro M, Carmo C, Oliveira-Sousa SI, Duarte AI, Hayden MR, Rego AC. Histone Deacetylase Inhibitors Protect Against Pyruvate Dehydrogenase Dysfunction in Huntington's Disease. J Neurosci. 2017 Mar 8;37(10):2776-2794.

Nakatogawa H, Suzuki K, Kamada Y, Ohsumi Y. Dynamics and diversity in autophagy mechanisms: lessons from yeast. Nat Rev Mol Cell Biol. 2009 Jul;10(7):458-67.

Nakazawa T, Nakazawa C, Matsubara A, Noda K, Hisatomi T, She H, Michaud N, Hafezi-Moghadam A, Miller JW, Benowitz LI. Tumor necrosis factor-alpha mediates oligodendrocyte death and delayed retinal ganglion cell loss in a mouse model of glaucoma. J Neurosci. 2006 Dec 6;26(49):12633-41.

Napolitano G, Ballabio A. TFEB at a glance. J Cell Sci. 2016 Jul 1;129(13):2475-81.

Nguyen TN, Padman BS, Usher J, Oorschot V, Ramm G, Lazarou M. Atg8 family LC3/GABARAP proteins are crucial for autophagosome-lysosome fusion but not autophagosome formation during PINK1/Parkin mitophagy and starvation. J Cell Biol. 2016 Dec 19;215(6):857-874.

Nixon RA, Wegiel J, Kumar A, Yu WH, Peterhoff C, Cataldo A, Cuervo AM. Extensive involvement of autophagy in Alzheimer disease: an immuno-electron microscopy study. J Neuropathol Exp Neurol. 2005 Feb;64(2):113-22.

Nylandsted J, Gyrd-Hansen M, Danielewicz A, Fehrenbacher N, Lademann U, Høyer-Hansen M, Weber E, Multhoff G, Rohde M, Jäättelä M. Heat shock protein 70 promotes cell survival by inhibiting lysosomal membrane permeabilization. J Exp Med. 2004 Aug 16;200(4):425-35.

Ohsumi Y. Historical landmarks of autophagy research. Cell Res. 2014 Jan;24(1):9-23.

Ostenfeld MS, Høyer-Hansen M, Bastholm L, Fehrenbacher N, Olsen OD, Groth-Pedersen L, Puustinen P, Kirkegaard-Sørensen T, Nylandsted J, Farkas T, Jäättelä M. Anti-cancer agent siramesine is a lysosomotropic detergent that induces cytoprotective autophagosome accumulation. Autophagy. 2008 May;4(4):487-99.

Ostenfeld MS, Fehrenbacher N, Høyer-Hansen M, Thomsen C, Farkas T, Jäättelä M.
Effective tumor cell death by sigma-2 receptor ligand siramesine involves lysosomal leakage and oxidative stress. Cancer Res. 2005 Oct 1;65(19):8975-83.

Otomo T, Yoshimori T. Lysophagy: A Method for Monitoring Lysosomal Rupture Followed by Autophagy-Dependent Recovery. Methods Mol Biol. 2017;1594:141-149.

Palczewski K. G protein-coupled receptor rhodopsin. Annu Rev Biochem. 2006;75:743-67.

Palmieri M, Pal R, Nelvagal HR, Lotfi P, Stinnett GR, Seymour ML, Chaudhury A, Bajaj L, Bondar VV, Bremner L, Saleem U, Tse DY, Sanagasetti D, Wu SM, Neilson JR, Pereira FA, Pautler RG, Rodney GG, Cooper JD, Sardiello M. mTORC1-independent

TFEB activation via Akt inhibition promotes cellular clearance in neurodegenerative storage diseases. Nat Commun. 2017 Feb 6;8:14338.

Park G, Tan J, Garcia G, Kang Y, Salvesen G, Zhang Z. Regulation of Histone Acetylation by Autophagy in Parkinson Disease. J Biol Chem. 2016 Feb 12;291(7):3531-40.

Paquet-Durand F1, Azadi S, Hauck SM, Ueffing M, van Veen T, Ekström P. Calpain is activated in degenerating photoreceptors in the rd1 mouse. J Neurochem. 2006 Feb;96(3):802-14.

Petersen NH, Olsen OD, Groth-Pedersen L, Ellegaard AM, Bilgin M, Redmer S, Ostenfeld MS, Ulanet D, Dovmark TH, Lønborg A, Vindeløv SD, Hanahan D, Arenz C, Ejsing CS, Kirkegaard T, Rohde M, Nylandsted J, Jäättelä M. Transformation-associated changes in sphingolipid metabolism sensitize cells to lysosomal cell death induced by inhibitors of acid sphingomyelinase. Cancer Cell. 2013 Sep 9;24(3):379-93.

Petersen NH, Kirkegaard T, Olsen OD, Jäättelä M. Connecting Hsp70, sphingolipid metabolism and lysosomal stability. Cell Cycle. 2010 Jun 15;9(12):2305-9.

Pickford F, Masliah E, Britschgi M, Lucin K, Narasimhan R, Jaeger PA, Small S, Spencer B, Rockenstein E, Levine B, Wyss-Coray T. The autophagy-related protein beclin 1 shows reduced expression in early Alzheimer disease and regulates amyloid b54eta accumulation in mice. J Clin Invest. 2008 Jun;118(6):2190-9.

Pittler SJ, Keeler CE, Sidman RL, Baehr W. PCR analysis of DNA from 70-year-old sections of rodless retina demonstrates identity with the mouse rd defect. Proc Natl Acad Sci U S A. 1993 Oct 15;90(20):9616-9.

Platón-Corchado M, Barcelona PF, Jmaeff S, Marchena M, Hernández-Pinto AM, Hernández-Sánchez C, Saragovi HU, de la Rosa EJ. p75NTR antagonists attenuate photoreceptor cell loss in murine models of retinitis pigmentosa. Cell Death Dis. 2017 Jul 13;8(7):e2922.

Ravikumar B, Duden R, Rubinsztein DC. Aggregate-prone proteins with polyglutamine and polyalanine expansions are degraded by autophagy. Hum Mol Genet. 2002 May 1;11(9):1107-17.

Reggiori F, Komatsu M, Finley K, Simonsen A. Autophagy: more than a nonselective pathway. Int J Cell Biol. 2012;2012:219625.

Reme, CE, Young, RW, 1977. The effects of hibernation on cone visual cells in the ground squirrel. Investig. Ophthalmol. Vis. Sci. 16, 815e840

Remé CE, Wolfrum U, Imsand C, Hafezi F, Williams TP. Photoreceptor autophagy: effects of light history on number and opsin content of degradative vacuoles. Invest Ophthalmol Vis Sci. 1999 Sep;40(10):2398-404.

Repnik U, Distefano MB, Speth MT, Ng MYW, Progida C, Hoflack B, Gruenberg J, Griffiths G. LLOMe does not release cysteine cathepsins to the cytosol but inactivates them in transiently permeabilized lysosomes. J Cell Sci. 2017 Jul 28. pii: jcs.204529.

Rivas MA, Vecino E. Animal models and different therapies for treatment of retinitis pigmentosa. Histol Histopathol. 2009 Oct;24(10):1295-322.

Rodríguez-Muela N1, Koga H, García-Ledo L, de la Villa P, de la Rosa EJ, Cuervo AM, Boya P. Balance between autophagic pathways preserves retinal homeostasis. Aging Cell. 2013 Jun;12(3):478-88.

Rodríguez-Muela N, Boya P. Axonal damage, autophagy and neuronal survival. Autophagy. 2012 Feb 1;8(2):286-8.

Rodríguez-Muela N, Germain F, Mariño G, Fitze PS, Boya P. Autophagy promotes survival of retinal ganglion cells after optic nerve axotomy in mice. Cell Death Differ. 2012 Jan;19(1):162-9.

Rosato RR, Almenara, JA, Dai, Y. Simultaneous activation of the intrinsic and extrinsic pathways by histone deacetylases (HDAC) inhibitors and tumor necrosis factor-related apoptosis-inducing ligand (TRAIL) synergistically induces mithocondrial damage and apoptosis in human leukemia cells. Mol Cancer Ther .2003;2: 1273-1284.

Rossmiller B, Mao H, Lewin AS. Gene therapy in animal models of autosomal dominant retinitis pigmentosa. Mol Vis. 2012;18:2479-96.

Sahara S, Yamashima T. Calpain-mediated Hsp70.1 cleavage in hippocampal CA1 neuronal death. Biochem Biophys Res Commun. 2010 Mar 19;393(4):806-11.

Sahel JA, Mohand-Said S, Léveillard T, Hicks D, Picaud S, Dreyfus H. Rod-cone interdependence: implications for therapy of photoreceptor cell diseases. Prog Brain Res. 2001;131:649-61.

Sahu R, Kaushik S, Clement CC, Cannizzo ES, Scharf B, Follenzi A, Potolicchio I, Nieves E, Cuervo AM, Santambrogio L. Microautophagy of cytosolic proteins by late endosomes. Dev Cell. 2011 Jan 18;20(1):131-9.

Salazar M, Carracedo A, Salanueva IJ, Hernández-Tiedra S, Lorente M, Egia A, Vázquez P, Blázquez C, Torres S, García S, Nowak J, Fimia GM, Piacentini M, Cecconi F, Pandolfi PP, González-Feria L, Iovanna JL, Guzmán M, Boya P, Velasco G. Cannabinoid action induces autophagy-mediated cell death through stimulation of ER stress in human glioma cells. J Clin Invest. 2009 May;119(5):1359-72.

Salvador N, Aguado C, Horst M, Knecht E. Import of a cytosolic protein into lysosomes by chaperone-mediated autophagy depends on its folding state. J Biol Chem. 2000 Sep 1;275(35):27447-56.

Sancho-Pelluz, J., Paquet-Durand, F. HDAC inhibition prevents Rd1 mouse photoreceptor degeneration. Advances in experimental medicine and biology 2012;723: 107-113.

Sancho-Pelluz, J., Alavi, M. V., Sahaboglu, A., Kustermann, S., Farinelli, P., Azadi, S., Van Veen, T., Romero, F. J., Paquet-Durand, F., Ekström, P. Excessive HDAC activation is critical for neurodegeneration in the rd1 mouse. Cell Death and Disease 2010 1: e24.

Sancho-Pelluz J, Arango-Gonzalez B, Kustermann S, Romero FJ, van Veen T, Zrenner E, Ekström P, Paquet-Durand F. Photoreceptor cell death mechanisms in inherited retinal degeneration. Mol Neurobiol. 2008 Dec;38(3):253-69.

Sargent G, van Zutphen T, Shatseva T, Zhang L, Di Giovanni V, Bandsma R, Kim PK. PEX2 is the E3 ubiquitin ligase required for pexophagy during starvation. J Cell Biol. 2016 Sep 12;214(6):677-90.

Schotte P, Declercq W, Van Huffel S, Vandenabeele P, Beyaert R. Non-specific effects of methyl ketone peptide inhibitors of caspases. FEBS Lett. 1999 Jan 8;442(1):117-21.

Scott SV, Nice DC, Nau JJ, Weisman LS, Kamada Y, Keizer-Gunnink I, Funakoshi T, Veenhuis M, Ohsumi Y, Klionsky DJ. Apg13p and Vac8p are part of a complex of phosphoproteins that are required for cytoplasm to vacuole targeting. J Biol Chem. 2000 Aug 18;275(33):25840-9.

Serrano-Puebla A, Boya P. Lysosomal membrane permeabilization in cell death: new evidence and implications for health and disease. Ann N Y Acad Sci. 2016 May;1371(1):30-44.

Settembre C, Fraldi A, Medina DL, Ballabio A. Signals from the lysosome: a control centre for cellular clearance and energy metabolism. Nat Rev Mol Cell Biol. 2013 May;14(5):283-96.

Settembre C, Fraldi A, Jahreiss L, Spampanato C, Venturi C, Medina D, de Pablo R, Tacchetti C, Rubinsztein DC, Ballabio A. A block of autophagy in lysosomal storage disorders. Hum Mol Genet. 2008 Jan 1;17(1):119-29.

Shao A, Wang Z, Wu H, Dong X, Li Y, Tu S2, Tang J, Zhao M, Zhang J, Hong Y. Enhancement of Autophagy by Histone Deacetylase Inhibitor Trichostatin A Ameliorates Neuronal Apoptosis After Subarachnoid Hemorrhage in Rats. Mol Neurobiol. 2016 Jan;53(1):18-27.

Shimizu S, Konishi A, Nishida Y, Mizuta T, Nishina H, Yamamoto A, Tsujimoto Y. Involvement of JNK in the regulation of autophagic cell death. Oncogene. 2010 Apr 8;29(14):2070-82.

Shimizu S, Kanaseki T, Mizushima N, Mizuta T, Arakawa-Kobayashi S, Thompson CB, Tsujimoto Y. Role of Bcl-2 family proteins in a non-apoptotic programmed cell death dependent on autophagy genes. Nat Cell Biol. 2004 Dec;6(12):1221-8. Epub 2004 Nov 21.

Sizova OS, Shinde VM, Lenox AR, Gorbatyuk MS. Modulation of cellular signaling pathways in P23H rhodopsin photoreceptors. Cell Signal. 2014 Apr;26(4):665-672.

Smith EL, Schuchman EH. The unexpected role of acid sphingomyelinase in cell death and the pathophysiology of common diseases. FASEB J. 2008 Oct;22(10):3419-31.

Song XB, Liu G, Liu F, Yan ZG, Wang ZY, Liu ZP, Wang L. Autophagy blockade and lysosomal membrane permeabilization contribute to lead-induced nephrotoxicity in primary rat proximal tubular cells. Cell Death Dis. 2017 Jun 8;8(6):e2863.

Sun S, Han Y, Liu J, Fang Y, Tian Y, Zhou J, Ma D, Wu P. Trichostatin A targets the mitochondrial respiratory chain, increasing mitochondrial reactive oxygen species production to trigger apoptosis in human breast cancer cells. PLoS One. 2014 Mar 13;9(3):e91610.

Takamura A, Komatsu M, Hara T, Sakamoto A, Kishi C, Waguri S, Eishi Y, Hino O, Tanaka K, Mizushima N. Autophagy-deficient mice develop multiple liver tumors. Genes Dev. 2011 Apr 15;25(8):795-800.

Takeshige K, Baba M, Tsuboi S, Noda T, Ohsumi Y. Autophagy in yeast demonstrated with proteinase-deficient mutants and conditions for its induction. J Cell Biol. 1992 Oct; 119(2):301-11.

Tanaka M, Machida Y, Niu S, Ikeda T, Jana NR, Doi H, Kurosawa M, Nekooki M, Nukina N. Trehalose alleviates polyglutamine-mediated pathology in a mouse model of Huntington disease. Nat Med. 2004 Feb;10(2):148-54.

Tanida I, Ueno T, Kominami E. LC3 conjugation system in mammalian autophagy. Int J Biochem Cell Biol. 2004 Dec;36(12):2503-18.

Taniguchi M, Okazaki T. The role of sphingomyelin and sphingomyelin synthases in cell death, proliferation and migration-from cell and animal models to human disorders. Biochim Biophys Acta. 2014 May;1841(5):692-703.

Tasdemir E, Maiuri MC, Galluzzi L, Vitale I, Djavaheri-Mergny M, D'Amelio M, Criollo A, Morselli E, Zhu C, Harper F, Nannmark U, Samara C, Pinton P, Vicencio JM, Carnuccio R, Moll UM, Madeo F, Paterlini-Brechot P, Rizzuto R, Szabadkai G, Pierron G, Blomgren K, Tavernarakis N, Codogno P, Cecconi F, Kroemer G. Regulation of autophagy by cytoplasmic p53. Nat Cell Biol. 2008 Jun;10(6):676-87.

Thiele DL, Lipsky PE. Regulation of cellular function by products of lysosomal enzyme activity: elimination of human natural killer cells by a dipeptide methyl ester generated from L-leucine methyl ester by monocytes or polymorphonuclear leukocytes. Proc Natl Acad Sci U S A. 1985 Apr;82(8):2468-72.

Till A, Lakhani R, Burnett SF, Subramani S. Pexophagy: the selective degradation of peroxisomes. Int J Cell Biol. 2012;2012:512721.

Toops KA, Tan LX, Jiang Z, Radu RA, Lakkaraju A. Cholesterol-mediated activation of acid sphingomyelinase disrupts autophagy in the retinal pigment epithelium. Mol Biol Cell. 2015 Jan 1;26(1):1-14.

Tsukada M, Ohsumi Y. Isolation and characterization of autophagy-defective mutants of Saccharomyces cerevisiae. FEBS Lett. 1993 Oct 25;333(1-2):169-74.

Venè R, Arena G, Poggi A, D'Arrigo C, Mormino M, Noonan DM, Albini A, Tosetti F. Novel cell death pathways induced by N-(4-hydroxyphenyl)retinamide: therapeutic implications. Mol Cancer Ther. 2007 Jan;6(1):286-98.

Venters SJ, Mikawa T, Hyer J. Early divergence of central and peripheral neural retina precursors during vertebrate eye development. Dev Dyn. 2015 Mar;244(3):266-76.

Vila M, Bové J, Dehay B, Rodríguez-Muela N, Boya P. Lysosomal membrane permeabilization in Parkinson disease. Autophagy. 2011 Jan;7(1):98-100.

Villalpando Rodriguez GE, Torriglia A. Calpain 1 induce lysosomal permeabilization by cleavage of lysosomal associated membrane protein 2. Biochim Biophys Acta. 2013 Oct;1833(10):2244-53.

Vuong LN, Hedges TR 3rd. Ganglion cell layer complex measurements in compressive optic neuropathy. Curr Opin Ophthalmol. 2017 Nov;28(6):573-578.

Vousden KH, Prives C. Blinded by the Light: The Growing Complexity of p53. Cell. 2009 May 1;137(3):413-31.

Walls KC, Ghosh AP, Franklin AV, Klocke BJ, Ballestas M, Shacka JJ, Zhang J, Roth KA. Lysosome dysfunction triggers Atg7-dependent neural apoptosis. J Biol Chem. 2010 Apr 2;285(14):10497-507.

Wang C, Liu Z, Huang X. Rab32 is important for autophagy and lipid storage in Drosophila. PLoS One. 2012;7(2):e32086.

Wang H, Wan H, Li X, Liu W, Chen Q, Wang Y, Yang L, Tang H, Zhang X, Duan E, Zhao X, Gao F, Li W. Atg7 is required for acrosome biogenesis during spermatogenesis in mice. Cell Res. 2014 Jul;24(7):852-69.

Wang J, Saul A, Cui X, Roon P, Smith SB. Absence of Sigma 1 Receptor Accelerates Photoreceptor Cell Death in a Murine Model of Retinitis Pigmentosa. Invest Ophthalmol Vis Sci. 2017 Sep 1;58(11):4545-4558.

Wang M, Kaufman RJ. Protein misfolding in the endoplasmic reticulum as a conduit to human disease. Nature. 2016 Jan 21;529(7586):326-35.

Wang SC, Wang ST, Liu HT, Wang XY, Wu SC, Chen LC, Liu YW. Trichostatin A induces bladder cancer cell death via intrinsic apoptosis at the early phase and Sp1‑survivin downregulation at the late phase of treatment. Oncol Rep. 2017 Sep;38(3):1587-1596.

Wang Y, Li L, Hou C, Lai Y, Long J, Liu J, Zhong Q, Diao J. SNARE-mediated membrane fusion in autophagy. Semin Cell Dev Biol. 2016 Dec;60:97-104.

Webb JL, Ravikumar B, Atkins J, Skepper JN, Rubinsztein DC. Alpha-Synuclein is degraded by both autophagy and the proteasome. J Biol Chem. 2003 Jul 4;278(27):25009-13.

Weleber RG. The effect of age on human cone and rod ganzfeld electroretinograms. Invest Ophthalmol Vis Sci. 1981 Mar;20(3):392-9.

Wild P, McEwan DG, Dikic I. The LC3 interactome at a glance. J Cell Sci. 2014 Jan 1;127(Pt 1):3-9.

Wu BX, Fan J, Boyer NP, Jenkins RW, Koutalos Y, Hannun YA, Crosson CE. Lack of Acid Sphingomyelinase Induces Age-Related Retinal Degeneration. PLoS One. 2015 Jul 13;10(7):e0133032.

Xiong J. Atg7 in development and disease: panacea or Pandora's Box? Protein Cell. 2015 Oct;6(10):722-34.

Xiong X, Tao R, DePinho RA, Dong XC. The autophagy-related gene 14 (Atg14) is regulated by forkhead box O transcription factors and circadian rhythms and plays a critical role in hepatic autophagy and lipid metabolism. J Biol Chem. 2012 Nov 9;287(46):39107-14.

Xue LY, Chiu SM, Oleinick NL. Atg7 deficiency increases resistance of MCF-7 human breast cancer cells to photodynamic therapy. Autophagy. 2010 Feb;6(2):248-55.

Yamada T, Carson AR, Caniggia I, Umebayashi K, Yoshimori T, Nakabayashi K, Scherer SW. Endothelial nitric-oxide synthase antisense (NOS3AS) gene encodes an autophagy-related protein (APG9-like2) highly expressed in trophoblast. J Biol Chem. 2005 May 6;280(18):18283-90.

Yamashima T, Saido TC, Takita M, Miyazawa A, Yamano J, Miyakawa A, Nishijyo H, Yamashita J, Kawashima S, Ono T, Yoshioka T. Transient brain ischaemia provokes Ca2+, PIP2 and calpain responses prior to delayed neuronal death in monkeys. Eur J Neurosci. 1996 Sep;8(9):1932-44.

Yang DS, Stavrides P, Mohan PS, Kaushik S, Kumar A, Ohno M, Schmidt SD, Wesson D, Bandyopadhyay U, Jiang Y, Pawlik M, Peterhoff CM, Yang AJ, Wilson DA, St George-Hyslop P, Westaway D, Mathews PM, Levy E, Cuervo AM, Nixon RA. Reversal of autophagy dysfunction in the TgCRND8 mouse model of Alzheimer's disease ameliorates amyloid pathologies and memory deficits. Brain. 2011 Jan;134(Pt 1):258-77.

Yang RY, Hsu DK, Liu FT. Expression of galectin-3 modulates T-cell growth and apoptosis. Proc Natl Acad Sci U S A. 1996 Jun 25;93(13):6737-42.

Yang Y, Yin W, Wu F, Fan J. Combination of azacitidine and trichostatin A decreased the tumorigenic potential of lung cancer cells. Onco Targets Ther. 2017 Jun 14;10:2993-2999.

Yao J, Jia L, Shelby SJ, Ganios AM, Feathers K, Thompson DA, Zacks DN. Circadian and noncircadian modulation of autophagy in photoreceptors and retinal pigment epithelium. Invest Ophthalmol Vis Sci. 2014 Apr 29;55(5):3237-46.

Yoshida Y, Yasuda S, Fujita T, Hamasaki M, Murakami A, Kawawaki J, Iwai K, Saeki Y, Yoshimori T, Matsuda N, Tanaka K. Ubiquitination of exposed glycoproteins by SCFFBXO27 directs damaged lysosomes for autophagy. Proc Natl Acad Sci U S A. 2017 Aug 8;114(32):8574-8579.

Yoshizawa K, Kiuchi K, Nambu H, Yang J, Senzaki H, Kiyozuka Y, Shikata N, Tsubura A. Caspase-3 inhibitor transiently delays inherited retinal degeneration in C3H mice carrying the rd gene. Graefes Arch Clin Exp Ophthalmol. 2002 Mar;240(3):214-9.

Young RW. Cell death during differentiation of the retina in the mouse. J Comp Neurol. 1984 Nov 1;229(3):362-73.

Yu L, Alva A, Su H, Dutt P, Freundt E, Welsh S, Baehrecke EH, Lenardo MJ. Regulation of an ATG7-beclin 1 program of autophagic cell death by caspase-8. Science. 2004 Jun 4;304(5676):1500-2.

Yuan XM, Li W, Dalen H, Lotem J, Kama R, Sachs L, Brunk UT. Lysosomal destabilization in p53-induced apoptosis. Proc Natl Acad Sci U S A. 2002 Apr 30;99(9):6286-91.

Yuan XM, Li W, Dalen H, Lotem J, Kama R, Sachs L, Brunk UT. Lysosomal destabilization in p53-induced apoptosis. Proc Natl Acad Sci U S A. 2002 Apr 30;99(9):6286-91.

Zhang J, Ng S, Wang J, Zhou J, Tan SH, Yang N, Lin Q, Xia D, Shen HM. Histone deacetylase inhibitors induce autophagy through FOXO1-dependent pathways. Autophagy. 2015 Apr 3;11(4):629-42.

Zhang X, Yan H, Yuan Y, Gao J, Shen Z, Cheng Y, Shen Y, Wang RR, Wang X, Hu WW, Wang G, Chen Z. Cerebral ischemia-reperfusion-induced autophagy protects against neuronal injury by mitochondrial clearance. Autophagy. 2013 Sep;9(9):1321-33.

Zhang Y, Cross SD, Stanton JB, Marmorstein AD, Le YZ, Marmorstein LY. Early AMD-like defects in the RPE and retinal degeneration in aged mice with RPE-specific deletion of Atg5 or Atg7. Mol Vis. 2017 Apr 14;23:228-241.

Zhang Y, Goldman S, Baerga R, Zhao Y, Komatsu M, Jin S. Adipose-specific deletion of autophagy-related gene 7 (atg7) in mice reveals a role in adipogenesis. Proc Natl Acad Sci U S A. 2009 Nov 24;106(47):19860-5.

Zhao C, Yasumura D, Li X, Matthes M, Lloyd M, Nielsen G, Ahern K, Snyder M, Bok D, Dunaief JL, LaVail MM, Vollrath D. mTOR-mediated dedifferentiation of the retinal pigment epithelium initiates photoreceptor degeneration in mice. J Clin Invest. 2011 Jan;121(1):369-83.

Zhou Z, Vinberg F, Schottler F, Doggett TA, Kefalov, VJ, Ferguson, TA, Sene, A,Apte, RS. Autophagy supports color vision. Autophagy. 2015a;11(10):1821-32.

Zhou Z, Doggett TA, Sene A, Apte RS, Ferguson TA. Autophagy supports survival and phototransduction protein levels in rod photoreceptors. Cell Death Differ. 2015b Mar;22(3):488-98.

Zhu H, Yoshimoto T, Imajo-Ohmi S, Dazortsava M, Mathivanan A, Yamashima T. Why are hippocampal CA1 neurons vulnerable but motor cortex neurons resistant to transient ischemia? J Neurochem. 2012 Feb;120(4):574-85.

Zhu K, Dunner K Jr, McConkey DJ. Proteasome inhibitors activate autophagy as a cytoprotective response in human prostate cancer cells. Oncogene. 2010 Jan 21;29(3):451-62.

Zhu JY, Abate M, Rice PW, Cole CN. The ability of simian virus 40 large T antigen to immortalize primary mouse embryo fibroblasts cosegregates with its ability to bind to p53. J Virol. 1991 Dec;65(12):6872-80.

Zhu M, Zhang S, Tian X, Wu C. Mask mitigates MAPT- and FUS-induced degeneration by enhancing autophagy through lysosomal acidification. Autophagy. 2017 Aug 14:1-15.

Zhu W, Tao L, Quick ML, Joyce JA, Qu JM, Luo ZQ. Sensing cytosolic RpsL by macrophages induces lysosomal cell death and termination of bacterial infection. PLoS Pathog. 2015 Mar 4;11(3):e1004704.